Aus der Klinik und Poliklinik für Psychiatrie und Psychotherapie
der Ludwig-Maximilians-Universität München

ehem. Direktor: Prof. Dr. med. Hans-Jürgen Möller
komm. Direktor: Prof. Dr. Norbert Müller

Multimodal Approaches in Human Brain Mapping

Dissertation

zum Erwerb des Doktorgrades der Medizin
an der Medizinischen Fakultät
der Ludwig-Maximilians-Universität zu München

vorgelegt von Valerie Lisanne Kirsch
aus München

2012

Mit Genehmigung der Medizinischen Fakultät

der Universität München

Berichterstatter:	Prof. Dr. med. Christoph Mulert
Mitberichterstatter:	Priv. Doz. Dr. Jennifer Linn Priv. Doz. Dr. Angela Deutschländer Prof. Dr. Michael Soyka
Mitbetreuung durch den promovierten Mitarbeiter	Dr. med. Gregor Leicht
Dekan:	Prof. Dr. med. Dr. h.c. M. Reiser, FACR, FRCR

Tag der mündlichen Prüfung: 19.07.2012

Acknowledgements

I would like to express deep gratitude to those who have helped and supported me during my doctoral studies. This thesis would not have been possible without the guidance and trust of Prof. Christoph Mulert. As my supervisor he offered me continued support and numerous opportunities, including that of accompanying him to Harvard Medical School. It was his consistently innovative vision and expertise which led to the conception and execution of this work. I would also like to address my gratitude to Prof. Robert W. McCarley, Prof. Martha Shenton, Ass.-Prof. Dean F. Salisbury and Ass.-Prof. Kevin M. Spencer for their hospitality, supervision and support during my stay in their labs. It was an inspirational experience and I cherish the memory. Many special thanks go to Dr. Gregor Leicht and Dr. Susanne Karch for introducing me to my first methods and offering their advice throughout the years. My special gratitude also goes to Matthias Ertl with whom I thoroughly enjoyed working on new ideas and shared many inspiring discussions. I am deeply thankful to Daniel Keeser for sharing his expertise and providing his generous support. I am obliged to Ass-Prof Dr. Marek Kubicki, Dr. Thomas J. Whitford, Jorge Alverado, Paula Pelavin and Toni Mahowald from whom I received crucial help whilst my stay in Boston. A particular note of appreciation goes to Marie Fairbanks whose kind help allowed me to survive all the administrative procedures. I am also grateful for the sense of gemeinschaft with my fellow doctoral students in the Munich department.

I wholeheartedly thank my aunt Marie for reviewing my written words. I thank my friends for their tolerance and unfailing support. I cannot express sufficient gratitude to my mom and sister for providing their invaluable assistance and endless patience. They have been a constant source of encouragement and thoughtful feedbacks. I share this moment with my dad whom I miss tremendously.

Zusammenfassung

Diese Dissertation beschäftigt sich mit zwei Themen: Zum einen untersucht sie die veränderte Synchronisation neuronaler Netzwerke als einen möglichen Pathomechanismus in der Schizophrenie mittels funktioneller (Elektroenzephalographie, EEG) und struktureller (Diffusion Tensor Imaging, DTI) Methoden (1.-3. Veröffentlichung). Zum anderen schlägt sie ein neues Messverfahren zur Optimierung EEG informierter fMRI (funktionelle Magnetresonanztomographie) Analysen vor (4. Veröffentlichung).

Die ersten drei Studien lokalisieren *(i)* das frühe akustisch evozierte Gamma-Band um dann *(ii)* sowohl Langstrecken- Synchronisationen als auch *(iii)* Veränderungen in der weißen Substanz des Hörtrakts mit auditiven verbalen Halluzinationen in der Schizophrenie zu verknüpfen. Die Ergebnisse der ersten Studie weisen auf eine gestörte gamma- modulierte Wechselwirkung zwischen dem anterioren cingulären Kortex und dem Hörkortex bei schizophrenen Patienten hin. Die Ergebnisse der zweiten und dritten Studie ergänzen sich und legen zusammengenommen nahe, dass eine gesteigerte Neigung zu Halluzinationen bei schizophrenen Patienten sowohl mit einer verstärkten Phasensynchronisierung hochfrequenter Oszillationen im Hörkortex, als auch mit einem erhöhten Volumen der akustischen interhemisphärischen Fasern einhergehen.

Die vierte Studie befasst sich mit einem kritischen Schwachpunkt in der simultanen EEG- fMRI-Datenauswertung. In vivo EEG- fMRI- Daten liefern nicht- invasiv ein besseres Verständnis der zeitlich- räumlichen Dynamik neuronaler Netzwerke. Derartig aufgezeichnete EEG-Signale sind allerdings besonders stark von pulssynchronen, oder auch ballistocardiographischen (BCG) Artefakten beeinträchtigt. Die Studie beschreibt eine Methode, die den Einfluss dieser Artefakte in ERP-Studien schon während der Aufnahme verringert. Durch eine Echtzeit-Erkennung des Pulses wird das evozierte Potential in ein artefaktfreies Zeitintervall gesetzt. In der vorliegenden Studie kann das Signal-Rausch-Verhältnis des EEG hierdurch deutlich verbessert werden. Dies dürfte insbesondere bei komplexeren Auswertungsansätzen, wie zum Beispiel der EEG-Informierter fMRI Analyse, ausschlaggebend sein.

Abstract

This thesis focuses on two issues: Firstly, altered synchronization of neural networks as a potential pathophysiological mechanism in schizophrenia is examined using complementary functional (electroencephalography, EEG) and structural (Diffusion Tensor Imaging, DTI) human brain mapping approaches (1st- 3rd publication). Secondly, a new method to improve simultaneous EEG-fMRI (functional magnetic resonance imaging) measurements is proposed (4th publication).

The first three studies *(i)* localize the early auditory evoked gamma band response (GBR) and then link *(ii)* long-range synchronization and *(iii)* its changes in white matter volume and organization in the auditory tract to auditory verbal hallucinations (AVH) in schizophrenia patients (SZ). The results of the first study point to a disturbed gamma- modulated interaction between the ACC and the auditory cortex in schizophrenia patients. The findings in study two and three complement each other. Taken together, they suggest that a greater propensity for hallucinations in schizophrenia is associated with both increased phase locking of high-frequency oscillations in the auditory cortex and an increased volume of the auditory interhemispheric pathway fibers.

The fourth study focuses on an ongoing matter of concern regarding electroencephalography (EEG) and functional magnetic resonance imaging (fMRI) integration. *In vivo* simultaneous acquisition of EEG–fMRI data non- invasively offers a deeper understanding of the tempo-spatial dynamics of human brain activity. EEG signals recorded in MR-environment, however, remain particularly strongly affected heavily contaminated by pulse related, or ballistocardiogram (BCG) artifacts. This study suggests a measurement method which avoids these artifacts in ERP-studies already during data acquisition. Through real-time pulse detection the stimulus can be presented with respect to the BCG artifact and consequently the evoked potential is set in an artifact-free time interval. In the present study the signal-to-noise-ratio of the EEG can be improved significantly. This might prove to be a decisive factor, particularly in more complex analyses approaches, such as the EEG-informed fMRI analysis.

Table of contents

Chapter 1

Introduction

Comprehending a system as complex as the human brain requires joint anatomical and physiological observations. Approaches based on multimodal human brain mapping seek to combine both types of observation. As in a cubist piece of art brain activations are broken up, analyzed and re-assembled in an abstract form, thus providing a multitude of viewpoints rather than just one. In the long term this more complex account of human brain functions might optimize diagnostics and enable us to monitor therapies, thus providing not only clinically essential information but also new insights into the basic mechanisms of brain function and malfunction.

The present work focuses on two major problems: The *first* part investigates the pathophysiological role of inhibitory γ (gamma) aminobutyric acid (GABA)-ergic, parvalbumin- positive interneurons within the dysfunction of neural microcircuits and their relation with positive symptoms in schizophrenia using complementary functional (Chapter 2.1 and 2.2) and structural (Chapter 2.3) human brain mapping approaches. The *second* part focuses on an ongoing matter of concern regarding electroencephalography (EEG) and functional magnetic resonance imaging (fMRI) integration. *In vivo* simultaneous acquisition of EEG–fMRI data non-invasively offers a deeper understanding of the tempo-spatial dynamics of human brain activity. However, recorded EEG signals remain especially heavily contaminated by pulse related artifacts. Chapter 2.4 therefore suggests a measurement method which avoids these artifacts during data acquisition.

The aims of this thesis were both to profit from and ameliorate different multimodal human brain mapping approaches, namely EEG, fMRI, DTI and combined EEG-fMRI. As in any method used it is important to define the limitations of a technique in order to understand its potential capabilities. Chapter 1 will therefore give a brief introduction to the methods used subsequently. Chapter 2 represents the main component of the thesis and consists of published manuscripts whose specific objectives will be briefly discussed beforehand. Chapter 3 finally gives a summary of the present work and suggests lines of future research.

1.1 EEG

Electroencephalography (EEG) is a key tool in the non-invasive and direct study of neural activity in high temporal resolution (Berger, 1929; Caton, 1875; Nunez et al., 1994). Synchronous gamma oscillations characterize neuronal network function in various brain regions (Bartos et al., 2007; Fries et al., 2007; Uhlhaas et al., 2009). Conversely, fundamental synchrony changes seem to underlie cognitive dysfunctions, such as can those in schizophrenia (Lewis et al., 2005; Spencer et al., 2003). So, what exactly can EEG tell us (cp. Chapter 1.1.1)? What is the gamma band for (cp. Chapter 1.1.2)? And what exactly is not "in sync" in schizophrenia (cp. Chapter 1.1.3)?

1.1.1 What can EEG tell us?

The EEG signal reflects changes in extra-cranial electric field potentials generated by synchronized synaptic source activity in cortical pyramid neurons (Nunez and Sirinivasan, 2005), thus providing a direct measure of spontaneous or stimulus-evoked underlying neuronal activity on a millisecond time-scale (Speckmann and Elger, 1999). Ongoing EEG activity originates from summated postsynaptic potentials (PSP) in the dendrites of pyramid neurons and becomes measurable on the scalp when larger patches of cortical tissue are synchronously active (Davidson et al., 2000). Note that EEG is not a direct product of action potentials (AP), since multi-directional axon geometry as well as the brief duration of the signal (Nunez and Silberstein, 2000) mean that a very strong degree of phase-locking precision would be required in order to provide a summation of signals. Moreover PSPs, being graded potentials characterized by either a hyperpolarization (inhibitory postsynaptic potential; IPSP) or a depolarization (excitatory postsynaptic potentials; EPSP) of the cell membrane, may eventually lead to an AP. However, there are some methodical constraints, which need to be considered: *Firstly* the conducting layers of tissue and bone lead to a distorted spatial distribution of EEG signals, which prevents the discrimination between distinct but spatially closed neural sources (Baumgartner, 2004). In consequence the amplitude of EEG potentials is much smaller than that in a single neuron (Kandel et al., 2000), requiring large clusters of neighboring neurons with simultaneous activity to generate a detectable EEG signal (Nunez and Silberstein, 2000). Note that most synaptic fields are never recorded on the scalp (Cooper et al., 1965; Penfield, 1954). *Secondly* owing to the proximity to recording electrodes, the morphology of cortical pyramidal cells and the high density of cortico- cortical synapses, tissue volumes which are both normal and close to the scalp surface are more likely to contribute to extra-cranial electric fields (Ritter and Villringer, 2006). And *finally*, the greatest constraint is the fact that it is impossible to identify a sole localization for underlying EEG signals. This is called the "inverse problem" (Helmholtz, 1853). It means that spatial localization of generators provide only inexact solutions and requires an assumption regarding the number and initial location of intracranial generators (Marin et al., 1998; Srinivasan et al., 1996; Yan et al., 1991). Nonetheless grasping how the brain processes information requires consideration of real temporal dynamics of neural activity (Engel et al., 2001). EEG can provide that.

1.1.2 What is the gamma band for?

The brain constitutes a complicated structural network (Bullmore and Sporns, 2009; Rodriguez et al., 1999; Traub et al., 1996) whose neural elements operate in parallel, exchange their results via reciprocal re-entrant connections and through self-organizing dynamics create coherent states (Silva et al., 1991; Singer, 1999; Uhlhaas et al., 2009). The connectivity topology resembles small world networks (Strogatz, 2001), which means that there are certain areas which sustain more connections than others (hubs) but there is no singular supraordinate coordinating center where all information converges (Uhlhaas et al., 2009). In particular, synchronous neural oscillations in the 30–80 Hz range (centered near 40 Hz and referred to as the "gamma band") are believed to be a fundamental mechanism by which the brain dynamically "binds" spatially distributed sets of neurons to form coherent functional assemblies (Bartos et al., 2007; Bressler, 1995; Friston, 2002). Synchronous gamma oscillations have been documented in various brain regions, including the visual (Fries et al., 2001; Womelsdorf et al., 2006), the auditory (Brosch et al., 2002; Edwards et al., 2005), the somatosensory (Bauer et al., 2006), the motor (Brown et al., 1998; Murthy and Fetz, 1992; Schoffelen et al., 2005), the parietal cortex (Pesaran et al., 2002) and the hippocampus (Bragin et al., 1995; Csicsvari et al., 2003). They can also be found in a variety of species, from insects (Stopfer et al., 1997) to mammals (Engel et al., 1991; Gray et al., 1989; Kreiter and Singer, 1996) including humans (Canolty et al., 2006; Schoffelen et al., 2005; Tallon-Baudry et al., 1996) and during conditions ranging from attention (Doesburg et al., 2008; Fan et al., 2007; Lakatos et al., 2008), memory (Herrmann et al., 2004; Wu et al., 2008) and sensory integration (Lakatos et al., 2007) and beyond (Stopfer et al., 1997). The likely mechanism is that coincident EPSPs summate more effectively in target structures than temporally dispersed EPSPs (Usrey and Reid, 1999; Wespatat et al., 2004). Complex brains have developed inhibitory interneuron "clocking" networks for the grouping of principal cells into temporal coalitions (Buzsaki and Chrobak, 1995; Buzsaki et al., 2004). Interestingly, fast-spiking basket types of GABA-(γ (gamma) butyric acid)- ergic interneurons −expressing Ca2+-binding protein parvalbumin− play a key role in emerging gamma frequency oscillations by synchronization of pyramidal cells firing via negative feedback inhibition (Fuchs et al., 2001; Gray and McCormick, 1996; Whittington et al., 1995). A simplified way to describe mechanisms underlying the generation of gamma oscillations and synchrony is that after excitatory input, the network of inhibitory interneurons imposes rhythmic inhibition onto the entire local network. Pyramidal cells will only be able to fire during the time window of fading inhibition. Importantly, then interneurons will in their turn discharge with some phase delay relative to the pyramidal cells. The resulting network inhibition terminates the firing and the next gamma cycle starts anew (Fisahn et al., 1998; Fries et al., 2007; Mann et al., 2005). Thus, together they exhibit a characteristic phase relation, which in its turn leads to synchronization of spiking activity and is thought to result in the integrated and seamless experience of normal cognitive functioning (Joliot et al., 1994; Rodriguez et al., 1999; Singer, 1993; Traub et al., 1996). In schizophrenia this mechanism of synchronization supposedly does not work (cp. Chapter 1.1.3).

1.1.3 What exactly is not “in sync” in schizophrenia?

Schizophrenia patients exhibit deficits in many domains ranging from abnormalities in basic sensory registration and processing (Adler et al., 1982; McCarley et al., 1993; Shelley et al., 1991) to impairments in higher cognitive operations such as sustained attention, processing speed, memory and executive functioning (Gallinat et al., 2004; Heaton et al., 2001; Perry et al., 2000)-all domains in which gamma band oscillations can be observed (Light et al., 2006; Uhlhaas and Singer, 2010). It is therefore becoming increasingly clear that the heterogeneous symptoms in schizophrenia cannot be accounted for by a sole cortical region but relate to a distributed impairment in the fluid coordination of neural activity involving many cortical areas and their connectivity (Phillips and Silverstein, 2003; Spencer et al., 2004; Uhlhaas et al., 2009). This is also called dysconnectivity syndrome (Catani and ffytche, 2005; Friston, 1999). The changes in precisely synchronized high-frequency oscillations in schizophrenia are consistent with impairments in neurotransmitter systems (Benes and Berretta, 2001; Coyle, 2004; Lisman et al., 2008; Tsai et al., 1995) and anatomical abnormalities of GABA-ergic interneurons (Benes, 2000; Fuchs et al., 2001; Hajos et al., 2004; Lewis et al., 2005; Vreugdenhil et al., 2003), which act as a pacemaker in the generation of gamma band oscillations in cortical networks (Fuchs et al., 2007; McBain and Fisahn, 2001; Whittington and Traub, 2003). The study of gamma band oscillatory responses in the scalp-recorded EEG may therefore provide the means to investigate the functional integrity of neural circuits on a macroscopic level (Jefferys et al., 1996; Laughlin and Sejnowski, 2003; Lee et al., 2003; Spencer et al., 2003; Uhlhaas et al., 2008).

In this thesis gamma band oscillations in schizophrenia are investigated via EEG *firstly* “cognitively induced” when performing a higher order cognitive task without tight time locking to stimuli across trials (cp. Chapter 2.1) and *secondly* automatically generated in response to direct, repetitive stimulation, with precise phase locking of EEG responses to the stimuli in time (cp. Chapter 2.2). Low-resolution tomography (LORETA) (Pascual-Marqui, 2002; Pascual-Marqui et al., 1999; Pascual-Marqui et al., 1994) is a linear source localization method, that can be used to estimate oscillatory activity (Babiloni et al., 2010; Mulert et al., 2001; Mulert et al., 2004; Mulert et al., 2007; van der Loo et al., 2009) as well as interhemispheric phase synchrony. The approach offers the considerable advantage of combining source localization and the assessment of lagged phase synchrony thus minimizing possible misinterpretations due to volume conduction. Another interesting question is whether phase locking in the gamma-band range is related to positive symptoms of schizophrenia (cp. Chapter 2.2), such as hallucinations (Krishnan et al., 2009; Spencer et al., 2009) and if this is the case, changes in the structural connectivity of auditory areas are involved (cp. Chapter 2.3). Diffusion tensor imaging (cp. Chapter 1.2.2) provides a unique opportunity to visualize and quantify the entire interhemispheric auditory fibre pathway (Kubicki et al., 2007; Lim et al., 1999; Rotarska-Jagiela et al., 2008).

1.2 MRI

Magnetic resonance imaging (MRI) allows whole brain coverage as well as good spatial resolution (Hillebrand et al., 2005; Lauritzen, 2005). MRI measures dipole transitions in the B0 magnetic field between different energy states depending upon the properties of the nearby tissue or the physiological state of the brain (Mansfield and Grannell, 1973). The radio frequency excitation pulses and magnetic field gradients can be applied according to a variety of different timing and amplitude parameters. Adjustments to these parameters allow us to distinguish various properties of the brain (Shibasaki, 2008), including structure (cp. DTI in Chapter 1.2.1), flow or neural activity (cp. fMRI in Chapter 1.2.2).

1.2.1 What can DTI tell us?

Diffusion tensor magnetic resonance imaging (DTI) non-invasively generates three-dimensional representations of the white matter fibre tracts (Basser et al., 2000; Conturo et al., 1999; Mori and van Zijl, 2002; Poupon et al., 2000), thus providing a unique insight into structural networks of the living human brain (Bullmore and Sporns, 2009; Johansen-Berg and Rushworth, 2009; Mesulam, 2005). Its technique makes use of directional movement or diffusion of water molecules (Beaulieu and Allen, 1994; Le Bihan et al., 2001; Mori and Zhang, 2006) being relatively more restricted perpendicular than parallel (anisotropic) to micro structural boundaries such as white matter fibers (Basser, 1995; Basser et al., 1994). The directional dependency of the diffusion signal is quantified by a tensor which is shaped like an ellipsoid and is fully characterized by its three orthogonal eigenvectors and their associated lengths (Johansen-Berg and Rushworth, 2009). On the one hand the diffusion tensor therefore gives information on the magnitude of diffusion anisotropy (Sundgren et al., 2004) reflecting the underlying volume and microstructural integrity of fiber tracts (Pierpaoli et al., 1996). On the other hand it allows fiber tracking algorithms to start from a distinct preselected “seed” region (Ciccarelli et al., 2008; Le Bihan, 2003) and then follow white matter pathways by inferring its continuity from adjacent voxels (Basser et al., 2000; Mori and van Zijl, 2002; Poupon et al., 2000), thus visualizing and investigating fibre pathways and brain connectivity between different regions of the brain (Behrens et al., 2003a). However DTI requires careful validation and clear definition of its limitations and scope (Johansen-Berg and Rushworth, 2009): *Firstly*, it is not possible to differentiate anterograde from retrograde connections, to detect the presence of synapses, or to determine whether a pathway is functional or not (Conturo et al., 1999). *Secondly*, owing to discrepancies between the axonal diameter and the imaging voxel size there is no particular parameter derived from diffusion imaging for each white matter component (Assaf and Pasternak, 2008; Jespersen et al., 2007), which means anatomical features of interest are confounded. *Thirdly*, while some pathways are easy to track (e.g., corpus callosum), others are challenging. Furthermore streamlining techniques can easily reconstruct major fiber bundles but cannot continue tracing as fibers approach grey matter or pass through regions of fiber crossing and anisotropy reduces (Tournier et al., 2004; Wedeen et al., 2008). However alternative approaches allow

tracking in the presence of uncertainty (Behrens et al., 2003b; Frank, 2002; Parker and Alexander, 2005) and can be extended to fit multiple fiber populations (Alexander, 2005; Behrens et al., 2007; Tuch, 2004; Tuch et al., 2003). Quintessentially, DTI allows a new insight onto the relationship between brain structure and function (Behrens et al., 2003a; Johansen-Berg et al., 2005; Passingham et al., 2002; Thomason and Thompson, 2011). In recent years the hypothesis of disconnection syndrome as a crucial contributor to psychiatric disorders, especially schizophrenia, has become increasingly popular (Catani and ffytche, 2005; Kanaan et al., 2005; Kubicki et al., 2007; Lim and Helpern, 2002; Magaro and Page, 1983). In Chapter 2.3 we contribute to this discussion by investigating the relationship between fractional anisotropy (FA) of fiber tracts connecting homotopic auditory areas and auditory hallucinations in ten first episode paranoid schizophrenia patients.

1.2.2 What can fMRI tell us?

Functional MRI (fMRI) detects neuronal activations non-invasively (Blamire et al., 1992; Ogawa et al., 1990). Importantly, its signal is approximately proportional to a measure of local, neural activity (Logothetis, 2003) whilst covering the whole brain on a millimetre scale, without requiring any assumption about the number and the location of active neuronal clusters (Heeger and Ress, 2002). The mechanism that describes the coupling of neuronal activity and metabolic demand is called neurovascular coupling and can be summarized by two assumptions (Malonek and Grinvald, 1996): *Firstly* the regional blood flow is coupled to the metabolic demand (Fox et al., 1988; Schwartz et al., 1979) and *secondly* the metabolic demand is mainly defined by synaptic activity (Shulman and Rothman, 1998; Sibson et al., 1998). Magnetic changes associated with the concomitant decrease in local deoxygenated hemoglobin (Bandettini et al., 1992; Frahm et al., 1994) form the physical basis for the fMRI blood oxygen level dependent (BOLD) signal. The proportion of deoxygenated and oxygenated hemoglobin −which determines the greyscale of the tissue in the end− depends on the change in cerebral oxygen extraction rate, cerebral blood flow and cerebral blood volume (Malonek et al., 1997; Vanzetta and Grinvald, 1999). Therefore, the BOLD contrast is an indirect and delayed metabolic correlate of neuronal processes (Lauritzen and Gold, 2003) requiring a model of the fMR response time-course (Friston et al., 1998) to describe the translation between function, neuronal activity and the fMRI signal to create functional brain maps. Moreover fMRI voxels are typically several millimetres in diameter. However, the vascular supply is not regulated on the scale of individual neurons which not only might vary between brain areas and subjects but also falsify the results (Ritter and Villringer, 2006). And finally fMRI measures do not assess with any relevant precision the chronometry of processing (Boynton et al., 1996; Friston et al., 1994) or the underlying multidimensional quality of neural activity (Engel et al., 2001). Nonetheless fMRI especially combined with EEG yields complimentary spatial and temporal information on brain functions. Chapter 1.3 addresses the issue of combined EEG-fMRI measurements.

1.3 EEG-fMRI

The integration of EEG and fMRI is motivated by the aim to characterize joint fluctuations of brain activity with high spatial and temporal resolution in the same environment, conditions of stimulation and subject state. But what is the relationship between fMRI signal and underlying neuronal activity? Currently, an ongoing matter of concern for EEG–fMRI integration is the quality of EEG recordings obtained inside the MRI scanner. In particular the correction of the ballistocardiogram (BCG) artifact remains as yet unsatisfactorily solved and limits the methodical coupling of EEG and fMRI information.

1.3.1 What can simultaneous EEG-fMRI tell us?

A number of studies have presented data suggesting a linear relationship between neural activity and the subsequent hemodynamic response (Arthurs and Boniface, 2003; Ngai et al., 1999; Ogawa et al., 2000). Simultaneous recordings of intracortical neural and fMRI signal showed the BOLD signal to be temporally correlated in particular with local field potential (LFP) as an index of postsynaptic membrane oscillations, which mostly reflect a weighted average of synchronized dendro-somatic components of the input signals of a neural population (Logothetis et al., 2001). Although the mechanism of neurovascular coupling is complex and not fully understood (Logothetis and Wandell, 2004), some advances have been made in terms of formulating the mathematical relations (Rees et al., 2000 a). There are three theoretical situations when EEG and fMRI signals may diverge: *(i) fMRI signal without EEG correlate:* Neural activity might be related to BOLD signal changes but not to scalp EEG changes if the location is too deep to be measured by EEG or if the spatial orientation of the electrical generators is unfavorable (Nunez and Silberstein, 2000). *(ii) EEG signal without fMRI correlate:* Highly synchronous activity of a small number of neurons might result in a detectable EEG signal change, but the associated hemodynamic changes might not be sufficiently above baseline values to survive statistical testing (Disbrow et al., 2000; Malonek and Grinvald, 1996). *(iii) Contradictory EEG and fMRI signals:* Scalp EEG amplitudes and hemodynamic activity can change in opposite directions because of different contributions of neuronal activity to each signal (Ahlfors and Simpson, 2004; Ureshi et al., 2005). Simultaneous EEG and fMRI recordings provide fundamental advantages over separate recording protocols (Dale and Halgren, 2001; Horwitz and Poeppel, 2002), not only guaranteeing identical environment and condition of sensory stimulation (Debener et al., 2006) *(j)*, same subject perception and behavior (Ullsperger and von Cramon, 2001) *(jj)*, but also providing joint high temporal and spatial resolution *(jjj)*, which could so far only be obtained in direct intracranial recordings (Baudena et al., 1995; Halgren et al., 1995a; Halgren et al., 1995b). Additionally once the occurring artifacts (cp. Chapter 1.3.2) have been corrected, simultaneous EEG-fMRI acquisition allows the investigator of brain state fluctuations to adopt more sophisticated approaches to data analysis (Calhoun et al., 2006; Dale et al., 2000; Daunizeau et al., 2007; Debener et al., 2006; Eichele et al., 2007; Kilner et al., 2005; Moosmann et al., 2007; Mulert et al., 2009; Mulert et al., 2008; Sotero and Trujillo-Barreto, 2008).

1.3.2 What limits EEG quality?

Simultaneous EEG-fMRI measurements entail artifacts that are consequential to reciprocal interferences between the two recording systems (George et al., 2001; Goldman et al., 2000). After proving the feasibility (Herrmann and Debener, 2007; Huang-Hellinger et al., 1995; Ives et al., 1993; Laufs et al., 2008) and refining the techniques (Lemieux et al., 2001; Salek-Haddadi et al., 2002) for simultaneous EEG-fMRI data acquisition, core concerns were (i) patient safety during measurement, (ii) MR signal distortions due to the EEG set-up and most importantly (iii) MR-related artifacts in the EEG signal. Whilst patients safety during measurement (Lemieux et al., 1997) and distortions of the MR signal caused by the EEG setup (Bonmassar et al., 2001; Krakow et al., 2000) can be considered as solved, an ongoing matter of concern is the quality of the EEG signal obtained inside the MRI scanner. Even with an optimized EEG- fMRI setup, EEG-fMRI analyses are heavily compromised by the limited quality of the recorded EEG data (Goldman et al., 2000; Kruggel et al., 2000), which typically suffer from two major artifacts (Laufs et al., 2008; Ritter and Villringer, 2006). *Firstly*, the gradient artifact reflects the switching of magnetic fields during MRI image acquisition (Allen et al., 2000; Anami et al., 2003). Owing to its technical origin the gradient artifact can be reliably corrected by averaged artifact template subtraction without limiting further EEG-fMRI analyses (Ritter et al., 2007). *Secondly,* the ballistocardiogram (BCG) artifact poses a bigger methodological challenge and remains a core limitation for more sophisticated EEG-fMRI integration methods (Yan et al., 2009). The BCG is thought to be predominantly caused by three major sources related to cardiac activity (Huang-Hellinger et al., 1995): *(j)* small movement of the electrodes due to expansion and contraction of scalp arteries between systolic and diastolic phase (Nakamura et al., 2006), *(jj)* small cardiac related movements of the body caused by change of blood flow in large body vessels (Sijbers et al., 2000)– and presumably to a lesser extent *(jjj)* fluctuation of the Hall-voltage due to the pulsatile speed changes of the arterial blood flow (Tenforde et al., 1983). But what makes the BCG artifact correction so difficult? *Firstly,* a major problem is its variability. The BCG artifact occurs about 150–500ms relative to the QRS complex onset (Debener et al., 2008) with its morphology, amplitude and peak latency being different between channels and subjects (Allen et al., 1998). BCG artifact correction methods, therefore, have to adjust to both inter- and intrapersonal particularities. *Secondly*, the BCG artifact contributes to the ERP frequency range (0.5–25 Hz) (Srivastava et al., 2005). This property makes the correction of BCG artifacts both difficult and crucial considering that EEG informed fMRI analysis requires single-trial information of event-related amplitude modulations without the possibility of increasing the signal-to-noise ratio by averaging prior to analysis. *Thirdly*, the amplitude of BCG artifacts is directly proportional to the strength of the magnetic field and, as a consequence, both the absolute magnitude and the spatial variability of the BCG are increased (Debener et al., 2008). Finding a reliable BCG artifact correction method becomes even more important when one considers the increasing use of high field MR-scanners.

1.3.3 What corrects BCG artifacts?

Several methods have been proposed to reduce BCG artifacts offline. Roughly, these methods can be subdivided into two main categories (Vanderperren et al., 2010). The *first* category takes advantage of the repetitive pattern of the BCG artifact, makes an assumption about the shape of the source signals and uses template matching. Its various methods merely differ in the way the template is generated (Debener et al., 2007). A cutting-edge proposal uses a dynamic averaged artifact template, which is then channel-wise subtracted from the original signal (Allen et al., 1998) without considering its intrapersonal variance. Subsequent methods tackle this issue by first normalizing the template through Gaussian weighted averaging (Goldman et al., 2000) and mean- (Sijbers et al., 2000) or median-filtering (Ellingson et al., 2004). The *second* category identifies brain- and artifact related sources from a set of signals, makes *no* assumption about the shape of the source signals, does *not* require the use of a reference signal and is based on blind source separation (BSS). Its various methods use several ways to perform this separation. Most notable is the independent component analysis (ICA) (Benar et al., 2003; Briselli et al., 2006; Mantini et al., 2007; Nakamura et al., 2006; Srivastava et al., 2005), which uses a linear mixing of independent source signals (Comon, 1994). Also quite popular is the principal component analysis (PCA), which uses singular value decomposition (Niazy et al., 2005; Siniatchkin et al., 2007). More recent approaches make use of non-kirchhoffian overcomplete representation (Dyrholm et al., 2009), canonical correlation analysis (Assecondi et al., 2010) or suggest semi- automatic ICA techniques to simplify the identification of BCG artifact related components (Gao et al., 2010; Ghaderi et al., 2010; Leclercq et al., 2009; Viola et al., 2009). Wanting to take advantage of both categories some authors suggest waveform pattern removal approaches prior to spatial pattern removal approaches (Debener et al., 2005). In summary all these algorithms affect the data differently, whilst having their own advantages and drawbacks (Grouiller et al., 2007). Needless to say there is little consensus on which method ensures the best data quality, but experts agree that the *offline* artifact correction remains unsatisfactorily solved (Vanderperren et al., 2010).

Clearly, continuous EEG-fMRI acquisition with fewer or no BCG artifacts would be preferable in the first place. So far only two published methods propose to correct the BCG artifacts in real-time (Bonmassar et al., 2002; Masterton et al., 2007) and no published method simply tries to *avoid* the BCG artifact *online* and *in real-time.* In Chapter 2.4 we propose a novel and simple method to avoid the effects of the BCG artifacts in event-related EEGs when collected simultaneously with fMRI. A time-locked pulse-triggered (PT) stimulus presentation exploits the observation that the main influence of the BCG artifact is largely limited to a fixed interval (Allen et al., 1998; Debener et al., 2008).

Chapter 2

Original articles

- **Leicht G, Kirsch V, Giegling I, Karch S, Hantschk I, Möller HJ, Pogarell O, Hegerl U, Rujescu D, Mulert C. Reduced early auditory evoked gamma-band response in patients with schizophrenia. Biological Psychiatry. 2010 Feb 1;67(3):224-31.**

- **Mulert C, Kirsch V, Pascual-Marqui R, McCarley RW. Spencer KM. Long-range synchrony of gamma oscillations and auditory hallucination symptoms in schizophrenia. International Journal of Psychophysiology. 2011 Jan;79(1):55-63.**

- **Mulert C, Kirsch V, Whitford TJ, Alvarado J, Pelavin P, McCarley RW, Kubicki M, Salisbury D, Shenton ME. Hearing voices: A role of interhemispheric aufitory connectivity? World Journal of Biological Psychiatry. 2011 May 30. [Epub ahead of print]**

- **Ertl M[*], Kirsch V[*1], Leicht G, Karch S, Olbrich S, Reiser M, Hegerl U, Pogarell O, Mulert C. Avoiding the ballistocardiogram (BCG) artifact of EEG data acquired simultaneously with fMRI by pulse-triggered presentation of stimuli. Journal of Neuroscience Methods. 2010 Feb 15;186(2):231-41**

[1] These authors contributed equally to this work. Ms. Kirsch and Mr. Ertl were equally responsible for the study design. Mr. Ertl simulated the experiment using Matlab. Ms. Kirsch and Mr. Ertl were then equally involved in the acquisition and analysis of the data and the evaluation of the results. Ms. Kirsch did the statistics, translated the results in tabular form and wrote the article.

Diese Autoren haben beide gleichermaßen zu dieser Arbeit beigetragen. Frau Kirsch und Herr Ertl überlegten sich gemeinsam das Studiendesign. Herr Ertl simulierte die Studie mittels Matlab. Frau Kirsch und Herr Ertl waren gleichermaßen an der Akquisition und Auswertung der Daten beteiligt. Frau Kirsch wertete die Daten statistisch aus, erstelle die Abbildungen und Tabellen und schrieb den Fachartikel.

2.1 Reduced early Auditory Evoked Gamma-Band Response in Patients with Schizophrenia

Synchronous neural oscillations in the 30–80 Hz range (referred to as the “gamma band”) are believed to be a fundamental mechanism by which the brain dynamically “binds” spatially distributed sets of neurons to form coherent functional assemblies (Bartos et al., 2007; Singer, 1999). It is becoming increasingly clear that the heterogeneous symptoms in schizophrenia relate to a distributed impairment in the fluid coordination of neural activity involving many cortical areas and their connectivity (Friston, 1999; Phillips and Silverstein, 2003). Here we investigate the early auditory evoked gamma (γ)-band response (GBR) (Tiitinen et al., 1993) and its sources in a large sample of schizophrenic patients and their age-, gender-, and education-matched healthy controls. The early evoked GBR is typically related to auditory stimuli, found between 25 and 100 ms poststimulus (Ahveninen et al., 2000; Pantev et al., 1991) and might be involved in attentional top-down control (Debener et al., 2003; Engel et al., 2001). Whereas it has been shown in many cases that auditory processing seems to be disturbed in schizophrenia (Spencer et al., 2004; Spencer et al., 2008), there is no direct evidence providing a reduced early auditory evoked GBR so far. Patients with schizophrenia show a significant reduction of power and phase-locking of the early auditory evoked GBR due to a reduced activity in the auditory cortex and the anterior cingulate cortex/ medial frontal gyrus region through low-resolution brain electromagnetic tomography analysis (LORETA). Our findings both are in line with the literature on early auditory GBR (Mulert et al., 2007) and underpin the assumed dysfunction of neural microcircuits in schizophrenia (Uhlhaas and Singer, 2010)− this time assessed by the early auditory GBR power.

Reduced Early Auditory Evoked Gamma-Band Response in Patients with Schizophrenia

Gregor Leicht, Valerie Kirsch, Ina Giegling, Susanne Karch, Irmgard Hantschk, Hans-Jürgen Möller, Oliver Pogarell, Ulrich Hegerl, Dan Rujescu, and Christoph Mulert

Background: There is growing evidence for abnormalities of certain γ-aminobutyric acid (GABA)-ergic interneurons and their interaction with glutamatergic pyramidal cells in schizophrenia. These interneurons are critically involved in generating neural activity in the γ-band (30–100 Hz) of the electroencephalogram. One example of such γ oscillations is the early auditory evoked γ-band response (GBR). Although auditory processing is obviously disturbed in schizophrenia, there is no direct evidence providing a reduced early auditory evoked GBR so far. We addressed two questions: 1) Is the early auditory evoked GBR decreased regarding power and phase-locking in schizophrenic patients?; and 2) Is this possible decrease a result of reduced activity in the auditory cortex and/or the anterior cingulate cortex (ACC), which were identified as sources of the GBR previously?

Methods: We investigated the early auditory evoked GBR and its sources in the ACC and the auditory cortex in 90 medicated patients with schizophrenia and in age-, gender-, and education-matched healthy control subjects with an auditory reaction task.

Results: Patients with schizophrenia showed a significant reduction of power and phase-locking of the early auditory evoked GBR. This effect was due to a reduced activity in the auditory cortex and the ACC/medial frontal gyrus region (low-resolution brain electromagnetic tomography analysis).

Conclusions: Generally, these findings are in line with earlier reports on the impaired ability of schizophrenic patients in generating γ activity. In addition, this is the first study to demonstrate disturbance of γ activity in auditory processing as assessed by the early auditory GBR power.

Key Words: ACC, auditory cortex, EEG, gamma, LORETA, schizophrenia, γ

Recent hypotheses on the pathophysiology of schizophrenia propose a dysfunction of neural microcircuits and a key pathophysiological role of inhibitory γ-aminobutyric acid (GABA)-ergic, parvalbumin-positive interneurons (e.g., 1–3). In this context, a circuit-based framework of neuronal and glutamatergic, GABAergic, dopaminergic, and cholinergic function in schizophrenia was developed (4). Postmortem studies showed abnormalities of such interneurons in schizophrenia (5,6). Interestingly, the GABAergic interneurons and their interaction with glutamatergic pyramidal cells are critically involved in the generation of synchronous neural activity in the γ-band of the electroencephalogram (EEG) (7,8). Knocking out certain glutamate receptor subtypes on GABAergic interneurons reduced γ power in an in vitro study, suggesting that the reduced glutamatergic excitation of the interneurons led to a decreased GABAergic inhibition of glutamatergic pyramidal cells in terms of a disturbed feedback loop (9). This interaction between interneurons and pyramidal cells was reconstructed in computational network models (1,10).

Current pathophysiologic theories assume that the cognitive deficits appearing in schizophrenia are a correlate of the disturbed coordination of distributed processes involving multiple brain areas (11,12). Meanwhile, there are different findings that indicate macroscopic disturbances in anatomical and functional connectivity in patients with schizophrenia (13). Functional neuroimaging studies provided evidence for a disturbed fronto-temporal connectivity in schizophrenia (14,15). To investigate the real temporal dynamics of the deficits in the sensory information processing concerning synchronization and functional connectivity, EEG measurements especially of high-frequency oscillations might give new insights (16,17).

Synchronous high-frequency activity of the EEG in the γ-band range (30–100 Hz) was proposed to be involved in integrating parallel neuronal activity (18,19). Gamma-band oscillations were suspected to be a correlate of the binding of sensory and high-order cortical areas (20). Especially early sensory-evoked γ oscillations were investigated, because they seem to be involved in the integration of early sensory and, for example, attentional or motivational processes (21–25). One example for this is the "early" auditory evoked γ-band response (GBR) (26), which is usually found between 25 and 100 msec after stimulus presentation, in contrast to the "later" GBR occurring within the time frame of 220–350 msec (27). For the early evoked GBR, a close relationship with selective attention was described (26,28). Some authors reported that early evoked γ-activity might also contribute to midlatency potentials such as the auditory evoked P50 potential (29).

There are some findings concerning the neural generators of the early evoked GBR in attentional tasks. Apart from an obligatory generator of the early evoked GBR in the auditory cortex (30) because of thalamo-cortical interactions (31), an additional contribution of the frontal lobe—more precisely the ACC—was suggested (32). Recently, generators of the GBR in the auditory cortex and also in a midline region including the dorsal (cognitive) anterior cingulate cortex (dACC) and the medial frontal gyrus were suggested with source estimation with the low-resolution brain electromagnetic tomography (LORETA) approach (21) and proved by single trial coupling of the GBR-

From the Department of Psychiatry and Psychotherapy (GL, VK, IG, SK, IH, H-JM, OP, UH, DR, CM), Ludwig-Maximilians-University, Munich; and the Department of Psychiatry and Psychotherapy (UH), University of Leipzig, Leipzig, Germany.

Address correspondence to Gregor Leicht, M.D., Department of Psychiatry, LMU Munich, Nußbaumstraße 7D-80336 München, Germany; E-mail: gregor.leicht@med.uni-muenchen.de.

Received Jan 24, 2009; revised Jul 15, 2009; accepted Jul 19, 2009.

0006-3223/10/$36.00
doi:10.1016/j.biopsych.2009.07.033

amplitude and the corresponding blood oxygen level dependent (BOLD) signal (C. Mulert, M.D., unpublished data, 2009).

With an auditory oddball paradigm, Symond *et al.* (33) showed altered γ synchrony in first-episode schizophrenia, and Roach and Mathalon (34) found a deficit in the phase-locking factor (PLF) of the early evoked GBR in schizophrenic patients. The PLF reflects the variance of phase across single trials and ranges from 0 (random distribution) to 1 (perfect phase-locking). It is correlated with evoked power. Nevertheless, reductions of the evoked power of the GBR (minimized influence of non–stimulus-locked activity) in schizophrenia have only been reported later in the epoch after a stimulus (220–350 msec) (27) and not during the first 100 msec after stimulus presentation, as investigated in the present work. So far, there are no reports regarding reduced power of this early auditory evoked GBR in patients with schizophrenia, although this question has been explicitly addressed before (27,35) and although findings about reduced γ PLF and alterations during auditory steady-state-stimulation in the γ frequency range (36–38) could indicate this.

We investigated power and PLF of the early GBR and its sources with an auditory reaction paradigm in 90 medicated patients with schizophrenia and in age-, gender- and education-matched healthy control subjects. With regard to the references to neural circuitry abnormalities in schizophrenia described in the preceding text, we aimed to answer the following questions: 1) Is the early auditory GBR decreased with regard to power and phase-locking in schizophrenic patients?; and 2) Is this decrease a result of a reduced activity in the auditory cortex and/or the ACC identified as sources of the GBR previously (21)?

Methods and Materials

Subjects

The study was approved by the local ethics committee of the Ludwig-Maximilians-University of Munich. After the procedure was fully explained to them, all subjects gave written informed consent.

Schizophrenic Patients. Ninety individuals with schizophrenia (60 men and 30 women) were ascertained from the Munich area in Germany. Case participants had DSM-IV and ICD-10 diagnoses of schizophrenia with these subtypes: paranoid 78.8%, disorganized 15.5%, catatonic 3.3%, and undifferentiated 2.2%. Detailed medical and psychiatric histories were collected, including a clinical interview with the Structured Clinical Interview for DSM-IV (SCID), to evaluate lifetime Axis I and II diagnoses (39,40). Four physicians and one psychologist rated the SCID interviews and all measurements were double-rated by a senior researcher. Exclusion criteria included a history of head injury or neurological diseases.

All case participants were outpatients. Their mean age was 40.2 (SD 10.2, range 19–70) years; 28% of them had a low (secondary school), 28% a middle (junior high school), and 34% a high (general qualification for university entrance) educational level. Age at onset was 26.2 (SD 8.6, range 10–55) years. Most patients were taking antipsychotic medications at the time of EEG recording (81% atypical antipsychotics, 3% typical antipsychotics, 8% both atypical and typical antipsychotics, 7% no psychotropic medication, and 28% antipsychotics in combination with antidepressants).

Healthy Volunteers. Unrelated volunteers were randomly selected from the general population of Munich, Germany, and contacted by mail. To exclude subjects with central neurological diseases and psychotic disorders or subjects who had first-degree relatives with psychotic disorders, several screenings were conducted before volunteers were enrolled in the study: an assessment of detailed medical and neuropsychiatric histories for both themselves and their first-degree relatives, a comprehensive interview including the SCID I and SCID II to validate the absence of any lifetime psychotic disorder, the Family History Assessment Module (41) to exclude psychotic disorders among their first-degree relatives, a neurological examination to exclude subjects with current central nervous system impairment, and—in case the volunteers were older than 60 years—the Mini Mental Status Test (42) to exclude subjects with cognitive impairment (for more details see [43]).

The group of the 90 control subjects was matched with the patients group concerning age (mean age: 40.1 [SD 12.1, range 22–69] years; no significant group difference), gender (60 men and 30 women in each group), and educational level (same ratio as in the patients group). There was no significant difference concerning the handedness between groups [$\chi^2(2) = .69$, $p = .71$].

Paradigm

The experimental task was an auditory reaction paradigm as used previously (44,45). Sixty tones (duration: 250 msec, generated by using the BrainStim software package; Brain Products, Munich, Germany) of different pitches (50%: 800 Hz and 50%: 1300 Hz) were presented via earphones at 85 dB sound pressure level with pseudo-randomized sequence and interstimulus intervals (ISI; 2.5–7.5 sec). In the experimental run, the subjects had to press one of two buttons with the left or right hand, assigned in advance, to high and low tones, respectively. The run took 5 min. All subjects had hearing better than 30 dB at a pitch of 1000 Hz. Before the beginning of the measurement, a short test run was carried out. During the experimental run reaction times (from the onset of the stimulus to the button press) and errors were registered. Error responses were defined as not pressing any button within 1500 msec or pressing the wrong button in this period.

EEG Recording and Preprocessing

Recording took place in a sound-attenuated and electrically shielded room. Subjects were seated with open eyes in a slightly reclined chair with a head rest and were asked to look at the wall 2 m in front of them. The EEG was recorded with 27 electrodes referred to Cz (recording apparatus; Neuroscan Synamps, Munich, Germany) with an electrode cap. Electrodes were positioned according to the International 10/20 system with the additional electrodes FC1, FC2, FC5, FC6, CP5, CP6, PO9, and PO10. The FPz served as ground. Data were collected with a sampling rate of 1000 Hz and an analogous bandpass filter (.16–200 Hz). The EEG preprocessing was done with the BrainVision Analyzer (BVA) software Vers.1.05 (Brain Products). Two-hundred-millisecond pre-stimulus and 450-msec post-stimulus periods were evaluated for all sweeps. After re-referencing to common average reference, an amplitude criterion was used (± 70 μV) for artifact rejection, involving all channels at any time point during the averaging period. Moreover, a baseline correction with the period from 200 msec before stimulus to 50 msec before stimulus was performed. Each subject's first 30 correct trials were used for further analyses. Amplitude and latency values were detected automatically with the BVA software. The results were rechecked by visual inspection (no errors).

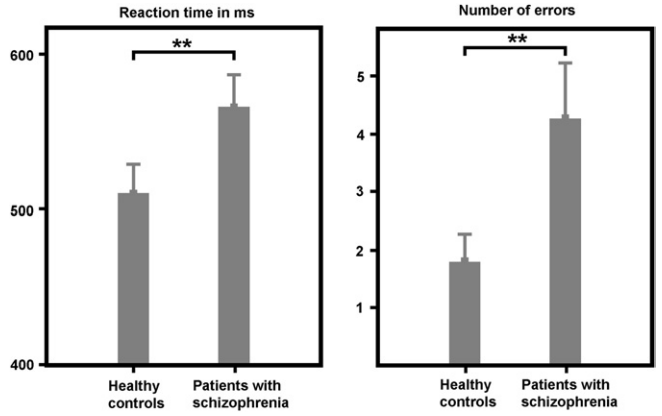

Figure 1. Task performance (means and SDs): patients with schizophrenia ($n = 90$) showed significantly elongated reaction times and a significantly higher number of errors compared with control subjects ($n = 90$). $^{**}p < .01$.

N1-, P2-, and P50-Component of the Auditory Evoked Potential

On the basis of prior knowledge (44), the N1-peak was defined as the most negative value within the time frame 70–150 msec after stimulus, and the P2-peak was defined as the most positive value within the time frame 130–220 msec after stimulus at Cz. For analysis of the P50-component, 50-Hz low-pass and 20-Hz high-pass filters (48 dB) were additionally applied before averaging. The P50-peak was defined as the most positive value within the time frame 30–70 msec after stimulus at Cz.

Evoked Gamma Activity and PLF

With the BVA software, evoked γ activity and PLF were described with a wavelet transformation [complex Morlet wavelet with the formula $w(t) = Aexp(-t^2/2)exp(i2\pi ct)$, Morlet parameter c = 5, Unit Energy Normalization], as used by other groups (25,46) and ourselves (21) before. Before using the wavelet transform, an additional 100-Hz low-pass filter was applied.

To reveal the phase-locked evoked fraction of the γ-activity, the wavelet transformation was performed on averaged event-related potentials. At first, the frequency range from 0 to 120 Hz was divided into 40 frequency steps (distributed on a logarithmic scale) for each subject to get a general idea of the frequency distribution. Secondly, the wavelet analysis focused on 40 Hz (frequency range 32–48 Hz) was extracted separately. The GBR-peak was defined as the highest value within the time frame 20–80 msec after stimulus at the electrode Cz in this frequency range. The PLFs were calculated by performing the wavelet transformation and extracting the complex phase information with all vector lengths normalized to the unit circle ("Complex Data Measures" solution, BVA software) before averaging of the phase information. Gamma PLF peaks were defined as the highest value within the time frame 20–80 msec after stimulus at the electrode Cz for the analysis focused on 40 Hz.

LORETA

For LORETA analysis, EEG preprocessing was done as described in the preceding text additionally with 45-Hz low-pass and 35-Hz high-pass filters (48 dB) before averaging. The LORETA method (47) is described in detail in Supplement 1.

LORETA Region-of-Interest Analysis

According to our previous works (21,48), region-of-interest (ROI) analyses were performed for a midline region including the dACC and the supplementary motor area (dACC-ROI), the primary (Brodmann area [BA] 41-ROI) as well as secondary (BA 42-ROI) auditory cortex, and the auditory association cortex (BA 22-ROI), and a control ROI analysis was performed in the ventral ACC (vACC-ROI) for the early evoked GBR within the time frame 30–70 msec (20 msec around the peak at Cz in the grand average). For the exact extension of the ROIs in the Talairach space, see Supplement 1. The ROI-analysis was done with the "ROI-Extracter" tool provided by Marco Congedo as used previously (21), which averages the current source density values in the specified voxels.

Statistics

Statistical comparisons between patients and healthy control subjects were performed with the SPSS-software package (13.0) (SPSS, Chicago, Illinois). To test for significant group differences as well as group × ROI interactions, analysis of variance (ANOVA) was used. In case of not normally distributed values, Mann–Whitney *U* tests were performed. Correlations were tested with the Pearson correlation coefficient. For the comparison of the handedness, a χ^2 test was used. Effect size was calculated as Cohen's d with means and SDs.

Results

Task Performance

The mean reaction time differed significantly between control subjects (510 msec, SD 89) and patients with schizophrenia (566 msec, SD 99; $Z = 3.8$, $p < .001$, see Figure 1A). The mean number of errors was significantly higher in patients (4.3, SD 4.5) than in control subjects (1.8, SD 2.3; $Z = 4.9$, $p < .001$, Figure 1B).

N1-, P2-, and P50-Component of the Auditory Evoked Potential

The amplitude of the N1-component of the auditory evoked potential (AEP) was significantly reduced at Cz in patients with schizophrenia (6.7 μV, SD 3.0) compared with control subjects (8.7 μV, SD 3.6; $Z = 4.4$, $p < .001$, Figure 2), whereas there was no significant difference regarding the latency (patients: 106 msec, SD 15; control subjects: 105 msec, SD 15). Amplitudes and latencies of the P2-component showed no significant differences between groups. The amplitude of the P50-component of the

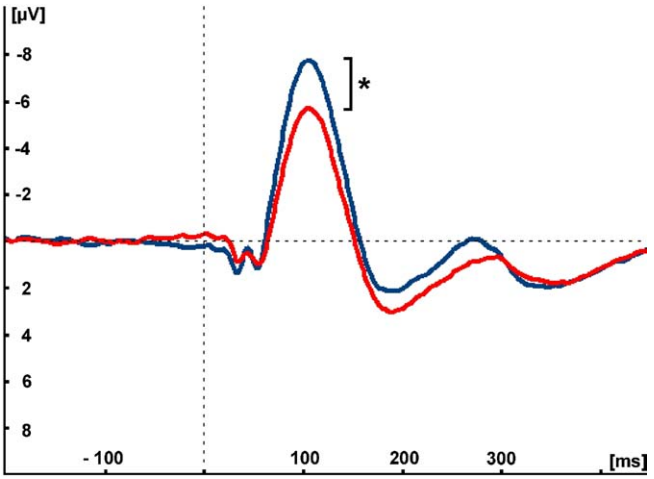

Figure 2. Auditory evoked potentials of patients with schizophrenia (red) and control subjects (blue). Patients showed significantly reduced N1-amplitudes ($^{*}p < .001$).

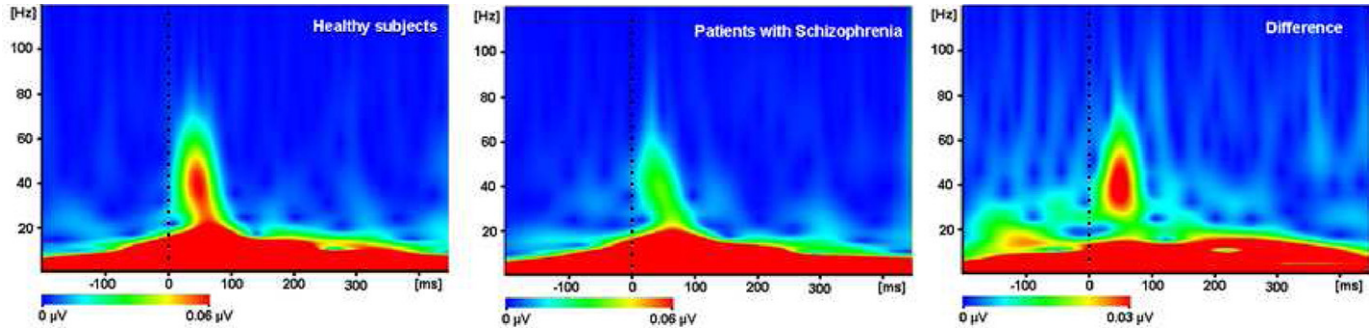

Figure 3. Time-frequency-analyses of the time frame 200 msec before the stimulus and 400 msec after stimulus averaged over all subjects of the control group (left), of the schizophrenic patients group (middle), and as a difference picture subtracting the result of the patients from the result of the control subjects (right). Scaling was uniform for both patients and control subjects. The early auditory evoked γ-band response can be seen as an increased activity at approximately 50 msec after stimulus presentation (dashed line) and in the frequency-range around 40 Hz.

AEP did not significantly differ between patients (.9 µV, SD .6) and control subjects (1.0 µV, SD .7). There was no significant difference regarding the latency of the P50-peak (patients: 52 msec, SD 11; control subjects: 53 msec, SD 11).

Evoked Gamma Activity and PLF

Generally, there was no increase of induced γ activity after stimulus onset in either of the groups. Approximately 50 msec after stimulus presentation in both groups, an increase of evoked γ activity was observed (Figure 3; for the scalp topography of the GBR see Figure 4B). This early evoked GBR was significantly reduced at Cz in patients with schizophrenia (.072 µV, SD .051) compared with control subjects (.090 µV, SD .061; $Z = 2.5$, $p = .013$, effect size = .32, Figure 4A). The PLF differed significantly between control subjects (.51, SD .18) and patients with schizophrenia (.44, SD .16; $Z = 2.9$, $p = .004$, see Figure 5). There was no significant difference between the groups concerning the latency of the GBR peak at Cz (control subjects: 52.8 msec, patients: 51.6 msec). In the patients group, no significant correlation was present between chlorpromazine equivalents and GBR. Moreover, neither GBR nor PLF were correlated with clinical symptom measures (Positive and Negative Syndrome Scale) or schizophrenia subtype.

LORETA Whole-Head-Analysis

For the control subjects maximum LORETA-activations of γ-activity within the time frame 30–70 msec were found in the left and right auditory cortex (including the transverse, the superior, and the middle temporal gyrus) and in a midline region including the ACC and the medial frontal gyrus, resembling our previous results (21). For the patients similar sources of the GBR within the time frame 30–70 msec were detected: maximum *t* values in the left auditory cortex and in the ACC/medial frontal gyrus region were found in nearly the same voxels as in the control group. In the right auditory cortex the voxel with the maximum *t* value was located more anterior (Table S1 in Supplement 1 and Figure 6).

LORETA ROI-Analysis

The ANOVA yielded a significant main effect of the factor ROI [$F(4,712) = 94.5$, $p < .001$] and a significant group × ROI interaction [$F(4,712) = 8.7$, $p < .001$]. Patients with schizophrenia, compared with control subjects, showed significantly lower current source density values in the dACC-ROI, the BA 22-ROI, the BA 41-ROI, and the BA 42-ROI but not in the vACC-ROI (see Table S2 in Supplement 1). We found a significant group × laterality effect [$F(1,178) = 5.9$, $p = .016$] regarding the auditory cortex ROIs, with larger group differences (lower values in patients) for the left compared with the right auditory cortex (not significant for the right BA 42-ROI; Table S3 in Supplement 1).

Discussion

This study investigated γ activity in a large sample of schizophrenic patients. To our best knowledge, this is the first report demonstrating a significant reduction of the power of the early auditory evoked GBR in schizophrenia. The findings of the GBR LORETA analysis point to a reduced activity in the auditory cortex and the dACC/medial frontal gyrus region in patients with schizophrenia underlying the reduced γ activity measured on the scalp. Our study is well in line with earlier investigations (30,49), with regard to the localization of the generators of the GBR in the

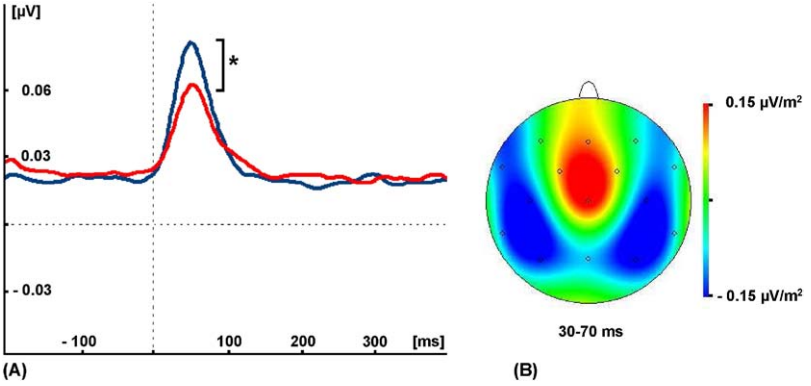

Figure 4. (A) The early auditory evoked γ-band response (GBR) is displayed as the result of the wavelet analysis (complex Morlet wavelet) focused on the γ activity around 40 Hz for patients with schizophrenia (red) and control subjects (blue). Patients showed a significantly reduced GBR (*$p < .013$). **(B)** Scalp topography of the early evoked GBR of the control group.

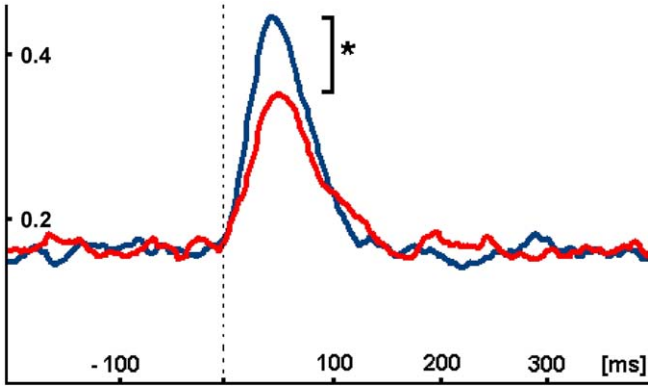

Figure 5. Phase-locking factor (PLF) analyses of the time frame 200 msec before the stimulus and 400 msec after stimulus averaged over all subjects for patients with schizophrenia (red) and control subjects (blue). The PLF values are displayed as the result of the wavelet analysis (complex Morlet wavelet) focused on the γ activity around 40 Hz. Patients showed a significantly reduced PLF (*$p < .004$).

auditory cortex. However, the additional midline (ACC and medial frontal gyrus) generator had also been suggested (32) and described before with EEG and combined measurement of EEG and functional magnetic resonance imaging (fMRI) (21 and C. Mulert, M.D., unpublished data, 2009). Patients with schizophrenia showed—echoing previous findings—slow reaction times and an increased number of errors performing the auditory reaction task (45,50).

In contrast to our present results, two recent studies had observed no abnormalities of the early auditory GBR evoked by simple tone stimuli of an oddball paradigm in schizophrenic patients (27,35). These diverging findings might be due to the smaller sample sizes of these studies or to the different, more difficult task used in the present study, considering that the early evoked GBR was shown to be related to task difficulty (21). Additionally, Spencer *et al.* (35) examined γ oscillations evoked by standard stimuli, whereas responses to target stimuli were investigated in the present study. Furthermore, possible differences between first-episode and chronic schizophrenia patients and the influence of medication should be directly addressed in further studies. In general, our findings are well in line with different reports on reduced γ activity in schizophrenia. Schizophrenic patients showed reduced evoked power and phase synchronization during 40-Hz auditory steady-state-stimulation that does not involve attentional requirements (36,37), indicating a global inability to generate or maintain γ activity. This might be due to similarly disturbed circuit and neuronal features like those that are involved in the generation of sensory evoked γ oscillations and is therefore related to the present findings. We were able to replicate—regarding γ phase-locking—recent findings on decreased PLFs in the first 100 msec after an auditory stimulus in schizophrenic patients (33,34), which generally matches reports on decreased trial-to-trial time locking to stimulus onset in schizophrenia (51). However, there have also been reports on increased γ phase synchrony in first-episode schizophrenia (52). In our data, the reduced PLF is clearly related to the finding of reduced GBR power, although both measurements are sensitive to independent aspects of the same activity.

There is growing evidence that the reduction of EEG γ activity in schizophrenia might be a correlate of a dysfunction of neural microcircuits, especially of the interaction between cortical pyramidal cells and inhibitory GABAergic interneurons (4). In particular, fast-spiking basket types of these interneurons play a key role in emerging γ-frequency oscillations by synchronization of pyramidal cells firing via negative feedback inhibition (9,10,53). Different studies showed alterations of the GABAergic inhibitory system in schizophrenia that are mainly restricted to the fast-spiking interneurons (54–56). The *N*-methyl-D-aspartate (NMDA) glutamate receptors of interneurons seem to play an important role for the excitation of interneurons and hence for feedback inhibition of pyramidal cells (1,57). In accordance with this, NMDA receptor antagonists produce disinhibition of pyramidal cells (2,58,59). Moreover, they induce symptoms resembling schizophrenia in healthy human subjects (60) and strongly enforce the symptoms of patients with schizophrenia (61). By contrast, activation of metabotropic glutamate receptors reverses the effects of NMDA receptor hypofunction (62), which led to successful attempts of treating schizophrenic patients with substances improving the glutamate receptor function (63,64). In this context, our present findings might correlate with an earlier report that antagonists of the NMDA receptor reduce γ activity (65), although there have been contrary results on this (66).

Anatomical auditory cortex abnormalities have been consistently reported in schizophrenia (67,68). Accordingly, deficits in auditory processes like the mismatch negativity in patients were noted, which are also an expression of alterations of neural properties in the auditory cortex, like the NMDA hypofunction (69). Our findings on reduced γ activity in the auditory cortex is in line with this. The detected hemispheric asymmetry of the auditory cortex ROIs matches anatomical and functional data indicating left auditory cortex dysfunction in schizophrenia (70). Our results of reduced activity of the dACC as a generator of the early evoked GBR could suggest an involvement of this region in the impaired auditory information processing in schizophrenia. Several studies point toward the involvement of the dACC in auditory information processing (e.g., the strong efferent influence of the dACC on the auditory association area BA 22) (71). Moreover, there is a functional relationship between dACC and auditory cortex activity, for example in the context of language processes (72). By interpreting findings on the relationship between the early auditory GBR and the difficulty of different auditory reaction tasks (similar to the one used here), we previously suggested a functional interaction between both regions affected by attentional requirements (21,73). The ACC dysfunction in schizophrenic patients is well-documented in studies with fMRI (74) or EEG (44). Structural MRI investigations reported volumetric alterations of the ACC in schizophrenic subjects (75,76). The disturbance of the modulatory influence of the ACC on the prefrontal and superior temporal cortex is suggested to be responsible for a disturbance of fronto-temporal connectivity in schizophrenia (77). Postmortem studies showed an altered distribution of parvalbumin-positive GABAergic interneurons (78) and described a reduction of nonpyramidal cells in the ACC layer II and increased vertical axon numbers as well as smaller neuronal clusters (5). Woo *et al.* (79) reported a decrease of the density of GABAergic interneurons in the ACC that express the NMDA NR2A subunit and also are essentially involved in the generation of γ oscillations as described earlier. According to these findings and the binding-hypothesis of the EEG γ activity, the results of the present study could point to a disturbed "gamma-modulated" functional interaction between the ACC and the auditory cortex in schizophrenia underlined by reports from diffusion tensor imaging investigations on disrupted fronto-temporal connections in this disease (80).

One limitation of the present study is that the spatial accuracy

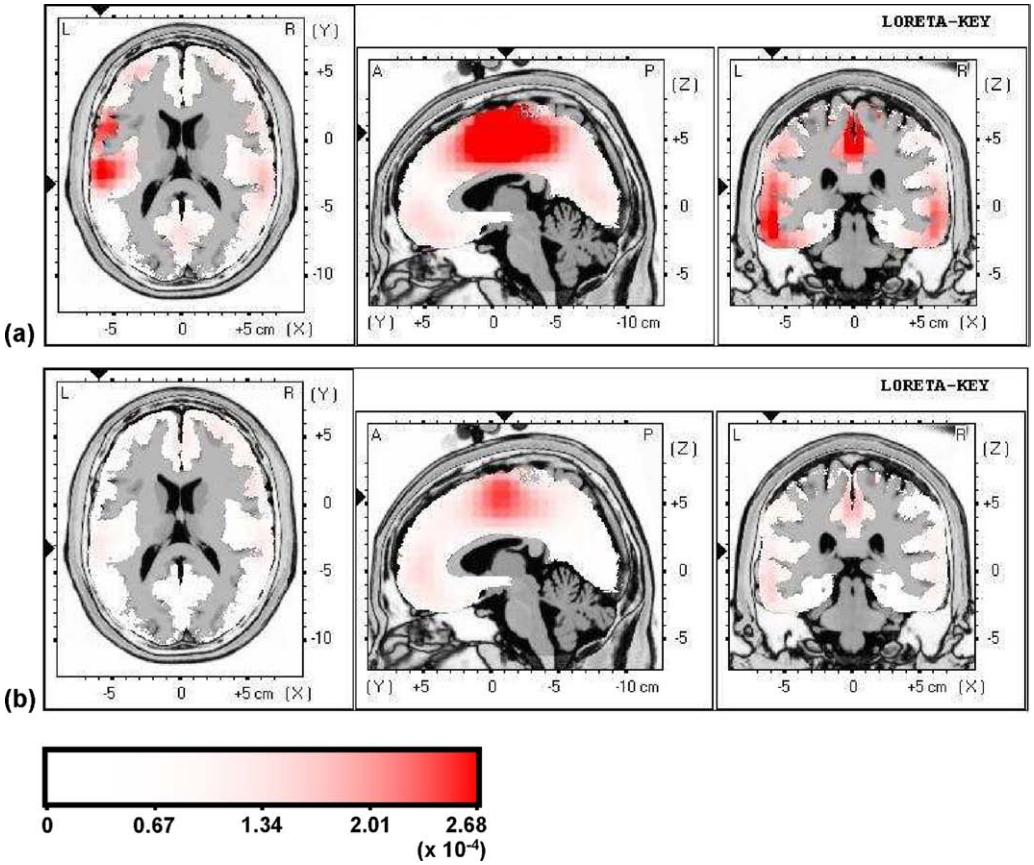

Figure 6. Maximum low-resolution brain electromagnetic tomography (LORETA)-activations (mean current source density in μA/mm^2) of evoked γ-band activity within the time frame 30–70 msec after stimulus presentation for control subjects **(A)** and patients with schizophrenia **(B)**. The black arrows indicate the activity in the primary auditory cortex (outer left and right figures, Talairach coordinates *x*, *y*, *z* = −59, −32, 15, superior temporal gyrus) and the absolute current density maximum of control subjects in the anterior cingulate cortex/supplementary motor area region (middle figures, Talairach coordinates *x*, *y*, *z* = −3, −11, 57, medial frontal gyrus). The γ-band response data for the LORETA-analyses were not calculated with a wavelet but with bandpass filters. *A* = anterior, *P* = posterior, *L* = left, *R* = right.

of the LORETA approach is not better than 1–2 cm, although recent cross-validation studies using simultaneous EEG and fMRI have suggested sufficient validity of the LORETA approach in general (81,82). In line with our present results are recent reports about GBR-specific fMRI activations in the auditory cortex, the ACC, and the thalamus with single-trial coupling of EEG and fMRI (C. Mulert, M.D., unpublished data, 2009). The applied LORETA software is limited to analysis of cortical activity. Therefore, the investigation of schizophrenic patients with simultaneous EEG and fMRI could give new insights concerning subcortical structures like the thalamus.

Although the P50-component of the AEP overlaps temporarily with the GBR, we found no significant differences between patients and control subjects concerning the P50-potential. This difference in the selectivity regarding patients and control subjects between P50 and GBR could support the idea of two different functional processes, whereas there are opposed findings (83). Because there is an influence of stimulus duration to amplitudes and latencies of GBRs (84) the question about differences between schizophrenic patients and control subjects regarding the interaction of an input continuing beyond the early GBR with this response should be addressed in further investigations.

Although there was no significant correlation between chlorpromazine equivalents and the early evoked GBR in the patients group, another difficulty for interpretation of the present results is the unknown influence of specific medication on the occurrence of γ oscillations due to the complex effect of antipsychotics on neural activity. Hong *et al.* (85) reported significantly higher γ power in atypically medicated patients with schizophrenia compared with patients with conventional antipsychotic treatment. Most patients in the present study were receiving treatment with atypical antipsychotics. Therefore—and due to the current thinking that antipsychotics might rather normalize disturbed functions—it can be assumed that antipsychotic medication might have rather reduced the differences concerning the GBR between patients and healthy subjects.

In conclusion, this study shows a significantly reduced early auditory evoked GBR in patients with schizophrenia, reflecting neural circuit dysfunction in this disease. We were able to show reduced activity in the auditory cortex and the ACC/medial frontal gyrus region in patients with schizophrenia, underlying the reduced γ activity measured on the scalp. These findings are in line with the hypothesis of a disturbed GABAergic interneural modulation of pyramidal cells in schizophrenia.

The recruitment was partially supported by GlaxoSmithKline.

The authors reported no biomedical financial interests or potential conflicts of interest.

Supplementary material cited in this article is available online.

1. Grunze HC, Rainnie DG, Hasselmo ME, Barkai E, Hearn EF, McCarley RW, *et al.* (1996): NMDA-dependent modulation of CA1 local circuit inhibition. *J Neurosci* 16:2034–2043.
2. Rujescu D, Bender A, Keck M, Hartmann AM, Ohl F, Raeder H, *et al.* (2006): A pharmacological model for psychosis based on N-methyl-D-aspartate receptor hypofunction: Molecular, cellular, functional and behavioral abnormalities. *Biol Psychiatry* 59:721–729.
3. Braun I, Genius J, Grunze H, Bender A, Moller HJ, Rujescu D (2007): Alterations of hippocampal and prefrontal GABAergic interneurons in an animal model of psychosis induced by NMDA receptor antagonism. *Schizophr Res* 97:254–263.
4. Lisman JE, Coyle JT, Green RW, Javitt DC, Benes FM, Heckers S, *et al.* (2008): Circuit-based framework for understanding neurotransmitter and risk gene interactions in schizophrenia. *Trends Neurosci* 31:234–242.
5. Benes FM (2000): Emerging principles of altered neural circuitry in schizophrenia. *Brain Res Brain Res Rev* 31:251–269.
6. Lewis DA, Hashimoto T, Volk DW (2005): Cortical inhibitory neurons and schizophrenia. *Nat Rev Neurosci* 6:312–324.
7. McBain CJ, Fisahn A (2001): Interneurons unbound. *Nat Rev Neurosci* 2:11–23.
8. Whittington MA, Traub RD (2003): Interneuron diversity series: Inhibitory interneurons and network oscillations in vitro. *Trends Neurosci* 26: 676–682.
9. Fuchs EC, Zivkovic AR, Cunningham MO, Middleton S, Lebeau FE, Bannerman DM, *et al.* (2007): Recruitment of parvalbumin-positive interneurons determines hippocampal function and associated behavior. *Neuron* 53:591–604.
10. Mann EO, Radcliffe CA, Paulsen O (2005): Hippocampal gamma-frequency oscillations: From interneurones to pyramidal cells, and back. *J Physiol* 562:55–63.
11. Friston KJ (1999): Schizophrenia and the disconnection hypothesis. *Acta Psychiatr Scand Suppl* 395:68–79.
12. Phillips WA, Silverstein SM (2003): Convergence of biological and psychological perspectives on cognitive coordination in schizophrenia. *Behav Brain Sci* 26:65–82; discussion:82–137.
13. Friston KJ, Frith CD (1995): Schizophrenia: A disconnection syndrome? *Clin Neurosci* 3:89–97.
14. Wolf DH, Gur RC, Valdez JN, Loughead J, Elliott MA, Gur RE, *et al.* (2007): Alterations of fronto-temporal connectivity during word encoding in schizophrenia. *Psychiatry Res* 154:221–232.
15. Winterer G, Coppola R, Egan MF, Goldberg TE, Weinberger DR (2003): Functional and effective frontotemporal connectivity and genetic risk for schizophrenia. *Biol Psychiatry* 54:1181–1192.
16. Lee KH, Williams LM, Breakspear M, Gordon E (2003): Synchronous gamma activity: A review and contribution to an integrative neuroscience model of schizophrenia. *Brain Res Brain Res Rev* 41:57–78.
17. Uhlhaas PJ, Haenschel C, Nikolic D, Singer W (2008): The role of oscillations and synchrony in cortical networks and their putative relevance for the pathophysiology of schizophrenia. *Schizophr Bull* 34:927–943.
18. Singer W (1999): Neuronal synchrony: A versatile code for the definition of relations? *Neuron* 24:49–65, 111–125.
19. Engel AK, Fries P, Singer W (2001): Dynamic predictions: Oscillations and synchrony in top-down processing. *Nat Rev Neurosci* 2:704–716.
20. Basar E, Basar-Eroglu C, Karakas S, Schurmann M (2001): Gamma, alpha, delta, and theta oscillations govern cognitive processes. *Int J Psychophysiol* 39:241–248.
21. Mulert C, Leicht G, Pogarell O, Mergl R, Karch S, Juckel G, *et al.* (2007): Auditory cortex and anterior cingulate cortex sources of the early evoked gamma-band response: Relationship to task difficulty and mental effort. *Neuropsychologia* 45:2294–2306.
22. Herrmann CS, Munk MH, Engel AK (2004): Cognitive functions of gamma-band activity: Memory match and utilization. *Trends Cogn Sci* 8:347–355.
23. Tallon-Baudry C, Bertrand O, Henaff MA, Isnard J, Fischer C (2005): Attention modulates gamma-band oscillations differently in the human lateral occipital cortex and fusiform gyrus. *Cereb Cortex* 15:654–662.
24. Gurtubay IG, Alegre M, Labarga A, Malanda A, Artieda J (2004): Gamma band responses to target and non-target auditory stimuli in humans. *Neurosci Lett* 367:6–9.
25. Senkowski D, Herrmann CS (2002): Effects of task difficulty on evoked gamma activity and ERPs in a visual discrimination task. *Clin Neurophysiol* 113:1742–1753.
26. Tiitinen H, Sinkkonen J, Reinikainen K, Alho K, Lavikainen J, Naatanen R (1993): Selective attention enhances the auditory 40-Hz transient response in humans. *Nature* 364:59–60.
27. Gallinat J, Winterer G, Herrmann CS, Senkowski D (2004): Reduced oscillatory gamma-band responses in unmedicated schizophrenic patients indicate impaired frontal network processing. *Clin Neurophysiol* 115: 1863–1874.
28. Tiitinen H, May P, Naatanen R (1997): The transient 40-Hz response, mismatch negativity, and attentional processes in humans. *Prog Neuropsychopharmacol Biol Psychiatry* 21:751–771.
29. Muller MM, Keil A, Kissler J, Gruber T (2001): Suppression of the auditory middle-latency response and evoked gamma-band response in a paired-click paradigm. *Exp Brain Res* 136:474–479.
30. Pantev C, Makeig S, Hoke M, Galambos R, Hampson S, Gallen C (1991): Human auditory evoked gamma-band magnetic fields. *Proc Natl Acad Sci U S A* 88:8996–9000.
31. Ribary U, Ioannides AA, Singh KD, Hasson R, Bolton JP, Lado F, *et al.* (1991): Magnetic field tomography of coherent thalamocortical 40-Hz oscillations in humans. *Proc Natl Acad Sci U S A* 88:11037–11041.
32. Ahveninen J, Kahkonen S, Tiitinen H, Pekkonen E, Huttunen J, Kaakkola S, *et al.* (2000): Suppression of transient 40-Hz auditory response by haloperidol suggests modulation of human selective attention by dopamine D2 receptors. *Neurosci Lett* 292:29–32.
33. Symond MP, Harris AW, Gordon E, Williams LM (2005): "Gamma synchrony" in first-episode schizophrenia: A disorder of temporal connectivity? *Am J Psychiatry* 162:459–465.
34. Roach BJ, Mathalon DH (2008): Event-related EEG time-frequency analysis: An overview of measures and an analysis of early gamma band phase locking in schizophrenia. *Schizophr Bull* 34:907–926.
35. Spencer KM, Niznikiewicz MA, Shenton ME, McCarley RW (2008): Sensory-evoked gamma oscillations in chronic schizophrenia. *Biol Psychiatry* 63:744–747.
36. Kwon JS, O'Donnell BF, Wallenstein GV, Greene RW, Hirayasu Y, Nestor PG, *et al.* (1999): Gamma frequency-range abnormalities to auditory stimulation in schizophrenia. *Arch Gen Psychiatry* 56:1001–1005.
37. Light GA, Hsu JL, Hsieh MH, Meyer-Gomes K, Sprock J, Swerdlow NR, *et al.* (2006): Gamma band oscillations reveal neural network cortical coherence dysfunction in schizophrenia patients. *Biol Psychiatry* 60:1231–1240.
38. Spencer KM, Salisbury DF, Shenton ME, McCarley RW (2008): Gamma-band auditory steady-state responses are impaired in first episode psychosis. *Biol Psychiatry* 64:369–375.
39. First MB, Spitzer RL, Gibbon M, Williams BW, Benjamin L (1990). *Structured Clin Interview Forest DSM-IV Axis II Personality Disorders (SCID-II)*. New York: Biometrics Research Department, New York State Psychiatric Institute.
40. First MB, Spitzer RL, Gibbon M, Williams JB (1995): *Structured Clinical Interview for DSM-IV Axis I Disorders—Patient Edition (SCID −I/P, Version 2.0)*. New York: Biometrics Research Department, New York State Psychiatric Institute.
41. Rice JP, Reich T, Bucholz KK, Neuman RJ, Fishman R, Rochberg N, *et al.* (1995): Comparison of direct interview and family history diagnoses of alcohol dependence. *Alcohol Clin Exp Res* 19:1018–1023.
42. Folstein MF, Folstein SE, McHugh PR (1975): Mini-mental state: A practical method for grading the cognitive state of patients for the clinician. *J Psychiatr Res* 12:189–198.
43. Rujescu D, Giegling I, Gietl A, Hartmann AM, Moller HJ (2003): A functional single nucleotide polymorphism (V158M) in the COMT gene is associated with aggressive personality traits. *Biol Psychiatry* 54:34–39.
44. Mulert C, Gallinat J, Pascual-Marqui R, Dorn H, Frick K, Schlattmann P, *et al.* (2001): Reduced event-related current density in the anterior cingulate cortex in schizophrenia. *Neuroimage* 13:589–600.
45. Mulert C, Gallinat J, Dorn H, Herrmann WM, Winterer G (2003): The relationship between reaction time, error rate and anterior cingulate cortex activity. *Int J Psychophysiol* 47:175–183.
46. Herrmann CS, Mecklinger A, Pfeifer E (1999): Gamma responses and ERPs in a visual classification task. *Clin Neurophysiol* 110:636–642.
47. Pascual-Marqui RD, Michel CM, Lehmann D (1994): Low resolution electromagnetic tomography: A new method for localizing electrical activity in the brain. *Int J Psychophysiol* 18:49–65.

48. Mulert C, Juckel G, Brunnmeier M, Karch S, Leicht G, Mergl R, *et al.* (2007): Prediction of treatment response in major depression: Integration of concepts. *J Affect Disord* 98:215–225.
49. Barth DS, MacDonald KD (1996): Thalamic modulation of high-frequency oscillating potentials in auditory cortex. *Nature* 383:78–81.
50. Gallinat J, Mulert C, Bajbouj M, Herrmann WM, Schunter J, Senkowski D, *et al.* (2002): Frontal and temporal dysfunction of auditory stimulus processing in schizophrenia. *Neuroimage* 17:110–127.
51. Patterson JV, Jin Y, Gierczak M, Hetrick WP, Potkin S, Bunney WE Jr, *et al.* (2000): Effects of temporal variability on p50 and the gating ratio in schizophrenia: A frequency domain adaptive filter single-trial analysis. *Arch Gen Psychiatry* 57:57–64.
52. Flynn G, Alexander D, Harris A, Whitford T, Wong W, Galletly C, *et al.* (2008): Increased absolute magnitude of gamma synchrony in first-episode psychosis. *Schizophr Res* 105:262–271.
53. Fisahn A, Pike FG, Buhl EH, Paulsen O (1998): Cholinergic induction of network oscillations at 40 Hz in the hippocampus in vitro. *Nature* 394: 186–189.
54. Perry TL, Kish SJ, Buchanan J, Hansen S (1979): Gamma-aminobutyric-acid deficiency in brain of schizophrenic patients. *Lancet* 1:237–239.
55. Zhang ZJ, Reynolds GP (2002): A selective decrease in the relative density of parvalbumin-immunoreactive neurons in the hippocampus in schizophrenia. *Schizophr Res* 55:1–10.
56. Benes FM, Lim B, Matzilevich D, Walsh JP, Subburaju S, Minns M (2007): Regulation of the GABA cell phenotype in hippocampus of schizophrenics and bipolars. *Proc Natl Acad Sci U S A* 104:10164–10169.
57. Jones RS, Buhl EH (1993): Basket-like interneurones in layer II of the entorhinal cortex exhibit a powerful NMDA-mediated synaptic excitation. *Neurosci Lett* 149:35–39.
58. Jackson ME, Homayoun H, Moghaddam B (2004): NMDA receptor hypofunction produces concomitant firing rate potentiation and burst activity reduction in the prefrontal cortex. *Proc Natl Acad Sci U S A* 101:8467–8472.
59. Homayoun H, Moghaddam B (2007): NMDA receptor hypofunction produces opposite effects on prefrontal cortex interneurons and pyramidal neurons. *J Neurosci* 27:11496–11500.
60. Umbricht D, Schmid L, Koller R, Vollenweider FX, Hell D, Javitt DC (2000): Ketamine-induced deficits in auditory and visual context-dependent processing in healthy volunteers: Implications for models of cognitive deficits in schizophrenia. *Arch Gen Psychiatry* 57:1139–1147.
61. Lahti AC, Koffel B, LaPorte D, Tamminga CA (1995): Subanesthetic doses of ketamine stimulate psychosis in schizophrenia. *Neuropsychopharmacology* 13:9–19.
62. Lecourtier L, Homayoun H, Tamagnan G, Moghaddam B (2007): Positive allosteric modulation of metabotropic glutamate 5 (mGlu5) receptors reverses N-methyl-D-aspartate antagonist-induced alteration of neuronal firing in prefrontal cortex. *Biol Psychiatry* 62:739–746.
63. Coyle JT, Tsai G (2004): The NMDA receptor glycine modulatory site: A therapeutic target for improving cognition and reducing negative symptoms in schizophrenia. *Psychopharmacology* 174:32–38.
64. Patil ST, Zhang L, Martenyi F, Lowe SL, Jackson KA, Andreev BV, *et al.* (2007): Activation of mGlu2/3 receptors as a new approach to treat schizophrenia: A randomized phase 2 clinical trial. *Nat Med* 13:1102–1107.
65. Cunningham MO, Hunt J, Middleton S, LeBeau FE, Gillies MJ, Davies CH, *et al.* (2006): Region-specific reduction in entorhinal gamma oscillations and parvalbumin-immunoreactive neurons in animal models of psychiatric illness. *J Neurosci* 26:2767–2776.
66. Pinault D (2008): N-methyl d-aspartate receptor antagonists ketamine and MK-801 induce wake-related aberrant gamma oscillations in the rat neocortex. *Biol Psychiatry* 63:730–735.
67. Hirayasu Y, McCarley RW, Salisbury DF, Tanaka S, Kwon JS, Frumin M, *et al.* (2000): Planum temporale and Heschl gyrus volume reduction in schizophrenia: A magnetic resonance imaging study of first-episode patients. *Arch Gen Psychiatry* 57:692–699.
68. Rojas DC, Bawn SD, Carlson JP, Arciniegas DB, Teale PD, Reite ML (2002): Alterations in tonotopy and auditory cerebral asymmetry in schizophrenia. *Biol Psychiatry* 52:32–39.
69. Javitt DC, Steinschneider M, Schroeder CE, Arezzo JC (1996): Role of cortical N-methyl-D-aspartate receptors in auditory sensory memory and mismatch negativity generation: Implications for schizophrenia. *Proc Natl Acad Sci U S A* 93:11962–11967.
70. Chance SA, Casanova MF, Switala AE, Crow TJ (2008): Auditory cortex asymmetry, altered minicolumn spacing and absence of ageing effects in schizophrenia. *Brain* 131:3178–3192.
71. Pandya DN, Van Hoesen GW, Mesulam MM (1981): Efferent connections of the cingulate gyrus in the rhesus monkey. *Exp Brain Res* 42:319–330.
72. Hunter MD, Eickhoff SB, Miller TW, Farrow TF, Wilkinson ID, Woodruff PW (2006): Neural activity in speech-sensitive auditory cortex during silence. *Proc Natl Acad Sci U S A* 103:189–194.
73. Mulert C, Seifert C, Leicht G, Kirsch V, Ertl M, Karch S, *et al.* (2008): Single-trial coupling of EEG and fMRI reveals the involvement of early anterior cingulate cortex activation in effortful decision making. *Neuroimage* 42:158–168.
74. Dehaene S, Artiges E, Naccache L, Martelli C, Viard A, Schurhoff F, *et al.* (2003): Conscious and subliminal conflicts in normal subjects and patients with schizophrenia: The role of the anterior cingulate. *Proc Natl Acad Sci U S A* 100:13722–13727.
75. Hirayasu Y, Shenton ME, Salisbury DF, Kwon JS, Wible CG, Fischer IA, *et al.* (1999): Subgenual cingulate cortex volume in first-episode psychosis. *Am J Psychiatry* 156:1091–1093.
76. Goldstein JM, Goodman JM, Seidman LJ, Kennedy DN, Makris N, Lee H, *et al.* (1999): Cortical abnormalities in schizophrenia identified by structural magnetic resonance imaging. *Arch Gen Psychiatry* 56:537–547.
77. Fletcher P, McKenna PJ, Friston KJ, Frith CD, Dolan RJ (1999): Abnormal cingulate modulation of fronto-temporal connectivity in schizophrenia. *Neuroimage* 9:337–342.
78. Kalus P, Senitz D, Beckmann H (1997): Altered distribution of parvalbumin-immunoreactive local circuit neurons in the anterior cingulate cortex of schizophrenic patients. *Psychiatry Res* 75:49–59.
79. Woo TU, Walsh JP, Benes FM (2004): Density of glutamic acid decarboxylase 67 messenger RNA-containing neurons that express the N-methyl-D-aspartate receptor subunit NR2A in the anterior cingulate cortex in schizophrenia and bipolar disorder. *Arch Gen Psychiatry* 61:649–657.
80. Kubicki M, Westin CF, Maier SE, Frumin M, Nestor PG, Salisbury DF, *et al.* (2002): Uncinate fasciculus findings in schizophrenia: A magnetic resonance diffusion tensor imaging study. *Am J Psychiatry* 159:813–820.
81. Mulert C, Jager L, Schmitt R, Bussfeld P, Pogarell O, Moller HJ, *et al.* (2004): Integration of fMRI and simultaneous EEG: Towards a comprehensive understanding of localization and time-course of brain activity in target detection. *Neuroimage* 22:83–94.
82. Mulert C, Jager L, Propp S, Karch S, Stormann S, Pogarell O, *et al.* (2005): Sound level dependence of the primary auditory cortex: Simultaneous measurement with 61-channel EEG and fMRI. *Neuroimage* 28:49–58.
83. Clementz BA, Blumenfeld LD, Cobb S (1997): The gamma band response may account for poor P50 suppression in schizophrenia. *Neuroreport* 8:3889–3893.
84. Busch NA, Debener S, Kranczioch C, Engel AK, Herrmann CS (2004): Size matters: Effects of stimulus size, duration and eccentricity on the visual gamma-band response. *Clin Neurophysiol* 115:1810–1820.
85. Hong LE, Summerfelt A, McMahon R, Adami H, Francis G, Elliott A, *et al.* (2004): Evoked gamma band synchronization and the liability for schizophrenia. *Schizophr Res* 70:293–302.

Supplementary Information

LORETA method

LORETA assumes that the smoothest of all activity distributions is most plausible ("smoothness assumption") and therefore, a particular current density distribution is found (1). This fundamental assumption of LORETA directly relies on the neurophysiological observation of coherent firing of neighboring cortical neurons during stimulus processing (2-4) and therefore can be seen as a physiologically based constraint. However, this coherent firing has been described on the level of cortical columns, which have a much smaller diameter than the voxels used in the LORETA software; the empirical basis for coherent firing in the millimeter range is not strong enough to fully accept this constraint as a physiological one, even if it might help to produce useful results. The characteristic feature of the resulting solution is its relatively low spatial resolution, which is a direct consequence of the smoothness constraint. Specifically, the solution produces a "blurred-localized" image of a point source, conserving the location of maximal activity, but with a certain degree of dispersion. It should be emphasized that this solution will typically produce a "blurred-localized" image of arbitrary distributions due to the principle of superposition. However, some distributions of point sources may superpose in such a way that they actually cancel out on the scalp and therefore cannot be correctly localized by any method. The version of LORETA used in the present study was the digitized Talairach atlas (5) available as digitized MRI from the Brain Imaging Center, Montreal Neurologic Institute, estimating the current source density (microAmperes/mm^2) distribution for either single timepoints or epochs of brain electric activity on a dense grid of 2394 voxels at 7mm spatial resolution (6). The solution space (the three-dimensional space in which the LORETA solution is projected) was restricted to the gray matter and hippocampus in the Talairach atlas (anatomically based constraint). Localization with regard to spherical and realistic head geometry was done using

EEG electrode coordinates reported by Towle *et al*. (7). A voxel was labeled as gray matter if it met the following three conditions: its probability of being gray matter was higher than that of being white matter, its probability of being gray matter was higher than that of being cerebrospinal fluid, and its probability of being gray matter was higher than 33% (6). LORETA has been widely used in the last years in order to localize electrical generators of scalp EEG data (8-11).

LORETA region of interest (ROI) analysis

According to our previous works (12; 13), the dACC-ROI (based on eighty-five $7mm^3$ voxels) covered a region extending in Talairach space from x: −10 to 11, y: −18 to 38, z: 15 to 50 and included voxels from Brodmann areas 24, 32 and 33. The primary auditory cortex BA41-ROI (based on ten $7mm^3$ voxels) covered a region extending in Talairach space from x: 46 to 60 and −38 to −59, y: −18 to −39, z: 8 to 15 and included all voxels from Brodmann area 41. The secondary auditory cortex BA42-ROI (based on eighteen $7mm^3$ voxels) covered a region extending in Talairach space from x: 60 to 67 and −59 to −66, y: −11 to −32, z: 8 to 15 and included all voxels from Brodmann area 42. The auditory association cortex BA22-ROI (based on eighty-eight $7mm^3$ voxels) covered a region extending in Talairach space from x: 46 to 67 and −45 to−66, y: 10 to −60, z: −6 to 22 and included all voxels from Brodmann area 22. The vACC-ROI (based on twenty-five $7mm^3$ voxels) covered a region extending in Talairach space from x: −10 to 11, y: 3 to 45, z: -6 to 8 and included voxels from Brodmann areas 24, 25 and 32.

Table S1. Early evoked gamma-band response (GBR): Localization of Maximum LORETA-activations within the timeframe 30-70 ms in patients with schizophrenia and controls.

	Localization	Talairach coordinates			Current source density in $\mu A/mm^2 \times 10^{-3}$
Healthy controls	SMA / dACC	-3	-11	64	0,43
	Auditory cortex left	-59	-18	-13	0,39
	Auditory cortex right	60	-32	-6	0,23
	Middle frontal gyrus	-45	10	29	0,31
Patients with schizophrenia	SMA / dACC	-3	-4	57	0,22
	Auditory cortex left	-59	-18	-13	0,26
	Auditory cortex right	53	3	-13	0,16

SMA, supplementary motor area; dACC = dorsal anterior cingulate cortex.

Table S2. Mean current source density values of the early evoked gamma activity for the different regions of interest (ROIs) within the timeframe 30-70 ms and for patients with schizophrenia and controls.

	dACC-ROI ($\mu A/mm^2 \times 10^{-3}$)	BA22-ROI ($\mu A/mm^2 \times 10^{-3}$)	BA41-ROI ($\mu A/mm^2 \times 10^{-3}$)	BA42-ROI ($\mu A/mm^2 \times 10^{-3}$)	vACC-ROI ($\mu A/mm^2 \times 10^{-3}$)
Healthy controls	0.51 (SD=0.23)	0.83 (SD=0.47)	0.84 (SD=0.56)	0.97 (SD=0.57)	0.52 (SD=0.30)
Patients with schizophrenia	0.44 (SD=0.21)	0.62 (SD=0.37)	0.58 (SD=0.36)	0.73 (SD=0.45)	0.45 (SD=0.27)
Statistics	$Z=2.2$, $p=0.027$	$Z=3.5$, $p=0.001$	$Z=3.7$, $p<0.001$	$Z=3.3$, $p=0.001$	No significant difference

BA, Brodmann Area; dACC, dorsal anterior cingulate cortex; SD, standard deviation; vACC, ventral anterior cingulate cortex.

Table S3. Mean current source density values of the early evoked gamma activity (timeframe 30-70 ms) for the auditory cortex ROIs in the bilateral comparison for patients with schizophrenia and controls.

	BA22-ROI left ($\mu A/mm^2 \times 10^{-3}$)	BA22-ROI right ($\mu A/mm^2 \times 10^{-3}$)	BA41-ROI left ($\mu A/mm^2 \times 10^{-3}$)	BA41-ROI right ($\mu A/mm^2 \times 10^{-3}$)	BA42-ROI left ($\mu A/mm^2 \times 10^{-3}$)	BA42-ROI right ($\mu A/mm^2 \times 10^{-3}$)
Healthy controls	0.91 (SD=0.64)	0.77 (SD=0.49)	0.96 (SD=0.73)	0.57 (SD=0.40)	1.1 (SD=0.79)	0.89 (SD=0.62)
Patients with schizophrenia	0.59 (SD=0.36)	0.64 (SD=0.44)	0.63 (SD=0.43)	0.46 (SD=0.33)	0.71 (SD=0.48)	0.74 (SD=0.54)
Statistics	$Z=3.9$, $p<0.001$	$Z=2.1$, $p=0.034$	$Z=3.7$, $p<0.001$	$F(1,178)=4.1$, $p=0.045$	$Z=3.7$, $p<0.001$	No significant difference

Abbreviations as above.

References

1. Pascual-Marqui RD, Michel CM, Lehmann D (1994): Low resolution electromagnetic tomography: a new method for localizing electrical activity in the brain. *Int J Psychophysiol* 18:49-65.
2. Gray CM, Konig P, Engel AK, Singer W (1989): Oscillatory responses in cat visual cortex exhibit inter-columnar synchronization which reflects global stimulus properties. *Nature* 338:334-7.
3. Llinas RR (1988): The intrinsic electrophysiological properties of mammalian neurons: insights into central nervous system function. *Science* 242:1654-64.
4. Silva LR, Amitai Y, Connors BW (1991): Intrinsic oscillations of neocortex generated by layer 5 pyramidal neurons. *Science* 251:432-5.
5. Talairach J, Tournoux P (1988): *Co-Planar Stereotaxic Atlas of the Human Brain*. Thieme, Stuttgart.
6. Pascual-Marqui RD, Lehmann D, Koenig T, Kochi K, Merlo MC, Hell D, *et al.* (1999): Low resolution brain electromagnetic tomography (LORETA) functional imaging in acute, neuroleptic-naive, first-episode, productive schizophrenia. *Psychiatry Res* 90:169-79.
7. Towle VL, Bolanos J, Suarez D, Tan K, Grzeszczuk R, Levin DN, *et al*. (1993): The spatial location of EEG electrodes: locating the best-fitting sphere relative to cortical anatomy. *Electroencephalogr Clin Neurophysiol* 86:1-6.
8. Gallinat J, Mulert C, Bajbouj M, Herrmann WM, Schunter J, Senkowski D, *et al.* (2002): Frontal and temporal dysfunction of auditory stimulus processing in schizophrenia. *Neuroimage* 17:110-27.
9. Mulert C, Pogarell O, Juckel G, Rujescu D, Giegling I, Rupp D, *et al.* (2004): The neural basis of the P300 potential. Focus on the time-course of the underlying cortical generators. *Eur Arch Psychiatry Clin Neurosci* 254:190-8.

10. Mulert C, Gallinat J, Pascual-Marqui R, Dorn H, Frick K, Schlattmann P, *et al.* (2001): Reduced event-related current density in the anterior cingulate cortex in schizophrenia. *Neuroimage* 13:589-600.

11. Pizzagalli D, Pascual-Marqui RD, Nitschke JB, Oakes TR, Larson CL, Abercrombie HC, *et al.* (2001): Anterior cingulate activity as a predictor of degree of treatment response in major depression: evidence from brain electrical tomography analysis. *Am J Psychiatry* 158:405-15.

12. Mulert C, Juckel G, Brunnmeier M, Karch S, Leicht G, Mergl R, *et al.* (2007): Prediction of treatment response in major depression: integration of concepts. *J Affect Disord* 98:215-25.

13. Mulert C, Leicht G, Pogarell O, Mergl R, Karch S, Juckel G, *et al.* (2007): Auditory cortex and anterior cingulate cortex sources of the early evoked gamma-band response: relationship to task difficulty and mental effort. *Neuropsychologia* 45:2294-306.

2.2 Long-range synchrony of gamma oscillations and auditory hallucination symptoms in schizophrenia

Disturbances in the functional and structural connectivity in schizophrenia have been suggested by several authors (Light et al., 2006; Spencer et al., 2008; Sweet et al., 2007; Whitford et al., 2010). Positive correlations between the phase synchronization of gamma oscillations and hallucination symptoms suggest that the propensity for hallucinations is associated with an increased tendency in the sensory cortex to enter states of oscillatory synchrony (Dierks et al., 1999; Gaser et al., 2004; Spencer et al., 2009; van de Ven et al., 2005). Much of this evidence has come from studies of auditory steady state responses (ASSRs), in which simple auditory stimuli such as clicks are delivered at rapid rates and entrain the EEG at the stimulation frequency (Galambos et al., 1981). The timing of neuronal spikes in oscillatory networks is the basis for information representation by phase (Buzsaki and Draguhn, 2004; Harris et al., 2003). The present study uses a new methodological approach to investigate long-range gamma band phase synchronization between the left and right auditory cortex in patients with schizophrenia and its relationship to auditory hallucinations. Subjects were 18 patients with chronic schizophrenia (SZ) and 16 healthy controls (HC). Current source density of the 40 Hz ASSR for the primary auditory cortices was significantly reduced in SZ. Furthermore a significant positive correlation was found between auditory hallucination symptom scores and phase synchronization between the primary auditory cortices. This suggests that long-range synchrony of gamma oscillations is disturbed in schizophrenia and that this deficit is related to clinical symptoms such as auditory hallucinations.

International Journal of Psychophysiology 79 (2011) 55–63

Contents lists available at ScienceDirect

International Journal of Psychophysiology

journal homepage: www.elsevier.com/locate/ijpsycho

Long-range synchrony of gamma oscillations and auditory hallucination symptoms in schizophrenia

C. Mulert [a,b,*], V. Kirsch [a,c], Roberto Pascual-Marqui [d], Robert W. McCarley [a], Kevin M. Spencer [a]

[a] Department of Psychiatry, VA Boston Healthcare System and Harvard Medical School, Massachusetts, USA
[b] University Medical Center Hamburg-Eppendorf, Department of Psychiatry and Psychotherapy, Psychiatry Neuroimaging Branch (PNB), Hamburg, Germany
[c] Ludwig-Maximilians-University, Department of Psychiatry and Psychotherapy, Munich, Germany
[d] The KEY Institute for Brain-Mind Research, University Hospital of Psychiatry, Zurich, Switzerland

ARTICLE INFO

Article history:
Received 18 March 2010
Received in revised form 5 August 2010
Accepted 5 August 2010
Available online 14 August 2010

Keywords:
EEG
ASSR
Gamma-band
40 Hz
Schizophrenia
Auditory stimulation
LORETA

ABSTRACT

Phase locking in the gamma-band range has been shown to be diminished in patients with schizophrenia. Moreover, there have been reports of positive correlations between phase locking in the gamma-band range and positive symptoms, especially hallucinations. The aim of the present study was to use a new methodological approach in order to investigate gamma-band phase synchronization between the left and right auditory cortex in patients with schizophrenia and its relationship to auditory hallucinations.

Subjects were 18 patients with chronic schizophrenia (SZ) and 16 healthy control (HC) subjects. Auditory hallucination symptom scores were obtained using the Scale for the Assessment of Positive Symptoms. Stimuli were 40-Hz binaural click trains. The generators of the 40 Hz-ASSR were localized using eLORETA and based on the computed intracranial signals lagged interhemispheric phase locking between primary and secondary auditory cortices was analyzed.

Current source density of the 40 ASSR response was significantly diminished in SZ in comparison to HC in the right superior and middle temporal gyrus ($p<0.05$). Interhemispheric phase locking was reduced in SZ in comparison to HC for the primary auditory cortices ($p<0.05$) but not in the secondary auditory cortices. A significant positive correlation was found between auditory hallucination symptom scores and phase synchronization between the primary auditory cortices ($p<0.05$, corrected for multiple testing) but not for the secondary auditory cortices.

These results suggest that long-range synchrony of gamma oscillations is disturbed in schizophrenia and that this deficit is related to clinical symptoms such as auditory hallucinations.

1. Introduction

Synchronous neural oscillations in the gamma band (>30 Hz) of the electroencephalogram (EEG) have been hypothesized to play an important role in the linking of neurons into cell assemblies both locally and in the inter-regional communications of the brain (Singer, 1999). While much of this evidence was provided in animal studies, investigations of gamma oscillations have now also been extensively done in healthy controls and patients with neuropsychiatric diseases. Experimental data obtained in both animals and in humans suggest that gamma-band oscillations are involved in perception and cognition (Herrmann et al., 2004; Ribary, 2005). For example, gamma-band phase synchronization between the inferior temporal lobe and the medial temporal lobe was recently demonstrated to play an important role in working memory using intracranial recordings (Axmacher et al., 2008). Interestingly, it was shown that anatomical connectivity rather than physical distance, determines the coupling strength of the oscillating neurons in the gamma-band range (Csicsvari et al., 2003).

The long-range synchrony of gamma oscillations has been demonstrated to be dependent on excitatory postsynaptic potentials (EPSPs) of γ-aminobutyric acid (GABA)ergic interneurons (Fuchs et al., 2001). Since gamma-band oscillations depend on intact function of the fast-spiking GABAergic (parvalbumin containing) interneurons (Fuchs et al., 2001; Hajos et al., 2004; Vreugdenhil et al., 2003), gamma-band oscillations may provide a means to investigate the function of GABAergic interneurons at a macroscopic level (Lisman et al., 2008). This might be especially interesting for the investigation of schizophrenia, since there is much evidence now suggesting disturbances of the GABAergic interneurons in schizophrenia, such as changes in the concentration of particular proteins, notably glutamate decarboxylase (GAD), the enzyme that synthesizes GABA, and the Ca2+-binding protein parvalbumin (Lewis et al., 2005; Woo et al., 1997). Reductions in the overall number of GABAergic interneurons have also been described by post-mortem analyses (Benes et al., 1991). Alterations in other neurotransmitter systems in schizophrenia (e.g. the dopaminergic and the glutamatergic

* Corresponding author. Martinistrasse 52, 20246 Hamburg, Germany. Tel.: +49 40 7410 59521; fax: +49 89 5160 59805.
E-mail address: c.mulert@uke.de (C. Mulert).

0167-8760/$ – see front matter © 2010 Elsevier B.V. All rights reserved.
doi:10.1016/j.ijpsycho.2010.08.004

system) can well be integrated in current models about the pathophysiology of schizophrenia suggesting a key-role for the disturbance of the GABAergic interneurons (Lisman et al., 2008). Dysfunction of GABAergic interneurons is likely to be a major factor of disturbed gamma-band oscillations and related changes in perception and cognition. In schizophrenia, there is now an increasing number of studies describing altered gamma-band oscillation patterns (Hall et al., 2009; Leicht et al., 2010; Spencer et al., 2004; Symond et al., 2005; Uhlhaas and Singer, 2010; Woo et al., 2010).

Although different kinds of paradigms have been used during the last few years, some of the most reliable findings so far come from studies of auditory steady state response (ASSR) (Brenner et al., 2009; Kwon et al., 1999; Spencer et al., 2008; Teale et al., 2008). The ASSR is an EEG response to periodic auditory stimulation (such as click trains or amplitude-modulated tones) in which the sensory cortex acts as a tuned oscillator, synchronizing to the phase and frequency of the presented stimulus. The ASSR appears to have a "resonant" frequency at ~40 Hz at which the power and phase locking of the ASSR are enhanced in comparison with other stimulation frequencies (Pastor et al., 2002). In addition to assessing the frequency response characteristics of sensory neural circuits, the ASSR may be a tool to investigate oscillatory mechanisms which might have a more general significance in the pathophysiology of schizophrenia. The typical finding in patients with schizophrenia is reduced power (related to the amplitude of the response) and phase-synchrony in the gamma-band across trials, measured at scalp electrodes or after source localization in the two auditory areas separately (Spencer et al., 2009; Teale et al., 2008).

Even more pronounced than in the visual or somatosensory system, there are extensive commissural links between the primary auditory cortices of both hemispheres linking tonotopically and binaurally matched subregions across the representational axis of characteristic frequency (Lee and Winer, 2008). Although there is a substantial degree of interhemispheric transfer at subcortical levels of the auditory system, the callosal pathway in hearing is generally assumed to play an important role e.g. due to the left hemisphere supremacy in language perception and the contralateral pathway dominance in auditory signal transmission (Bamiou et al., 2007). According to the "callosal relay" model, speech stimuli entering the right hemisphere will require callosal transfer to the left hemisphere in order to be processed (Hugdahl et al., 1997; Zaidel, 1986). The temporal–callosal pathway has been demonstrated to be related to phonological skills in children (Dougherty et al., 2007) and it was shown that an intact posterior third of the corpus callosum (where the fibers of the auditory cortex are crossing) is important for the integration of prosodic information (right hemisphere function) and syntactic information (left hemisphere function) which is necessary for language comprehension (Friederici et al., 2007).

During the last few years, structural connectivity in the brain has been investigated by means of Diffusion Tensor Imaging (DTI) (Kubicki et al., 2007). Comparing schizophrenic patients with auditory hallucinations versus patients without hallucinations, increased directionality (suggested as representing stronger connectivity) was found in that part of the corpus callosum (CC, see Hubl et al., 2004), Fig. 1, where the inter-hemispheric auditory fibers are assumed to cross (posterior part of the middle third and probably adjacent parts of the posterior third) (Bamiou et al., 2007). While structural connectivity can be assessed using DTI, EEG can be used to investigate functional connectivity (Teipel et al., 2009).

Accordingly, the aim of the present study was to investigate the gamma-band phase synchronization between the left and right auditory areas in patients with schizophrenia during auditory steady-state stimulation. We re-analyzed data from a previously-published study (Spencer et al., 2009) which utilized dipole source analysis to examine the ASSR deficit in schizophrenia. Since a positive correlation was found in that study between auditory hallucination symptoms and a left auditory cortex source, and since functional imaging studies have suggested that both unilateral and bilateral activation of the primary auditory cortex is relevant for auditory hallucinations, we also looked for a possible relationship between phase-synchrony coupling of the left and right primary auditory cortex in the gamma-band range and auditory hallucination symptoms. Here we utilized low-resolution tomography (LORETA) (Pascual-Marqui, 2002; Pascual-Marqui et al., 1994), a linear source localization method that has been widely used during the last few years by us (Mulert et al., 2004, 2006, 2007) and others (Babiloni et al., 2010; van der Loo et al., 2009) in order to estimate oscillatory activity in the left and right auditory cortex as well as interhemispheric phase synchrony. Previous studies have demonstrated substantial congruence between LORETA and fMRI localization (Mulert et al., 2005, 2010).

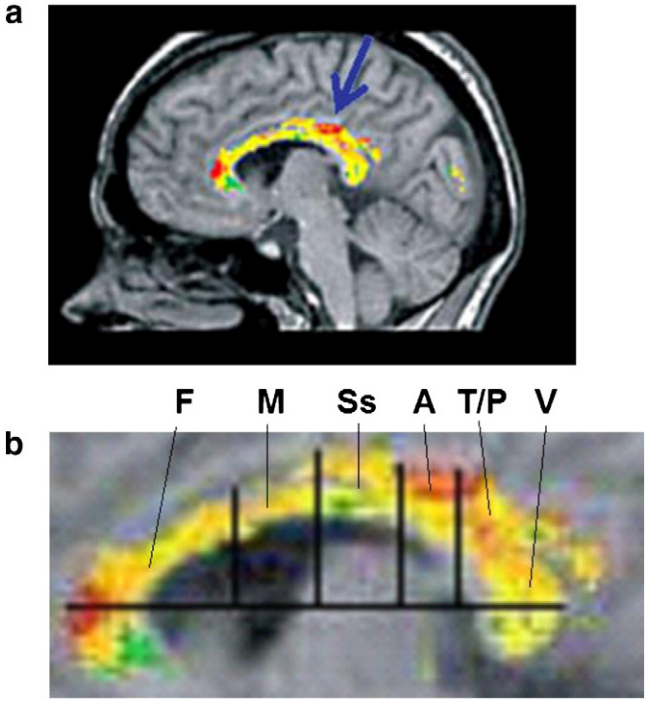

Fig. 1. Diffusion Tensor Imaging (DTI) results comparing schizophrenic patients with auditory hallucinations and schizophrenic patients without hallucinations; a) the blue arrow shows an area in the posterior part of the corpus callosum (CC) with significantly increased Fractional Anisotropy (FA) in patients with auditory hallucinations; b) The Witelson Classification suggests increased FA values in the part of the CC where the auditory fibers cross (Witelson, 1989). F: Frontal fibers, M: Motor fibers, Ss: Somatosensory fibers, A: Auditory fibers, T/P: Temporal and parietal fibers, V: Visual fibers. Reprinted and modified with permission from Hubl et al., Archives of General Psychiatry, 2004, 61(7):658-668, Copyright © (2004) American Medical Association. All rights reserved.

2. Methods

2.1. Subjects

This study was approved by the Institutional Review Boards of the VA Boston Healthcare System and Harvard Medical School. After complete description of the study to the subjects, written informed consent was obtained. All subjects were paid for their participation in the study.

Subjects were 18 patients with chronic schizophrenia (SZ) and 16 healthy control subjects (HC), all right-handed males (see Table 1). The HC were recruited from the local community. They were free of Axis I or II disorders (Structured clinical Interview for DSM III-R Non Patient Edition, Structured Clinical Interview for DSM IV Axis II Personality Disorders) as well as a history of Axis I disorders in first-degree relatives. SZ were diagnosed with schizophrenia according to the DSM-IV criteria (SCID). The diagnostic composition of the SZ

Table 1
Comparison of demographic and clinical variables for the HC and SZ groups.

	HC	SZ	Statistic
Age (years)	44.4 ± 6.8	39.8 ± 10.5	$t[32] = 1.47$, $p = 0.151$
Parental socio-economic status	3.1 ± 1.3	3.2 ± 0.9	$t[28] = -0.32$, $p = 0.754$
Handedness	0.78 ± 0.16	0.77 ± 0.25	$t[32] = 0.17$, $p = 0.864$
Age of onset (years)		26.1 ± 8.0	
Positive symptom total (SAPS)		9.0 ± 4.2	
Negative symptom total (SANS)		13.9 ± 4.9	
Medication dosage (chlorpromazine equivalents)		450 ± 306 range 83–1200	

Mean ± standard deviation are given for each variable.

group was: 10 paranoid, 5 undifferentiated, 2 schizoaffective, and 1 disorganized.

Subjects were all right-handed, selected without regard for ethnicity, and aged between 18 and 55 years. There was no history of electroconvulsive treatment, neurological illness, including epilepsy and no history of alcohol or drug dependence, nor abuse within the last year, nor long duration (>1 year) of past abuse (DSM-IV criteria). In addition, there was no present medication for medical disorders that would have deleterious EEG, neurological, or cognitive functioning consequences. For further details see Spencer et al., 2009.

Schizophrenic symptoms were rated with the Scale for the Assessment of Positive Symptoms (SAPS) (Andreasen, 1984) and the Scale for the Assessment of Negative Symptoms (Andreasen, 1983). Auditory hallucination symptoms were rated using the Auditory Hallucinations item of the SAPS. The groups did not differ on age (44 years for HC, 40 for SZ), handedness, or parental socioeconomic status (see Spencer et al., 2009 for details).

All patients received atypical antipsychotic drugs. Antipsychotic medication dosage was calculated in terms of chlorpromazine equivalents (Stoll, 2001), and ranged from 83 to 1200 (mean of 450).

2.2. Stimuli and experimental design

Subjects were seated in a quiet room in a comfortable chair 1 m in front of a computer monitor. Stimuli were presented through headphones (70 dB sound pressure level). Subjects passively listened to trains of 1 ms clicks presented at 40 Hz for 500 ms. 150 trains were presented binaurally. Subjects were instructed to look at the fixation cross on the monitor and listen to the stimuli.

2.3. Electrophysiological recording and analysis

The EEG was recorded with Neuroscan Synamp amplifiers (0.01–100 Hz, 500–Hz digitization) with sintered Ag/AgCl electodes in an electrode cap at 60 scalp sites, left and right earlobes, referenced to the right earlobe. The forehead (AFz) served as ground. Bipolar vertical and horizonatal electro-oculograms were recorded from electrodes above and below the right eye and the left and right outer canthi, respectively. Electrode impedances were <10 kΩ.

Single-trial epochs were extracted from −250 to 772 ms relative to stimulus onset and corrected for eye movements and blinks using independent component analysis (Makeig et al., 1996). Next, epochs containing artifacts were removed. The artifact criteria were >±90 μV change in one time point, and amplitude range within an epoch exceeding 200 μV. These criteria were verified via visual inspection. Finally, artifact-free single epochs were re-referenced to common average reference. There were no differences between the subject groups in the number of trials after artifact rejection (145 for HC and 140 for SZ on average).

All further analyses have been performed using the sLORETA/eLORETA software, as provided by Roberto Pascual-Marqui/The KEY Institute for Brain-Mind Research University Hospital of Psychiatry, Zurich at http://www.uzh.ch/keyinst/NewLORETA/LORETA01.htm, including the software update 2008-August 23. Localization of the neural generators of the ASSR was done using the eLORETA algorithm http://www.uzh.ch/keyinst/eLORETA/index.html. eLORETA is a 3D distributed, linear inverse solution that has no localization error to point sources under ideal (noise-free) conditions. Analysis was focussed on the frequency range 38–42 Hz.

Localization analysis was restricted to the 500 ms stimulation period using a sliding window approach. Time-varying frequency analysis was based on the short time Fourier transfor, using a sliding Bartlett–Hann window function with a width of 40 data points (80 ms). Given the temporal resolution of this approach, results were reported every 50 ms.

Lagged phase synchronization across regions was calculated between the left and right primary auditory cortex (Heschl´s gyrus, BA 41) and between the left and right secondary auditory cortex (superior temporal gyrus /STG, BA 42), focussed on the frequency range between 38 and 42 Hz. Regions of interest were defined using the anatomical definitions provided by the sLORETA/eLORETA software package which are based on the Talairach Daemon (http://www.talairach.org/), see Fig. 2. Regions of interest were selected a priori based on the most consistent reports about activations in the ASSR paradigm.

Lagged phase synchronization is defined as the phase synchronization between two signals after the instantaneous, zero phase contribution has been partialled out. Such a correction is necessary when using scalp EEG signals or estimated intracranial signals (EEG-tomography), because zero phase synchronization is often due to non-physiological effects, what might be termed intrinsic physics artifacts: volume conduction and low spatial resolution, see for example (Nolte et al., 2004; Stam et al., 2007).

The classical phase synchronization definition, which is highly contaminated by the instantaneous artifactual component, is:

$$\varphi^2_{x,y}(t,\omega) = \left|f_{x,y}(t,\omega)\right|^2 = \left\{Re\left[f_{x,y}(t,\omega)\right]\right\}^2 + \left\{Im\left[f_{x,y}(t,\omega)\right]\right\}^2 \quad (1)$$

with:

$$f_{x,y}(t,\omega) = \frac{1}{N_R}\sum_{k=1}^{N_R}\left[\frac{x_k(t,\omega)}{|x_k(t,\omega)|}\right]\left[\frac{y_k^*(t,\omega)}{|y_k(t,\omega)|}\right] \quad (2)$$

where $x_k(t,\omega)$ and $y_k(t,\omega)$ denote the discrete Fourier transforms of the two signals of interest for the k-th EEG epoch, $k = 1 \ldots N_R$, N_R being the number of epochs, at time instant t and at frequency ω; Re[c] and Im[c] denote the real and imaginary parts of a complex number c; $|c|$ denotes the modulus; and the superscript "*" denotes complex conjugate.

Lagged phase synchronization definition [RD Pascual-Marqui: Instantaneous and lagged measurements of linear and nonlinear dependence between groups of multivariate time series: frequency decomposition. arXiv:0711.1455 [stat.ME], 2007-November-09, http://arxiv.org/abs/0711.1455], which statistically partials out the intantaneous component, is:

$$\varphi^2_{x=y}(t,\omega) = \frac{\left\{Im\left[f_{x,y}(t,\omega)\right]\right\}^2}{1-\left\{Re\left[f_{x,y}(t,\omega)\right]\right\}^2} \quad (3)$$

In order to assess differences in the lagged phase synchrony between HC and SZ, statistical comparisons were calculated at the maximal values (peaks) of both HC and SZ during auditory stimulation. For the correlation analysis between the SAPS Auditory Hallucination scores and phase synchronization the whole segment information (single trial epochs) was used.

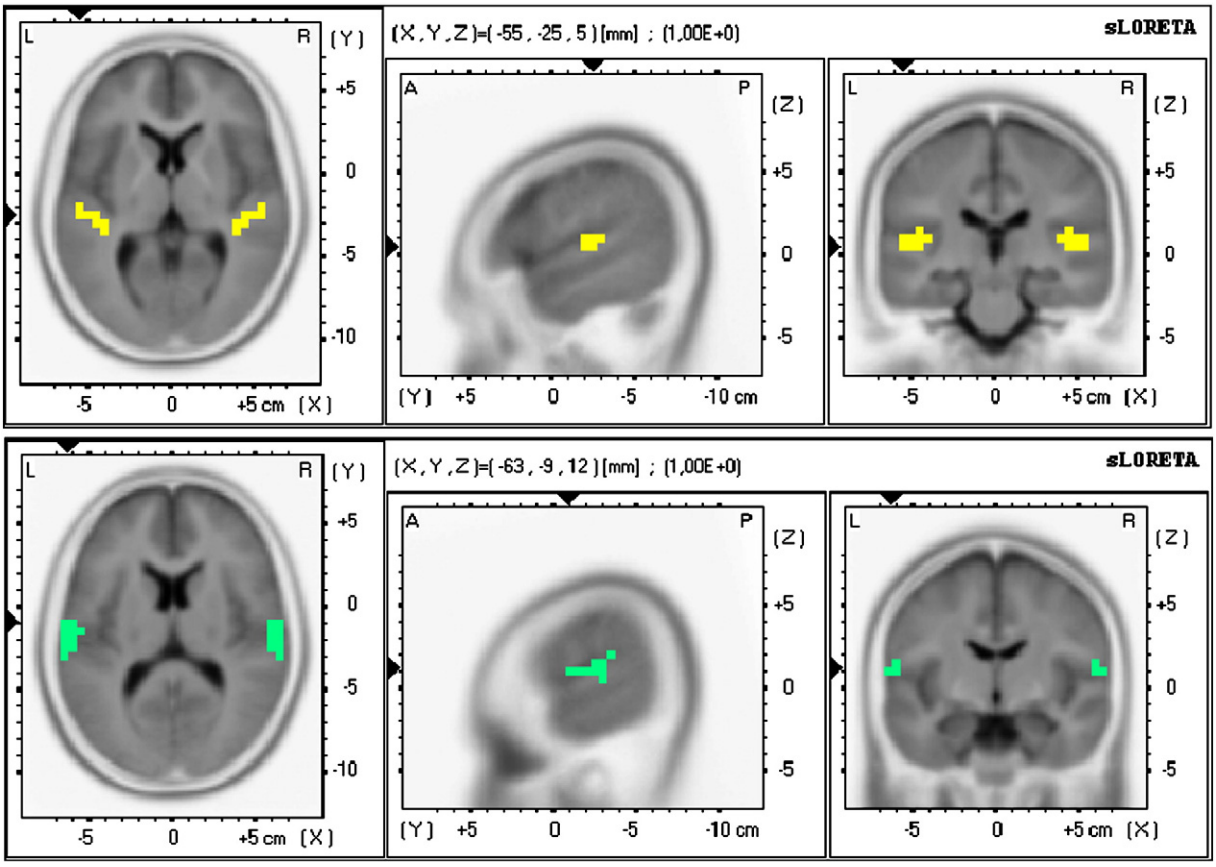

Fig. 2. Regions of interest for the lagged phase synchronization analyses. Yellow: Primary Auditory Cortex (BA 41, Heschl´s Gyrus). Green: Secondary Auditory Cortex (BA 42, Superior Temporal Gyrus).

Statistical comparisons between HC and SZ were done using the Statistical non-Parametric Mapping (SnPM) methodology provided in the sLORETA/eLORETA software package, following Nichols and Holmes (2002). The method is based on empirically estimating the probability distribution of the maximum-statistics under the null hypothesis, via randomizations, thus correcting for multiple testing and without the need to rely on Gaussianity.

2.4. Statistical analysis

Comparisons between the HC and SZ groups were performed with t-tests. Spearman´s Rho was used for correlation analyses (2-tailed). For the correlation analyses between Auditory Hallucination scores as assessed with the SAPS and phase synchronization values between left and right auditory areas (both primary and secondary auditory cortex) a Bonferroni correction with $\alpha = 0.05$ (hallucination score × 2 phase synchronization values) was applied. Other correlation analyses were also Bonferroni corrected.

3. Results

For the description of the scalp data please refer to Fig. 3.

3.1. Source localization

Both in HC and in SZ activation was found during the ASSR in superior and middle temporal gyrus and in Heschl´s gyrus (see Table 2). The highest current source density values were found in the middle temporal gyrus in both hemispheres in both groups. While in HC a right>left asymmetry was found, in SZ activation was stronger on the left side.

In the statistical comparison between SZ and HC, there was a significantly diminished activation in the right superior temporal gyrus (MNI coordinates: X, Y, and Z: 70, −25, and 5; $t = 5.45$, $p < 0.05$, two-tailed) and right middle temporal gyrus (MNI coordinates: X, Y, and Z: 70, −25, and −5; $t = 5.60$, $p < 0.05$, two-tailed) in patients. No region with increased activation in patients was found (see Fig. 4).

3.2. Lagged phase synchronization

3.2.1. Primary auditory cortex (Heschl´s gyrus)

In both HC and SZ an increase in the lagged phase synchronization was detected during stimulation. The highest synchronization values were found after 50 ms and after 150 ms in HC and after 500 ms in SZ. In the statistical comparison at the first synchronization-peak (after 50 ms) there was no significant difference to the SZ group. In the statistical comparison at the second synchronization-peak (after 150 ms) there was a significant reduction in the SZ group compared to the HC group ($t = 2.42$, $p < 0.05$, two-tailed). In contrast, the statistical comparison between HC and SZ at the maximal synchronization of SZ (after 500 ms) showed no significant results (see Fig. 5).

3.2.2. Secondary auditory cortex (STG)

In both HC and SZ an increase in the lagged phase synchronization was detected during stimulation. The highest synchronization was found after 50 ms in HC and after 500 ms in SZ. In both statistical comparisons (at the synchronization peaks of controls and patients) no significant difference across groups could be detected (see Fig. 5).

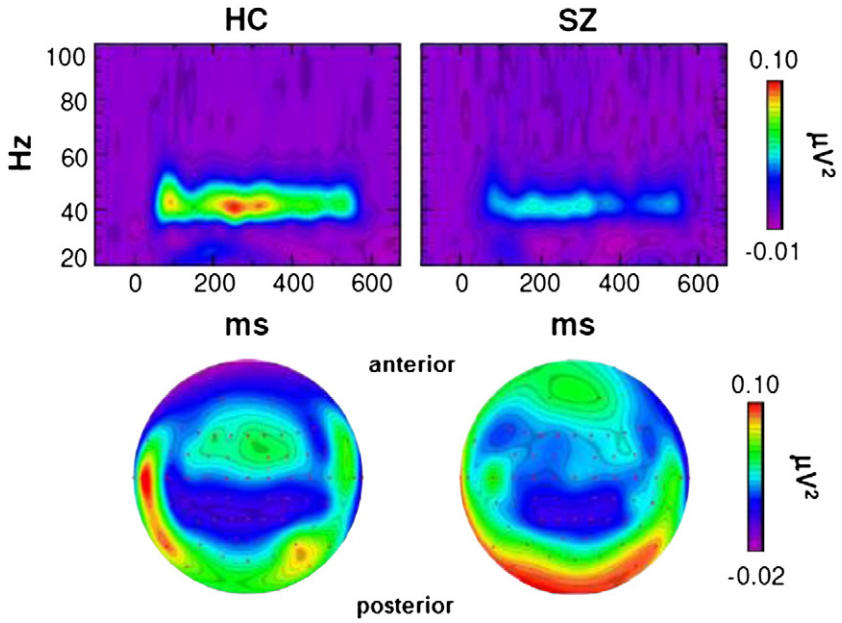

Fig. 3. Scalp EEG data: Time-frequency and topographic maps of evoked power for healthy controls (HC) and schizophrenia patients (SZ) at electrode Fz. Modified from Spencer et al., 2009 (BMC Neurosci 10:85).

3.3. Correlations with demographic variables and auditory hallucination scores

To rule out confounding effects, correlations were calculated between ASSR measures of interest and demographic variables. There were no correlations with age, parental socioeconomic status, handedness, medication dosage or time from admission for both groups.

In the correlation analysis between the Auditory Hallucination score as assessed with the SAPS and the lagged phase synchronization values between left and right *primary* auditory cortex we found a significant positive correlation (Spearman´s rho: 0.56, $p<0.05$, corrected for multiple comparisons, see Fig. 6).

In the correlation analysis between the SAPS Auditory Hallucination score and the lagged phase synchronization values between left and right *secondary* auditory cortex, however, there was no significant correlation.

Table 2
eLORETA localizations of ASSR activation patterns.

Localization	X,Y, Z (MNI)			Current source density in μA/mm² ($\times 10^{-5}$)
Healthy controls				
L temporal lobe, middle temporal gyrus	−65	−10	−15	3.60
L temporal lobe, superior temporal gyrus	−65	−20	0	3.16
L temporal lobe, transverse temporal gyrus	−60	−10	10	2.79
R temporal lobe, middle temporal gyrus	70	−20	−10	4.27
R temporal lobe, superior temporal gyrus	65	−10	0	4.04
R temporal lobe, transverse temporal gyrus	65	−10	10	3.84
Patients with schizophrenia				
L temporal lobe, middle temporal gyrus	−65	−30	−20	4.94
L temporal lobe, superior temporal gyrus	−45	−20	−10	4.26
L temporal lobe, transverse temporal gyrus	−65	−10	10	3.77
R temporal lobe, middle temporal gyrus	50	10	−30	3.78
R temporal lobe, superior temporal gyrus	50	−5	−10	3.73
R temporal lobe, transverse temporal gyrus	60	−10	10	3.21

4. Discussion

This study was intended to use a new methodological approach in order to investigate whether long-range synchrony of gamma oscillations is disturbed in schizophrenia and whether a relationship between inter-hemispheric phase synchronization and auditory hallucination symptoms can be found. The major finding was reduced phase synchronization in schizophrenia only between the left and right primary auditory cortex (Heschl´s gyrus), but not between the bilateral secondary auditory cortices. Furthermore, a positive correlation between auditory hallucination symptom scores and inter-hemispheric phase synchronization was present only for primary auditory cortices, but not for secondary auditory cortices.

In general, analyzing EEG phase synchronization may be a promising tool in order to investigate disturbed functional connectivity in schizophrenia. However, volume conduction effects have been a problem in the investigation of coherence or phase synchrony reports based on scalp channel data (Stam et al., 2007). A considerable strength of our approach was the combination of source localization and the assessment of lagged phase synchrony in a combined approach thus minimizing possible misinterpretations due to volume conduction.

Relevant disturbances in the functional and structural connectivity in schizophrenia have been suggested by several authors (Andreasen et al., 1998; Friston and Frith, 1995; Innocenti et al., 2003; McGlashan and Hoffman, 2000) and during the last few years there has been increasing empirical evidence in agreement with these proposals (Bassett et al., 2008; Garrity et al., 2007; Rotarska-Jagiela et al., 2008; Whitford et al., 2007). Recently, corresponding reductions have been described for both the grey matter of the Heschl´s gyri and the respective white matter tissue, assessed as the decrease of the Fractional Anisotropy (FA) as measured by means of Diffusion Tensor Imaging (DTI) in patients with adolescent schizophrenia (Douaud et

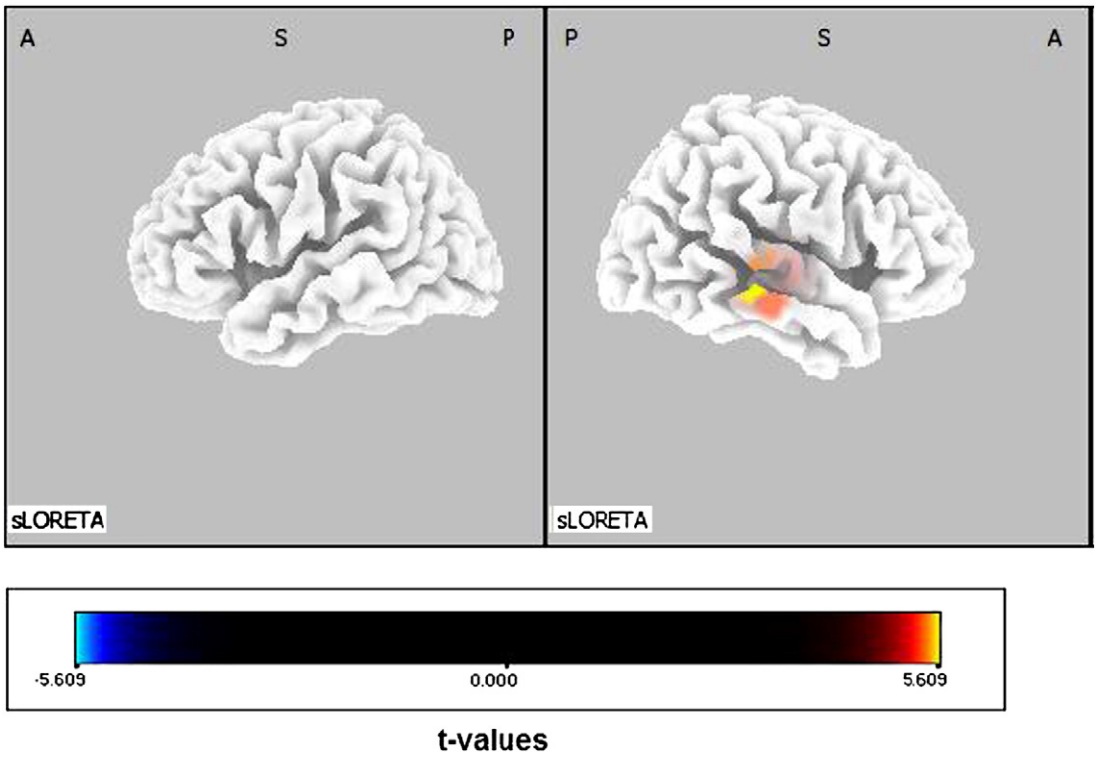

Fig. 4. Statistical map demonstrating differences between HC and SZ at $p<0.05$. There are only regions with increased activation in HC than in SZ (yellow-red): The right superior and middle temporal gyrus. No regions with increased activation in patients can be found. A: Anterior, S: Superior, P: Posterior.

al., 2007). Reductions of the Heschl´s gyri volumes have been described earlier (Hirayasu et al., 2000) and also a connection between Heschl´s gyrus volumes and the severity of auditory hallucinations (Gaser et al., 2004). Alterations of the corpus callosum, which is the major commissural structure for the connection of corresponding auditory areas in each hemisphere are also a common finding in schizophrenia (Arnone et al., 2008). Some authors were suggesting a "hyperconnection" in parts of the CC connecting temporal association cortices and suggested a relationship to positive symptoms (John et al., 2008). Most important for the current study are findings suggesting increased white matter directionality (supposed to represent increased connectivity) in the posterior part of the middle section of the CC/the posterior third of the CC—the area where the auditory fibers are crossing—in schizophrenic patients with auditory hallucinations in comparison to patients without hallucinations (Hubl et al., 2004).

Our results of decreased gamma-phase synchronization between left and right Heschl´s gyri in patients with schizophrenia and a positive correlation between interhemispheric connectivity are well in line with a recent study investigating structural connectivity in patients with schizophrenia. In this DTI study, schizophrenia patients exhibited FA reductions in their frontal fibers crossing via the corpus callosum but at the same time significant positive correlations were observed to the severity of their psychotic symptoms such as hallucinations and delusions (Whitford et al., 2010). These results have been interpreted in such a way that mild asynchronies between the activities of spatially discrete brain regions might give rise to psychotic symptoms. However, severe asynchronies, caused by severe white matter damage might not be incorporable into a coherent phenomenological framework and thus not give rise to psychotic symptoms (Whitford et al., 2010).

The interhemispheric auditory pathway has not yet been discussed in relationship to auditory verbal hallucinations (AVH). However, its relationship to phonological awareness and speech perception might help to understand its role in AVH (for review see Bamiou et al., 2007). The interhemispheric auditory pathway, mainly crossing in the posterior third of the corpus callosum, is responsible for the interhemispheric interplay of prosodic information and syntactic information that is necessary for speech comprehension. For example, patients with a lesion in the posterior third of the corpus callosum do not show an event-related N400 potential in a speech comprehension task requiring the interaction of prosodic and syntactic information (Friederici et al., 2007). In this paradigm a mismatch between the syntactic and prosodic structure of the initial sentence part is associated with an N400 potential in healthy controls. The N400 pattern has been interpreted as the neural correlate of a successful interaction of the left and right auditory areas. While identification of phonemes, words and the syntactic relation between them is processed mainly in the left hemisphere, emotional prosody is processed in the right hemisphere. Thus left and right auditory areas interact during normal on-line spoken language comprehension.

In the current study we found a disturbance in SZ only of the interhemispheric phase synchrony between the primary auditory cortices, but not between the secondary auditory cortices. While this finding has to be seen within the limitations of EEG source localization and needs independent replication, it is never the less interesting, since earlier studies suggest both a pronounced pathology in Heschl´s gyrus (Dierks et al., 1999; Gaser et al., 2004; Salisbury et al., 2007) and in the STG in schizophrenia (Rajarethinam et al., 2000).

In the present study utilizing LORETA we found a reduction of the ASSR in schizophrenia patients in the right temporal lobe. This finding is consistent with the dipole source analysis of the same data set (Spencer et al., 2009), in which ASSR power in a right auditory cortex source was significantly reduced in schizophrenia patients. Thus, two different source localization methods led to the same result. The present study, however, adds the information about disturbed long-range synchronization in the gamma-frequency range.

While disturbed gamma oscillations have been suggested to be related to basic pathopysiological mechanisms in schizophrenia (Uhlhaas and Singer, 2010) and AVH are a frequent symptom of this disease, it is nevertheless interesting to notice that gamma oscillations might be

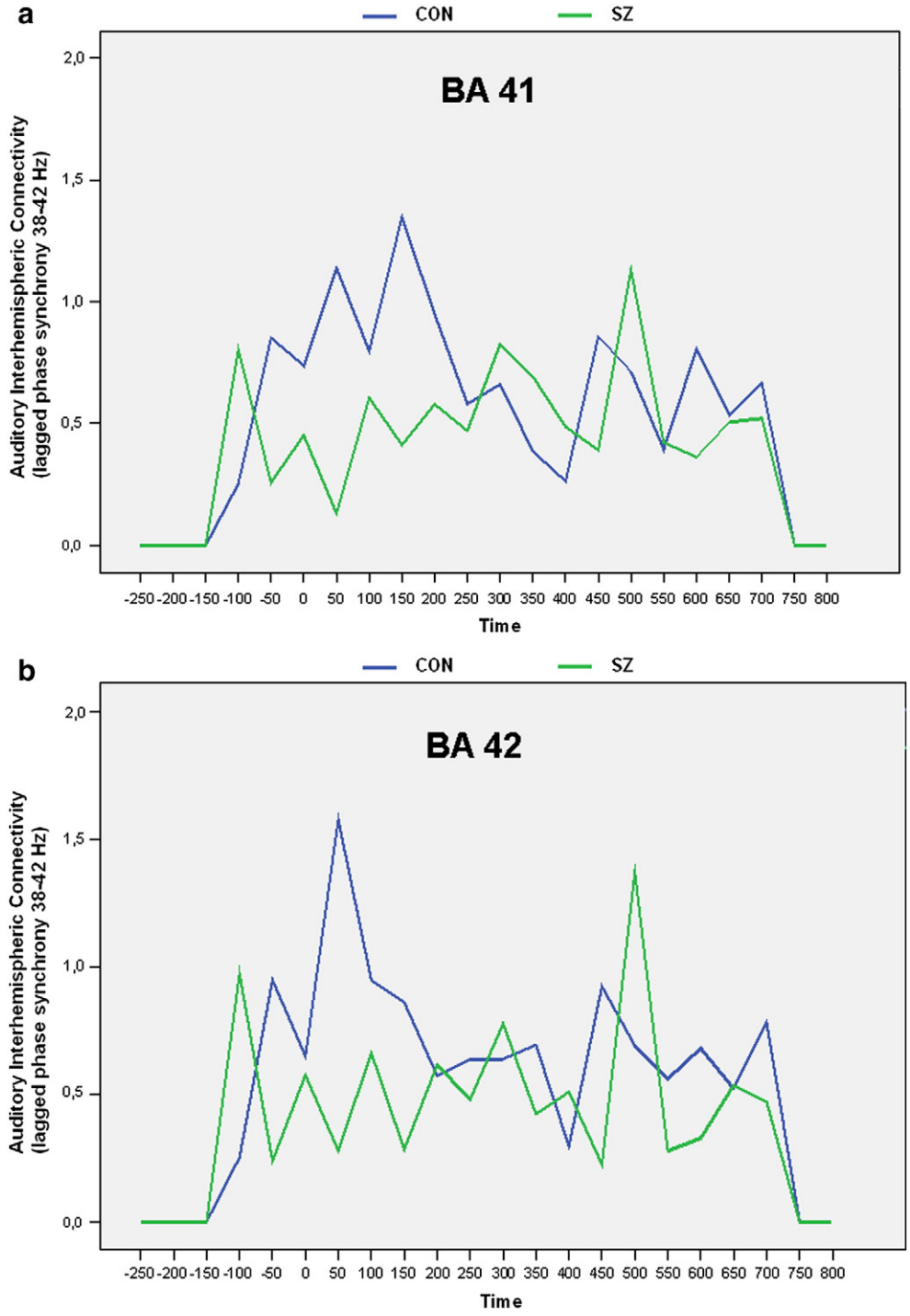

Fig. 5. Phase synchronization during the ASSR in HC (blue) and SZ (green); a) BA 41, b) BA42. Auditory stimulation starts at 0 ms and ends at 500 ms.

related to hallucinations in other modalities such as somatic hallucinations (Baldeweg et al., 1998).

This study focused on the auditory 40 Hz-SSR demonstrating significant findings in temporal areas. However, there also reports of contributions in the frontal lobe, parietal lobe and the cerebellum in the 40 Hz ASSR (Reyes et al., 2005). In addition, there are reports about disturbances in the SSR in schizophrenia in other frequency ranges, such as the 30 Hz response (Spencer et al., 2008). It might be an interesting goal for further investigations to address the question of long-range synchronization between the areas of the extended SSR network and in different frequency-bands.

In summary, the current study reports decreased interhemispheric phase synchrony in SZ between the primary auditory cortices and a positive correlation of this interhemispheric phase synchrony with auditory hallucination scores. The applied technique using a combination of source localization and calculation of lagged phase synchrony might be useful also concerning the investigation of other aspects of disturbed functional connectivity in schizophrenia.

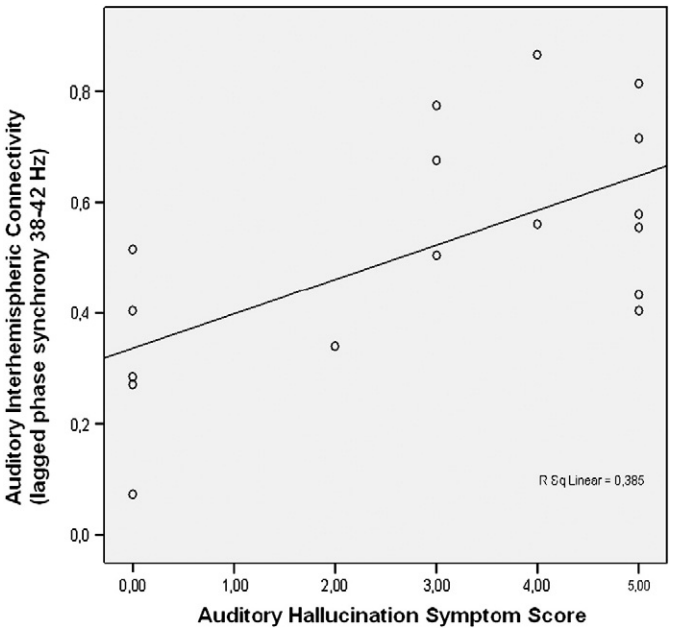

Fig. 6. Spearman´s Correlations between SAPS (scale for the assessment of positive symptoms) auditory hallucination scores and phase synchrony between left and right primary auditory cortex.

Acknowledgments

This work was supported by a US Department of Veterans Affairs Research Enhancement Award Program and Schizophrenia Center (RWM); US National Institute of Mental Health Grants R01 40799 (RWM), R03 076760 (KMS), and R01 MH080187 (KMS); and a NARSAD Young Investigator Award (KMS). CM was supported by a grant of the German Society for Psychiatry, Psychotherapy and Neurology (DGPPN).

References

Andreasen, N.C., 1983. The scale for the Assessment of Negative Symptoms (SANS). University of Iowa, Iowa City.
Andreasen, N.C., 1984. The Scale for the Assessment of Positive Symptoms (SAPS). University of Iowa, Iowa City.
Andreasen, N.C., Paradiso, S., O'Leary, D.S., 1998. "Cognitive dysmetria" as an integrative theory of schizophrenia: a dysfunction in cortical-subcortical-cerebellar circuitry? Schizophr. Bull. 24, 203–218.
Arnone, D., McIntosh, A.M., Tan, G.M., Ebmeier, K.P., 2008. Meta-analysis of magnetic resonance imaging studies of the corpus callosum in schizophrenia. Schizophr. Res. 101, 124–132.
Axmacher, N., Schmitz, D.P., Wagner, T., Elger, C.E., Fell, J., 2008. Interactions between medial temporal lobe, prefrontal cortex, and inferior temporal regions during visual working memory: a combined intracranial EEG and functional magnetic resonance imaging study. J. Neurosci. 28, 7304–7312.
Babiloni, C., Vecchio, F., Buffo, P., Buttiglione, M., Cibelli, G., Rossini, P.M., 2010. Cortical responses to consciousness of schematic emotional facial expressions: a high-resolution EEG study. Hum. Brain Mapp. 31, 1559–1569.
Baldeweg, T., Spence, S., Hirsch, S.R., Gruzelier, J., 1998. Gamma-band electroencephalographic oscillations in a patient with somatic hallucinations. Lancet 22;352 (9128), 620–621.
Bamiou, D.E., Sisodiya, S., Musiek, F.E., Luxon, L.M., 2007. The role of the interhemispheric pathway in hearing. Brain Res. Rev. 56, 170–182.
Bassett, D.S., Bullmore, E., Verchinski, B.A., Mattay, V.S., Weinberger, D.R., Meyer-Lindenberg, A., 2008. Hierarchical organization of human cortical networks in health and schizophrenia. J. Neurosci. 28, 9239–9248.
Benes, F.M., McSparren, J., Bird, E.D., SanGiovanni, J.P., Vincent, S.L., 1991. Deficits in small interneurons in prefrontal and cingulate cortices of schizophrenic and schizoaffective patients. Arch. Gen. Psychiatry 48, 996–1001.
Brenner, C.A., Krishnan, G.P., Vohs, J.L., Ahn, W.Y., Hetrick, W.P., Morzorati, S.L., et al., 2009. Steady state responses: electrophysiological assessment of sensory function in schizophrenia. Schizophr. Bull. 35, 1065–1077.
Csicsvari, J., Jamieson, B., Wise, K.D., Buzsaki, G., 2003. Mechanisms of gamma oscillations in the hippocampus of the behaving rat. Neuron 37, 311–322.
Dierks, T., Linden, D.E., Jandl, M., Formisano, E., Goebel, R., Lanfermann, H., et al., 1999. Activation of Heschl's gyrus during auditory hallucinations [see comments]. Neuron 22, 615–621.
Douaud, G., Smith, S., Jenkinson, M., Behrens, T., Johansen-Berg, H., Vickers, J., et al., 2007. Anatomically related grey and white matter abnormalities in adolescent-onset schizophrenia. Brain 130, 2375–2386.
Dougherty, R.F., Ben-Shachar, M., Deutsch, G.K., Hernandez, A., Fox, G.R., Wandell, B.A., 2007. Temporal-callosal pathway diffusivity predicts phonological skills in children. Proc. Natl Acad. Sci. USA 104, 8556–8561.
Friederici, A.D., von Cramon, D.Y., Kotz, S.A., 2007. Role of the corpus callosum in speech comprehension: interfacing syntax and prosody. Neuron 53, 135–145.
Friston, K.J., Frith, C.D., 1995. Schizophrenia: a disconnection syndrome? Clin. Neurosci. 3, 89–97.
Fuchs, E.C., Doheny, H., Faulkner, H., Caputi, A., Traub, R.D., Bibbig, A., et al., 2001. Genetically altered AMPA-type glutamate receptor kinetics in interneurons disrupt long-range synchrony of gamma oscillation. Proc. Natl Acad. Sci. USA 98, 3571–3576.
Garrity, A.G., Pearlson, G.D., McKiernan, K., Lloyd, D., Kiehl, K.A., Calhoun, V.D., 2007. Aberrant "default mode" functional connectivity in schizophrenia. Am. J. Psychiatry 164, 450–457.
Gaser, C., Nenadic, I., Volz, H.P., Buchel, C., Sauer, H., 2004. Neuroanatomy of "hearing voices": a frontotemporal brain structural abnormality associated with auditory hallucinations in schizophrenia. Cereb. Cortex 14, 91–96.
Hajos, N., Palhalmi, J., Mann, E.O., Nemeth, B., Paulsen, O., Freund, T.F., 2004. Spike timing of distinct types of GABAergic interneuron during hippocampal gamma oscillations in vitro. J. Neurosci. 24, 9127–9137.
Hall, M.H., Taylor, G., Sham, P., Schulze, K., Rijsdijk, F., Picchioni, M., et al., 2009. The early auditory gamma-band response is heritable and a putative endophenotype of schizophrenia. Schizophr. Bull. doi:10.1093/schbul/sbp134.
Herrmann, C.S., Munk, M.H., Engel, A.K., 2004. Cognitive functions of gamma-band activity: memory match and utilization. Trends Cogn. Sci. 8, 347–355.
Hirayasu, Y., McCarley, R.W., Salisbury, D.F., Tanaka, S., Kwon, J.S., Frumin, M., et al., 2000. Planum temporale and Heschl gyrus volume reduction in schizophrenia: a magnetic resonance imaging study of first-episode patients. Arch. Gen. Psychiatry 57, 692–699.
Hubl, D., Koenig, T., Strik, W., Federspiel, A., Kreis, R., Boesch, C., et al., 2004. Pathways that make voices: white matter changes in auditory hallucinations. Arch. Gen. Psychiatry 61, 658–668.
Hugdahl, K., Carlsson, G., Uvebrant, P., Lundervold, A.J., 1997. Dichotic-listening performance and intracarotid injections of amobarbital in children and adolescents. Preoperative and postoperative comparisons. Arch. Neurol. 54, 1494–1500.
Innocenti, G.M., Ansermet, F., Parnas, J., 2003. Schizophrenia, neurodevelopment and corpus callosum. Mol. Psychiatry 8, 261–274.
John, J.P., Shakeel, M.K., Jain, S., 2008. Corpus callosal area differences and gender dimorphism in neuroleptic-naive, recent-onset schizophrenia and healthy control subjects. Schizophr. Res. 103, 11–21.
Kubicki, M., McCarley, R., Westin, C.F., Park, H.J., Maier, S., Kikinis, R., Jolesz, F.A., Shenton, M.E., 2007. A review of diffusion tensor imaging studies in schizophrenia. J. Psychiatr. Res. 41 (1–2), 15–30 (Epub 2005 Jul 14. Review).
Kwon, J.S., O'Donnell, B.F., Wallenstein, G.V., Greene, R.W., Hirayasu, Y., Nestor, P.G., et al., 1999. Gamma frequency-range abnormalities to auditory stimulation in schizophrenia [see comments]. Arch. Gen. Psychiatry 56, 1001–1005.
Lee, C.C., Winer, J.A., 2008. Connections of cat auditory cortex: II. Commissural system. J. Comp. Neurol. 507, 1901–1919.
Leicht, G., Kirsch, V., Giegling, I., Karch, S., Hantschk, I., Moller, H.J., et al., 2010. Reduced early auditory evoked gamma-band response in patients with schizophrenia. Biol. Psychiatry 67, 224–231.
Lewis, D.A., Hashimoto, T., Volk, D.W., 2005. Cortical inhibitory neurons and schizophrenia. Nat. Rev. Neurosci. 6, 312–324.
Lisman, J.E., Coyle, J.T., Green, R.W., Javitt, D.C., Benes, F.M., Heckers, S., et al., 2008. Circuit-based framework for understanding neurotransmitter and risk gene interactions in schizophrenia. Trends Neurosci. 31, 234–242.
Makeig, S., Bell, A., Jung, T.P., Sejnowski, T.J., 1996. Independent component analysis of electroencephalographic data. Adv. Neural Inf. Process. Syst. 8, 145–151.
McGlashan, T.H., Hoffman, R.E., 2000. Schizophrenia as a disorder of developmentally reduced synaptic connectivity. Arch. Gen. Psychiatry 57, 637–648.
Mulert, C., Jager, L., Schmitt, R., Bussfeld, P., Pogarell, O., Moller, H.J., et al., 2004. Integration of fMRI and simultaneous EEG: towards a comprehensive understanding of localization and time-course of brain activity in target detection. Neuroimage 22, 83–94.
Mulert, C., Jäger, L., Propp, S., Karch, S., Störmann, S., Pogarell, O., Möller, H.J., Juckel, G., Hegerl, U., 2005. Sound level dependence of the primary auditory cortex: Simultaneous measurement with 61-channel EEG and fMRI. Neuroimage 15;28 (1), 49–58.
Mulert, C., Juckel, G., Giegling, I., Pogarell, O., Leicht, G., Karch, S., et al., 2006. A Ser9Gly polymorphism in the dopamine D3 receptor gene (DRD3) and event-related P300 potentials. Neuropsychopharmacology 31, 1335–1344.
Mulert, C., Leicht, G., Pogarell, O., Mergl, R., Karch, S., Juckel, G., et al., 2007. Auditory cortex and anterior cingulate cortex sources of the early evoked gamma-band response: relationship to task difficulty and mental effort. Neuropsychologia 45, 2294–2306.
Mulert, C., Leicht, G., Hepp, P., Kirsch, V., Karch, S., Pogarell, O., Reiser, M., Hegerl, U., Jäger, L., Moller, H.J., McCarley, R.W., 2010. Single-trial coupling of the gamma-band response and the corresponding BOLD signal. Neuroimage 49 (3), 2238–2247.
Nichols, T.E., Holmes, A.P., 2002. Nonparametric permutation tests for functional neuroimaging: a primer with examples. Hum. Brain Mapp. 15, 1–25.
Nolte, G., Bai, O., Wheaton, L., Mari, Z., Vorbach, S., Hallett, M., 2004. Identifying true brain interaction from EEG data using the imaginary part of coherency. Clin. Neurophysiol. 115, 2292–2307.
Pascual-Marqui, R.D., 2002. Standardized low-resolution brain electromagnetic tomography (sLORETA): technical details. Methods Find. Exp. Clin. Pharmacol. 24 (Suppl D), 5–12.

Pascual-Marqui, R.D., Michel, C.M., Lehmann, D., 1994. Low resolution electromagnetic tomography: a new method for localizing electrical activity in the brain. Int. J. Psychophysiol. 18, 49–65.
Pastor, M.A., Artieda, J., Arbizu, J., Marti-Climent, J.M., Penuelas, I., Masdeu, J.C., 2002. Activation of human cerebral and cerebellar cortex by auditory stimulation at 40 Hz. J. Neurosci. 22, 10501–10506.
Rajarethinam, R.P., DeQuardo, J.R., Nalepa, R., Tandon, R., 2000. Superior temporal gyrus in schizophrenia: a volumetric magnetic resonance imaging study. Schizophr. Res. 41, 303–312.
Reyes, S.A., Lockwood, A.H., Salvi, R.J., Coad, M.L., Wack, D.S., Burkard, R.F., 2005. Mapping the 40-Hz auditory steady-state response using current density reconstructions. Hear. Res. 204 (1–2), 1–15.
Ribary, U., 2005. Dynamics of thalamo-cortical network oscillations and human perception. Prog. Brain Res. 150, 127–142.
Rotarska-Jagiela, A., Schonmeyer, R., Oertel, V., Haenschel, C., Vogeley, K., Linden, D.E., 2008. The corpus callosum in schizophrenia-volume and connectivity changes affect specific regions. Neuroimage 39, 1522–1532.
Salisbury, D.F., Kuroki, N., Kasai, K., Shenton, M.E., McCarley, R.W., 2007. Progressive and interrelated functional and structural evidence of post-onset brain reduction in schizophrenia. Arch. Gen. Psychiatry 64, 521–529.
Singer, W., 1999. Neuronal synchrony: a versatile code for the definition of relations? Neuron 24, 49-25.
Spencer, K.M., Nestor, P.G., Perlmutter, R., Niznikiewicz, M.A., Klump, M.C., Frumin, M., et al., 2004. Neural synchrony indexes disordered perception and cognition in schizophrenia. Proc. Natl Acad. Sci. USA 101, 17288–17293.
Spencer, K.M., Salisbury, D.F., Shenton, M.E., McCarley, R.W., 2008. Gamma-band auditory steady-state responses are impaired in first episode psychosis. Biol. Psychiatry 64, 369–375.
Spencer, K.M., Niznikiewicz, M.A., Nestor, P.G., Shenton, M.E., McCarley, R.W., 2009. Left auditory cortex gamma synchronization and auditory hallucination symptoms in schizophrenia. BMC Neurosci. 10, 85.
Stam, C.J., Nolte, G., Daffertshofer, A., 2007. Phase lag index: assessment of functional connectivity from multi channel EEG and MEG with diminished bias from common sources. Hum. Brain Mapp. 28, 1178–1193.
Stoll, A.L., 2001. The Psychopharmacology Reference Card. McLean Hospital, Belmont, Massachusetts.
Symond, M.P., Harris, A.W., Gordon, E., Williams, L.M., 2005. "Gamma synchrony" in first-episode schizophrenia: a disorder of temporal connectivity? Am. J. Psychiatry 162, 459–465.
Teale, P., Collins, D., Maharajh, K., Rojas, D.C., Kronberg, E., Reite, M., 2008. Cortical source estimates of gamma band amplitude and phase are different in schizophrenia. Neuroimage 42, 1481–1489.
Teipel, S.J., Pogarell, O., Meindl, T., Dietrich, O., Sydykova, D., Hunklinger, U., Georgii, B., Mulert, C., Reiser, M.F., Möller, H.J., Hampel, H., 2009. Regional networks underlying interhemispheric connectivity: an EEG and DTI study in healthy ageing and amnestic mild cognitive impairment. Hum. Brain Mapp. 30 (7), 2098–2119.
Uhlhaas, P.J., Singer, W., 2010. Abnormal neural oscillations and synchrony in schizophrenia. Nat. Rev. Neurosci. 11, 100–113.
van der Loo, E., Gais, S., Congedo, M., Vanneste, S., Plazier, M., Menovsky, T., et al., 2009. Tinnitus intensity dependent gamma oscillations of the contralateral auditory cortex. PLoS ONE 4, e7396.
Vreugdenhil, M., Jefferys, J.G., Celio, M.R., Schwaller, B., 2003. Parvalbumin-deficiency facilitates repetitive IPSCs and gamma oscillations in the hippocampus. J. Neurophysiol. 89, 1414–1422.
Whitford, T.J., Grieve, S.M., Farrow, T.F., Gomes, L., Brennan, J., Harris, A.W., et al., 2007. Volumetric white matter abnormalities in first-episode schizophrenia: a longitudinal, tensor-based morphometry study. Am. J. Psychiatry 164, 1082–1089.
Whitford, T.J., Kubicki, M., Schneiderman, J.S., O'Donnell, L.J., King, R., Alvarado, J.L., Khan, U., Markant, D., Nestor, P.G., Niznikiewicz, M., McCarley, R.W., Westin, C.F., Shenton, M.E., 2010. Corpus callosum abnormalities and their association with psychotic symptoms in patients with schizophrenia. Biol. Psychiatry May 20. [Epub ahead of print].
Witelson, S.F., 1989. Hand and sex differences in the isthmus and genu of the human corpus callosum. A postmortem morphological study. Brain 112 (Pt 3), 799–835.
Woo, T.U., Miller, J.L., Lewis, D.A., 1997. Schizophrenia and the parvalbumin-containing class of cortical local circuit neurons. Am. J. Psychiatry 154, 1013–1015.
Woo, T.U., Spencer, K.M., McCarley, R.W., 2010. Gamma oscillation deficits and the onset and early progression of schizophrenia. Harv. Rev. Psychiatry 18 (3), 173–189.
Zaidel, E., 1986. Callosal dynamics and right hemisphere language. In: Lepore, F., Ptito, M., Jasper, H.H. (Eds.), The Blackwell Dictionary of Neuropsychology. Blackell, Oxford, pp. 279–285.

2.3 Hearing voices: A role of interhemispheric auditory connectivity?

Diffusion tensor imaging (DTI) is in a unique position to test the relationship between brain structure and function (Johansen-Berg and Rushworth, 2009). Evidence from *in vivo* and post-mortem studies suggests that white matter volume and integrity are altered in patients with schizophrenia (Kubicki et al., 2007; Lim et al., 1999; Rotarska-Jagiela et al., 2008; Shenton et al., 2010). Auditory verbal hallucinations (AVH) are among the most common symptoms in schizophrenia and seem to go along with changes in the structural connectivity of auditory areas (Hubl et al., 2004; Lee et al., 2009; Seok et al., 2007; Whitford et al., 2010). The aim of this study was to specifically test the hypothesis that anatomical connections between bilateral auditory areas are related to the presence of AVH in schizophrenic patients. A combination of DTI and fibretractography was used to quantify fractional anisotropy values across fibre tracts connecting homotopic auditory areas via the corpus callosum (Oh et al., 2009) in first episode paranoid schizophrenic patients with and without auditory hallucinations. We found no difference in the fractional anisotropy (FA) of the interhemispheric auditory fibres between schizophrenic patients and healthy controls. However, the subgroup of patients hearing conversing voices showed increased FA relative to patients without these symptoms and trend wise to healthy controls. This study provides a complementary structural investigation of the pathophysiology of auditory hallucinations in schizophrenia. Our findings suggest that in addition to local deficits in the left auditory cortex and disturbed frontotemporal connectivity, the interhemispheric auditory pathway might be involved in the pathogenesis of auditory verbal hallucinations.

The World Journal of Biological Psychiatry, 2011; 00: 1–6

BRIEF REPORT

Hearing voices: A role of interhemispheric auditory connectivity?

CHRISTOPH MULERT[1,2,3], VALERIE KIRSCH[1,3], THOMAS J. WHITFORD[1,4], JORGE ALVARADO[1], PAULA PELAVIN[1], ROBERT W. MCCARLEY[1,5], MAREK KUBICKI, DEAN F. SALISBURY[6] & MARTHA E. SHENTON[1,5,7]

[1]*Department of Psychiatry, Psychiatry Neuroimaging Laboratory, Brigham and Women's Hospital, Harvard Medical School, Boston, MA, USA,* [2]*University Medical Center Hamburg-Eppendorf, Department of Psychiatry and Psychotherapy, Psychiatry Neuroimaging Branch, Hamburg, Germany,* [3]*Department of Psychiatry, LMU Munich, Germany,* [4]*Melbourne Neuropsychiatry Centre, Department of Psychiatry, University of Melbourne and Melbourne Health, Melbourne, VIC, Australia,* [5]*Department of Psychiatry, VA Boston Healthcare System and Harvard Medical School, Brockton, MA, USA,* [6]*Cognitive Neuroscience Laboratory, McLean Hospital, Department of Psychiatry, Harvard Medical School, Belmont, MA, USA, and* [7]*Surgical Planning Laboratory, MRI Division, Department of Radiology, Brigham and Women's Hospital, Harvard Medical School, Boston, MA*

Abstract

Objectives. Auditory verbal hallucinations (AVH) are among the most common symptoms in schizophrenia. Earlier studies suggest changes in the structural connectivity of auditory areas involved in the pathophysiology of auditory hallucinations. Combining diffusion tensor imaging (DTI) and fibre tractography provides a unique opportunity to visualize and quantify entire fibre bundles. *Methods.* Fibre tracts connecting homotopic auditory areas via the corpus callosum were identified with DTI in ten first episode paranoid schizophrenia patients and ten healthy controls. Regions of interest were drawn manually, to guide tractography, and fractional anisotropy (FA) – a measure of fibre integrity – was calculated and averaged over the entire tract for each subject. *Results.* There was no difference in the FA of the interhemispheric auditory fibres between schizophrenic patients and healthy controls. However, the subgroup of patients hearing conversing voices showed increased FA relative to patients without these symptoms ($P = 0.047$) and trendwise increased FA relative to healthy controls ($P = 0.066$). In addition, a trendwise correlation between FA values and AVH symptoms ($P = 0.089$) was found. *Conclusions.* Our findings suggest that in addition to local deficits in the left auditory cortex and disturbed fronto-temporal connectivity, the interhemispheric auditory pathway might be involved in the pathogenesis of AVH.

Key words: *Schizophrenia, brain imaging, MRI, positive symptoms, biological psychiatry*

Introduction

Brain imaging has provided a unique and unprecedented opportunity to understand the biological basis of psychopathological symptoms in psychiatric diseases. While it has long been speculated that schizophrenia might be a disease with disturbed connectivity of brain regions (Friston and Frith 1995; Weinberger and Lipska 1995; Andreasen et al. 1998), current methodological advances in Diffusion Tensor Imaging (DTI) and fibre tracking have enabled us now to test specific hypotheses concerning the relationship between the connectivity of distinct brain regions and psychopathological symptoms of interest (for review see (Kubicki et al. 2007). Since auditory verbal hallucinations (AVH) are among the most prominent symptoms in schizophrenia, different brain imaging methods have been used in order to investigate them. For example, Functional Magnetic Resonance Imaging (fMRI) and Positron Emission Tomography (PET) during AVH have both shown that activation of the auditory cortex is observed (Dierks et al. 1999; Shergill et al. 2000), as well as other regions including the inferior frontal cortex and the anterior cingulate cortex (ACC). Interestingly, several authors have described bilateral activation of the auditory cortex during AVH (Copolov et al. 2003; Lennox et al. 2000), while others have described only unilateral activation, typically on the left side (Dierks et al. 1999; Suzuki et al. 1993) or both uni- and bilateral patterns in different

Correspondence: Christoph Mulert, Martinistrasse 52, 20246 Hamburg, Germany. Tel: +49 40 7410 59520. Fax: +49 40 7410 59805. E-mail: c.mulert@uke.de

(Received 27 September 2010; accepted 24 February 2011)

ISSN 1562-2975 print/ISSN 1814-1412 online © 2011 Informa Healthcare
DOI: 10.3109/15622975.2011.570789

patients within the same study (van de Ven et al. 2005) (for a review see Allen et al. 2008). In addition, it has been shown that there is a positive correlation between the subjective reality of hallucinations and the functional coupling of the inferior frontal cortex with the auditory cortex (Raij et al. 2009).

Using DTI, increased anisotropy was shown in a number of white matter structures in patients with AVH. Hubl et al. (2004) showed increased fractional anisotropy (FA) in the lateral temporoparietal section of the arcuate fasciculus. This tract connects language production areas with auditory processing areas. Other findings in this study included increased FA values in the corpus callosum both in anterior parts (where fibres connecting frontal areas are crossing) and posterior parts (in an area where fibres connecting auditory areas are crossing). In another investigation patients with AVH were shown to have increased anisotropy in the superior longitudinal fascicule and the anterior cingulum (Shergill et al. 2007). More recently, increased water diffusivity was reported in the left side superior temporal gyrus in patients with schizophrenia, which was associated with auditory hallucinations (Lee et al. 2009).

Since many brain imaging findings concerning AVH are related to either basic auditory areas or language production and perception areas, it is interesting to note that during more recent years there has been increasing evidence for an important role of the interhemispheric pathway connecting bilateral auditory areas for speech perception. For example, phonological awareness is associated with higher diffusivity perpendicular to the main axis of the corpus callosum in its posterior part that is connecting the temporal lobes (Dougherty et al. 2007). Phonological awareness refers to an individual's awareness of the sound structure, or phonological structure, of a spoken word. It includes the ability to auditorily distinguish units of speech, such as a word's syllables and a syllable's individual phonemes. This finding has been interpreted as suggesting that subjects with high phonological awareness have reduced interhemispheric connectivity and are better at processing rapidly changing auditory stimuli.

In a more recent study using an auditory speech perception task and probabilistic tractography, a significant relationship between the anatomical connectivity between the superior temporal lobe areas and speech perception performance has been described (Westerhausen et al. 2009). It is interesting that in both aforementioned studies specific structure–function associations between phonological awareness/auditory speech perception and the anatomical connections, between the bilateral auditory areas, as assessed by fibre tractography, were found in healthy subjects.

Accordingly, it was the aim of the present study to specifically test the hypothesis of whether or not anatomical connections between bilateral auditory areas are related to the presence of AVH in schizophrenic patients. Since increased anisotropy in posterior parts of the corpus callosum, probably connecting the bilateral auditory areas, was described earlier in schizophrenic patients with AVH (Hubl et al. 2004), we predicted increased anisotropy in schizophrenic patients with AVH across the connecting interhemispheric auditory pathway. We used a combination of DTI and fibre tractography that was recently introduced in order to allow a quantification of fractional anisotropy values across a fibre tract of interest (Oh et al. 2009).

Materials and methods

Subjects

Ten subjects with paranoid schizophrenia and ten healthy controls participated in this study (see Table I). The patients were recruited from inpatients at McLean Hospital, a private psychiatric hospital affiliated with Harvard Medical School. Healthy control subjects were recruited through newspaper and online advertisement. After a complete description of the study, written informed consent was obtained from all participants. The study was approved by the local institutional review boards at McLean Hospital, Brigham and Women's Hospital, the VA Boston Healthcare System, and Harvard Medical School. The protocols for diagnosis and clinical evaluations have been previously described in detail (see (Salisbury et al. 2007) and Supplementary Material available online). This study was conducted in accordance with the guidelines of the current version of the "Declaration of Helsinki".

DTI acquisition

Line-scan DTIs (Kubicki et al. 2004) were acquired with a quadrature head coil on a 1.5-Tesla GE Echospeed system (General Electric Medical Systems, Milwaukee, WI) using the following scanning parameters: six gradient directions at $b = 1000$ s/mm^2, two baseline images ($b = 5$ s/mm^2), FOV 220 $\times$ 165 mm; 128 $\times$ 96 scan matrix; slice thickness = 4 mm; interslice distance = 1 mm; receiver bandwidth $\pm$ 4 kHz; echo time = 64 ms; effective repetition time = 2592 ms; scan time = 60 s per slice selection.

ROI definition and preprocessing

In order to extract the fibre tracts connecting the bilateral auditory areas, we used a seeding

Table I. Demographic and clinical characteristics of subjects.

Demographic	SZ (total) $n = 10$ Mean ± SD	SZ (AVH) $n = 5$ Mean ± SD	SZ (NAVH) $n = 5$ Mean ± SD	HC $n = 10$ Mean ± SD	*P* value
Age (years)	26.9 ± 8.6	28.8 ± 2.3	25.0 ± 7.1	22.4 ± 2.2	0.126
Sex, male/female	8/2	4/1	4/1	8/2	1
Handedness	0.69 ± 0.36	0.86 ± 0.19	0.52 ± 0.43	0.66 ± 0.21	0.828
Socioeconomic status	2.8 ± 1.14	2.8 ± 1.10	2.8 ± 1.30	2.2 ± 0.63	0.162
Parents' socioeconomic status	1.2 ± 0.45	1.2 ± 0.45	1.2 ± 0.45	1.5 ± 0.71	0.264
Education (years)	14.0 ± 2.3	14.2 ± 1.8	13.8 ± 2.9	14.4 ± 1.8	0.635
Mini-Mental State Examination score	28.2 ± 1.75	28.2 ± 1.92	28.2 ± 1.79	29.8 ± 0.42	0.012
WAIS-III score					
Information	12.7 ± 2.70	14.6 ± 1.67	10.8 ± 2.17	13.9 ± 1.66	0.248
Digits span	9.8 ± 2.57	8.8 ± 1.79	10.8 ± 3.03	11.3 ± 2.16	0.175
Global Assessment Scale score	31.67 ± 5.82	30.0 ± 2.0	33.33 ± 8.50	N/A	N/A
Total Positive and Negative Syndrome Scale score	73.5 ± 14.6	67.0 ± 8.8	80.0 ± 17.2	N/A	N/A
Negative Syndrome Scale score	16.1 ± 6.2	13.6 ± 4.3	18.6 ± 7.2	N/A	
Positive Syndrome Scale score	20.5 ± 3.0	19.2 ± 3.6	21.8 ± 1.6	N/A	
Medication dose (chlorpromazine equivalent /mg/d)	239.6 ± 122.1	254.2 ± 71.2	225 ± 170.8	N/A	N/A
Duration of illness from first hospitalization to scan, median (range) (mo)	5.27 ± 6.21 (0.17–16)	5.70 ± 7.35 (1–16)	4.83 ± 5.68 (1–12)	N/A	N/A
Duration of medication use, median (range) (mo)	0.9 ± 0.44 (0.4–1.4)	1.12 ± 1.09 (0.3–2.7)	1.0 ± 0.75 (0.3–2.7)	N/A	N/A

SZ, schizophrenia; HC, healthy control; N/A, not applicable; WAIS, Wechsler Adult Intelligence Scale; mo, months; AVH, auditory verbal hallucinations; SD, standard deviation.

tractography technique, followed by a selection process that only preserves tracts going through specific combinations of regions of interest (ROIs) (Conturo et al. 1999; Mori et al. 1999). Initial seeding was done in a midsagittal ROI covering the posterior third of the corpus callosum where the auditory fibres crossed. A single rater (V.K.), blind to diagnosis, gender and age drew the ROIs for all subjects.

Diffusion-tensor imaging and preprocessing

Diffusion Tensor Images (DTIs) were constructed from the Diffusion-Weighted Images using a least-squares estimation. Deterministic (streamline) tractography was implemented in the Slicer 2.7. software package (www.slicer.org), as described previously (Oh et al. 2007). Tractography was initiated from every voxel defined by the ROI (see above), and followed the direction defined by the principal eigenvector. A step size of 0.5 mm was employed, with a radius of curvature >0.87 mm. Tractography was terminated upon reaching a voxel of FA <0.15 (the stopping criterion). A coronal ROI was defined for each subject at the level of the splenium (i.e. where the tapetum could be discretely identified (Huang et al. 2005), and fibres were excluded if they failed to pass thorough this ROI. The purpose of the exclusion ROI was to ensure that only CC fibres connecting superior temporal cortices remained in the analysis. Figure 1 illustrates the auditory CC fibres extracted from one representative subject. For each subject, FA was calculated for every voxel through which any of the auditory CC fibres passed, and mean FA was calculated by averaging the FA of these voxels (Basser and Pierpaoli 1996).

Statistical analysis

Statistical analyses were performed using the SPSS-software package (16.0) with a personal computer. Due to the small sample size Kruskal–Wallis tests were performed to assess group differences between the three subgroups in demographic and clinical characteristics except for gender. We used Mann–Whitney *U*-tests in order to compare mean FA values between patients with schizophrenia and healthy controls. Correlation analyses between AVH symptoms and FA values were performed as Spearman correlation analyses. The significance level was set at $\alpha = 0.05$ in all analyses.

Results

The demographic and clinical characteristics of the present samples are shown in Table I. There were no

significant differences among the three groups in terms of age, gender, or years of education.

There was no difference in mean FA values in the comparison of all schizophrenic patients to the healthy control group. However, schizophrenic patients with AVH demonstrated increased FA values in the interhemispheric auditory pathway in comparison to patients without AVH (Mean FA = 0.514 ± 0.032; $Z = -1.984$; $P = 0.047$, see Figure 1). Moreover, schizophrenic patients with AVH demonstrated marginally increased FA values compared to healthy controls (Mean FA = 0.547 ± 0.175 vs. 0.506 ± 0.060; $Z = -1.837$; $P = 0.066$).

We found a statistical trend towards a positive correlation between FA values and AVH symptoms (Spearman $\rho = 0.46$, $P = 0.089$).

In an exploratory analysis of correlations between FA and psychopathological measures and between FA and the chlorpromazine equivalents, we found no statistically significant correlations between FA reduction and factors or items from the Positive and Negative Syndrome Scale nor between FA values and chlorpromazine equivalent values.

Discussion

This study investigated the relationship between the auditory interhemispheric pathway and AVH in patients with a first episode of schizophrenia. We used a combination of DTI and fibre tractography in order to quantify mean diffusion values specifically across the fibre bundles of interest. In line with our hypothesis we found increased FA values in the interhemispheric pathway in patients with AVH, but not in patients without AVH.

While this is the first study to specifically test this hypothesis, a previous study using DTI also showed (among other findings) increased FA values in the posterior part of the corpus callosum in schizophrenic patients (in an area where the interhemispheric auditory fibres cross) (Hubl et al. 2004), and a more recent study showed a positive correlation between auditory hallucination scores and FA values in the superior temporal gyrus (Lee et al. 2009).

According to an influential concept, hallucinations result from attributing one's own inner speech to an external agency (Frith 1992). This has been hypothesized to be related to a functional disconnection of frontal brain areas and brain areas concerned with perception (Friston and Frith 1995). This concept is consistent with the finding of increased FA values in the arcuate fasciculus (Hubl et al. 2004), a tract that connects language production areas in the frontal lobe (e.g., Broca's area) with auditory processing and language perception areas in the temporal lobe.

While the interhemispheric pathway has been investigated with respect to phonological awareness and speech perception, it has (to the best of our knowledge) not been investigated with respect to its association with AVH. However, our finding is in line with a recent electroencephalography (EEG) study describing a positive correlation between synchronization of bilateral auditory areas and hallucination symptom scores (Mulert et al. 2010). Apart from that, the relationship to phonological awareness and speech perception might help to understand the role of the interhemispheric pathway the pathophysiology of AVH. The interhemispheric auditory pathway, crossing in the posterior third of the corpus callosum, is responsible for the interhemispheric

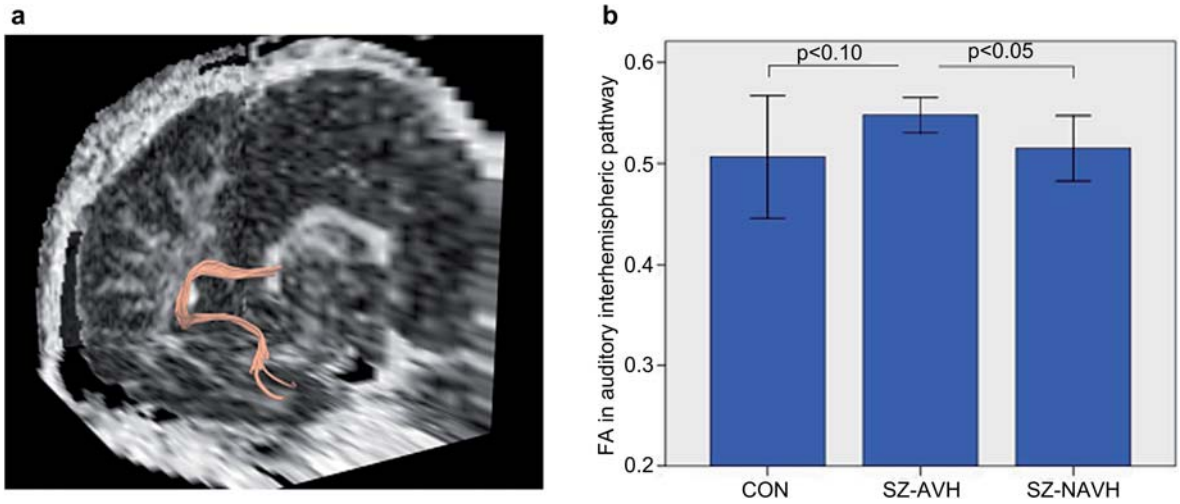

Figure 1. (a) 3D reconstruction of the right-hemisphere fibre tracking (temporo-callosal pathway) for a single subject in native space. (b) Group comparisons of fractional anisotropy (FA) ± 1 SD in the auditory interhemispheric pathway in healthy controls (CON), schizophrenic patients with auditory verbal hallucinations (SZ-AVH) and schizophrenic patients without auditory verbal hallucinations (SZ-NAVH). Mann–Whitney *U*-tests showed significant increased FA values in SZ-AVH in comparison to SZ-NAVH ($P = 0.047$) and trendwise increased FA relative to healthy controls ($P = 0.066$).

interplay of prosodic information and syntactic information that is necessary for speech comprehension. For example, patients with a lesion in the posterior third of the corpus callosum do not show an event-related N400 potential in a speech comprehension task requiring the interaction of prosodic and syntactic information (Friederici et al. 2007). There are now also DTI tractography studies demonstrating a structure–function relationship between the auditory interhemispheric pathway and phonological awareness or speech comprehension (Dougherty et al. 2007; Westerhausen et al. 2009).

The overall picture concerning the relationship between DTI findings and psychopathological symptoms in schizophrenia such as AVH is far from being completely understood. While the present finding is in line with previous findings of positive correlations between FA values in different fibre tracts and positive symptoms such as AVH (Seok et al. 2007) there are also reports of reduced FA values in speech related fibre tracts and negative correlations between FA values and psychopathological measurements (Phillips et al. 2009). In a recent DTI study, schizophrenia patients exhibited FA reductions in their frontal fibres crossing via the corpus callosum but at the same time significant positive correlations were observed to the severity of their psychotic symptoms such as hallucinations and delusions (Whitford et al. 2010). These results have been interpreted in such a way that mild asynchronies between the activities of spatially discrete brain regions might give rise to psychotic symptoms. However, severe asynchronies, caused by severe white matter damage might not be incorporable into a coherent phenomenological framework and thus not give rise to psychotic symptoms (Whitford et al. 2010).

Limitations

Since the sample size in the present study is small, our results in ten first episode patients need to be viewed as preliminary, and require replication with increased sample sizes.

In summary, our results suggest that the inter-individual variability of the auditory interhemispheric pathway, known to be related to phonological awareness and speech perception, might also play an important role in the pathogenesis of AVH.

Acknowledgments

This work was supported by a grant of the German Society for Psychiatry, Psychotherapy and Neurology (Imaging Award 2007)(CM), by an Overseas-Based Biomedical Training Fellowship from the National Health and Medical Research Council of Australia (NHMRC 520627), administered through the Melbourne Neuropsychiatry Centre at the University of Melbourne (TW), by. the Department of Veterans Affairs (Merit Award to RWM and to MES, Schizophrenia Center Award to RWM and MES, Middleton Award to RWM), by the National Institute of Health (R01 MH 40799, R01 MH 052807, P50MH080272 to RWM; R01 MH58704 to DFS, and R01 MH 50740 to MES and a K05 MH 070047 award to MES), and NARSAD awards (DFS and MES). Kathrin Holzschneider was involved in the final editing of the paper.

Statement of Interest

None to declare.

References

Allen P, Laroi F, McGuire PK, Aleman A. 2008. The hallucinating brain: a review of structural and functional neuroimaging studies of hallucinations. Neurosci Biobehav Rev 32:175–191.

Andreasen NC, Paradiso S, O'Leary DS. 1998. "Cognitive dysmetria" as an integrative theory of schizophrenia: a dysfunction in cortical-subcortical-cerebellar circuitry? Schizophr Bull 24:203–218.

Basser PJ, Pierpaoli C. 1996. Microstructural and physiological features of tissues elucidated by quantitative-diffusion-tensor MRI. J Magn Reson B 111:209–219.

Conturo TE, Lori NF, Cull TS, Akbudak E, Snyder AZ, Shimony JS, et al. 1999. Tracking neuronal fiber pathways in the living human brain. Proc Natl Acad Sci USA 96:10422–10427.

Copolov DL, Seal ML, Maruff P, Ulusoy R, Wong MT, Tochon-Danguy HJ, Egan GF. 2003. Cortical activation associated with the experience of auditory hallucinations and perception of human speech in schizophrenia: a PET correlation study. Psychiatry Res 122:139–152.

Dierks T, Linden DE, Jandl M, Formisano E, Goebel R, Lanfermann H, Singer W. 1999. Activation of Heschl's gyrus during auditory hallucinations [see comments]. Neuron 22: 615–621.

Dougherty RF, Ben-Shachar M, Deutsch GK, Hernandez A, Fox GR, Wandell BA. 2007. Temporal-callosal pathway diffusivity predicts phonological skills in children. Proc Natl Acad Sci USA 104:8556–8561.

Friederici AD, von Cramon DY, Kotz SA. 2007. Role of the corpus callosum in speech comprehension: interfacing syntax and prosody. Neuron 53:135–145.

Friston KJ, Frith CD. 1995. Schizophrenia: a disconnection syndrome? Clin Neurosci 3:89–97.

Frith CD. 1992. The cognitive neuropsychology of schizophrenia. Hove: Lawrence Erlbaum.

Huang H, Zhang J, Jiang H, Wakana S, Poetscher L, Miller MI, et al. 2005. DTI tractography based parcellation of white matter: application to the mid-sagittal morphology of corpus callosum. Neuroimage 26:195–205.

Hubl D, Koenig T, Strik W, Federspiel A, Kreis R, Boesch C, et al. 2004. Pathways that make voices: white matter changes in auditory hallucinations. Arch Gen Psychiatry 61:658–668.

Kubicki M, Maier SE, Westin CF, Mamata H, Ersner-Hershfield H, Estepar R, et al. 2004. Comparison of single-shot

echo-planar and line scan protocols for diffusion tensor imaging. Acad Radiol 11:224–232.

Kubicki M, McCarley R, Westin CF, Park HJ, Maier S, Kikinis R, et al. 2007. A review of diffusion tensor imaging studies in schizophrenia. J Psychiatr Res 41:15–30.

Lee K, Yoshida T, Kubicki M, Bouix S, Westin CF, Kindlmann G, et al. 2009. Increased diffusivity in superior temporal gyrus in patients with schizophrenia: a Diffusion Tensor Imaging study. Schizophr Res 108:33–40.

Lennox BR, Park SB, Medley I, Morris PG, Jones PB. 2000. The functional anatomy of auditory hallucinations in schizophrenia. Psychiatry Res 100:13–20.

Mori S, Crain BJ, Chacko VP, van Zijl PC. 1999. Three-dimensional tracking of axonal projections in the brain by magnetic resonance imaging. Ann Neurol 45:265–269.

Mulert C, Kirsch V, Pascual-Marqui R, McCarley RW, Spencer KM. 2011. Long-range synchrony of gamma oscillations and auditory hallucination symptoms in schizophrenia. Int J Psychophysiol 79:55–63. Epub 2010 Aug 14.

Oh JS, Song IC, Lee JS, Kang H, Park KS, Kang E, Lee DS. 2007. Tractography-guided statistics (TGIS) in diffusion tensor imaging for the detection of gender difference of fiber integrity in the midsagittal and parasagittal corpora callosa. Neuroimage 36:606–616.

Oh JS, Kubicki M, Rosenberger G, Bouix S, Levitt JJ, McCarley RW, et al. 2009. Thalamo-frontal white matter alterations in chronic schizophrenia: a quantitative diffusion tractography study. Hum Brain Mapp 30:3812–3825.

Phillips OR, Nuechterlein KH, Clark KA, Hamilton LS, Asarnow RF, Hageman NS, et al. 2009. Fiber tractography reveals disruption of temporal lobe white matter tracts in schizophrenia. Schizophr Res 107:30–38.

Raij TT, Valkonen-Korhonen M, Holi M, Therman S, Lehtonen J, Hari R. 2009. Reality of auditory verbal hallucinations. Brain 132:2994–3001. Epub 2009 Jul 20.

Salisbury DF, Kuroki N, Kasai K, Shenton ME, McCarley RW. 2007. Progressive and interrelated functional and structural evidence of post-onset brain reduction in schizophrenia. Arch Gen Psychiatry 64:521–529.

Seok JH, Park HJ, Chun JW, Lee SK, Cho HS, Kwon JS, Kim JJ. 2007. White matter abnormalities associated with auditory hallucinations in schizophrenia: a combined study of voxel-based analyses of diffusion tensor imaging and structural magnetic resonance imaging. Psychiatry Res 156:93–104.

Shergill SS, Brammer MJ, Williams SC, Murray RM, McGuire PK. 2000. Mapping auditory hallucinations in schizophrenia using functional magnetic resonance imaging. Arch Gen Psychiatry 57:1033–1038.

Shergill SS, Kanaan RA, Chitnis XA, O'Daly O, Jones DK, Frangou S, et al. 2007. A diffusion tensor imaging study of fasciculi in schizophrenia. Am J Psychiatry 164:467–473.

Suzuki M, Yuasa S, Minabe Y, Murata M, Kurachi M. 1993. Left superior temporal blood flow increases in schizophrenic and schizophreniform patients with auditory hallucination: a longitudinal case study using 123I-IMP SPECT. Eur Arch Psychiatry Clin Neurosci 242:257–261.

van de Ven VG, Formisano E, Roder CH, Prvulovic D, Bittner RA, Dietz MG, et al. 2005. The spatiotemporal pattern of auditory cortical responses during verbal hallucinations. Neuroimage 27:644–655.

Weinberger DR, Lipska BK. 1995. Cortical maldevelopment, anti-psychotic drugs, and schizophrenia: a search for common ground. Schizophr Res 16:87–110.

Westerhausen R, Gruner R, Specht K, Hugdahl K. 2009. Functional relevance of interindividual differences in temporal lobe callosal pathways: a DTI tractography study. Cereb Cortex 19:1322–1329.

Whitford TJ, Kubicki M, Schneidermann JS, O'Donnell LJ, King R, Alvarado JL, et al. 2010. Corpus callosum abnormalities and their association with psychotic symptoms in patients with schizophrenia. Biol Psychiatry 68:70–77.

Supplementary material available online

Subjects

Supplementary Material for Mulert C, Kirsch V, Whitford TJ, Alvarado J, Pelavin P, McCarley RW, Kubicki M, Salisbury DF & Shenton ME. Hearing voices: A role of interhemispheric auditory connectivity? Biol Psychiatry, 2011 doi 10.3109/15622975.2011.570789.

Subjects

Patients and controls were aged 19 to 44 years, had estimated IQ greater than 75 (measured by the Wechsler Adult Intelligence Scale-third edition) were all right-handed and had a negative history of seizures, head trauma with loss of consciousness, neurologic disorder, and alcohol or drug detox within 5 years. Medication history, prior to first hospitalization, if present, was assessed by patient report and by reviewing the medical record when possible. Healthy control subjects had no axis I or II psychiatric disorder, according to the Structured Clinical Interview for DSM IV (SCID) Non Patient Edition (SCID-I/NP), Structured Clinical Interview for DSM IV Axis II Personality Disorders). Patients were diagnosed with schizophrenia according to the DSM-IV criteria (SCID) using the SCID edition for patients (SCID-I/P) and information from the medical record. All patients included in this study were diagnosed as paranoid. At the time of scan, patients were variously receiving second generation antipsychotics. Antipsychotic medication dosage was calculated in terms of chlorpromazine equivalents. The following formula was applied: chlorpromazine* 1 + thioridazine*1 + mesoridazine*2 + loxapine*8.33 + perphenazine*10 + molindone*10 + trifluoperazine*20 + thiothixine*20 + fluphenazine* 50 + haloperidol*50 + pimozide*100 + clozapine* 0.5 + quetiapine*1 + olanzapine*20 + risperidone*100 + ziprasidone*5 + aripriprazol*16.67. Within the SZ group, the following numbers of subjects received additional medications: mood stabilizers: 3, anti-depressant drugs: 6, anxiolytic drugs: 3.

Clinical evaluations within 2-3 weeks of scanning included the Positive and Negative Syndrome Scale; the Mini-Mental State Examination (MMSE); the information, digits forward and digits backward subscales of WAIS-III; and the Global Assessment Scale. We also evaluated handedness using the Edinburgh Inventory (Oldfield 1971) and the socioeconomic status of patients and control subjects and of their parents using the Hollingshead Two-Factor measure. Information about Hallucination symptoms in the patients was obtained using the Scale for the Assessment of Positive Symptoms (SAPS). In order to get subgroups with equal numbers of subjects, subgroups of patients according to the presence of auditory verbal hallucinations (AVH) was based on the presence of conversing voices (5 from 10 patients) in the SAPS. Demographic and clinical data and inter-group comparisons are summarized in Table 1. The groups did not differ on age, gender proportion, handedness, education, parental socioeconomic status, however there was a small but significant group difference concerning the Mini-Mental scores ($p = 0.043$) and the WAIS-III Information scores ($p = 0.040$).

Reference

Oldfield RC (1971): The assessment and analysis of handedness: the Edinburgh inventory. *Neuropsychologia* 9:97–113.

2.4 Avoiding the ballistocardiogram (BCG) artifact of EEG data acquired simultaneously with fMRI by puls-triggered presentation of stimuli

This study focuses on an ongoing matter of concern relating to the quality of EEG–fMRI integration. *In vivo* simultaneous acquisition of electroencephalography (EEG) and functional magnetic resonance imaging (fMRI) data non- invasively offer a much deeper understanding of the analysis of tempo-spatial dynamics of brain activity in cognitive processing (Benar et al., 2007; Debener et al., 2006; Eichele et al., 2005; Karch et al., 2010; Mulert et al., 2009; Mulert et al., 2008; Ritter and Villringer, 2006). However EEG signals recorded simultaneously to fMRI are heavily contaminated by artifacts (Goldman et al., 2000; Ives et al., 1993; Kruggel et al., 2000). In particular the correction of the balistocardiogram (BCG) remains as yet unsatisfactorily solved and limits the methodical coupling of EEG and fMRI information (Debener et al., 2007; Grouiller et al., 2007; Laufs et al., 2008; Vanderperren et al., 2010; Viola et al., 2009). Methods that are currently available typically remove the BCG artifact either in post-recording or real-time signal processing (Bonmassar et al., 2002; Masterton et al., 2007; Niazy et al., 2005; Siniatchkin et al., 2007; Srivastava et al., 2005). The present work suggests a measurement method that avoids BCG artifacts during data acquisition by taking advantage of the observation that the main influence on the BCG artifact is generally limited to a time interval of 150- 500 ms post- QRS complex (Allen et al., 1998; Debener et al., 2008). In our simulations we are able to show that pulse-triggered (PT) stimuli presentation can significantly improve the estimation of the simulated evoked potential. Additionally we demonstrate in preliminary data that PT measurement works in a real-life situation. This study contributes to an optimization of evoked potential estimations in the MR scanner.

Journal of Neuroscience Methods 186 (2010) 231–241

Contents lists available at ScienceDirect

Journal of Neuroscience Methods

journal homepage: www.elsevier.com/locate/jneumeth

Avoiding the ballistocardiogram (BCG) artifact of EEG data acquired simultaneously with fMRI by pulse-triggered presentation of stimuli

Matthias Ertl[a,b,1], Valerie Kirsch[a,1], Gregor Leicht[a,c], Susanne Karch[a], Sebastian Olbrich[d], Maximilian Reiser[e], Ulrich Hegerl[d], Oliver Pogarell[a], Chistoph Mulert[a,c,*]

[a] Department of Psychiatry, LMU, Munich, Germany
[b] Munich University of Applied Science, Munich, Germany
[c] University Medical Center Hamburg-Eppendorf, Department of Psychiatry and Psychotherapy, Centre for Psychosocial Medicine, Hamburg, Germany
[d] Department of Psychiatry, University of Leipzig, Leipzig, Germany
[e] Department of Radiology, LMU, Munich, Germany

ARTICLE INFO

Article history:
Received 12 March 2009
Received in revised form 9 November 2009
Accepted 10 November 2009

Keywords:
EEG–FMRI
Simultaneous EEG–fMRI measurement
BCG artifact

ABSTRACT

Simultaneous acquisition of electroencephalography (EEG) and functional magnetic resonance imaging (fMRI) data could offer a much deeper understanding of brain function, e.g. in the analysis of tempo-spatial dynamics of brain activity in cognitive processing. However, more sophisticated analysis methods such as single-trial coupling of EEG and fMRI are often handicapped by the limited quality of EEGs acquired in the MRI scanner. In particular, the ballistocardiogram (BCG) artifact is still a relevant problem. Methods that are currently available typically remove the BCG artifact either in post-recording or real-time signal processing. Here, we would like to suggest a new strategy to avoid BCG artifacts during data acquisition. In our proposal, stimuli are presented pulse-triggered (PT), thus avoiding interference of BCG artifacts with the evoked potentials investigated during EEG recording. This method is based on the observation that the main influence of the BCG artifact is generally limited to the time interval of 150–500 ms post-QRS complex. Based on real measurements, we simulated different signal presentation methods relative to the onset of the BCG artifact for 14 subjects. Stimuli were either presented independently of the BCG artifact or pulse-triggered at fixed time-points (280 ms, 480 ms and 680 ms post-QRS complex) and with a jitter (short: 120 ms or long: 240 ms). In combination with an averaged artifact subtraction method signal distortion was reduced at best by 47%.

1. Introduction

Combined recording and analysis of electroencephalography (EEG) and functional magnetic resonance imaging (fMRI) provide complementary information regarding the spatial and temporal resolution of brain activity (Mulert et al., 2008a; Ritter and Villringer, 2006) thus offering the possibility of enhancing the current understanding of brain (dys-) functions non-invasively. This technique has been used for the investigation of fMRI correlates of event-related potentials (ERPs) (Bonmassar et al., 1999; Kruggel et al., 2000), spontaneous sleep (Czisch et al., 2004) and alpha rhythms (Goldman et al., 2002; Moosmann et al., 2003) as well as epileptic activity (Iannetti et al., 2002; Lemieux et al., 2001). More precise insights are expected to come from more sophisticated analysis methods, i.e. when integrating EEG and fMRI information at the single-trial level. The idea behind this approach is to perform an fMRI analysis informed by paradigm-induced amplitude modulations of simultaneously acquired single-trial ERPs. Therefore, obtained spatiotemporal matches provide information at millimeter-accuracy about regional responses using fMRI with a temporal resolution in milliseconds, provided by the EEG (Benar et al., 2007; Debener et al., 2005; Eichele et al., 2005; Mulert et al., 2008b, 2009).

However, EEG–fMRI analyses are typically compromised by the limited quality of the recorded EEG data (Bonmassar et al., 1999; Goldman et al., 2000; Kruggel et al., 2000). Generally, EEG data recorded simultaneously with fMRI suffer from two major artifacts. The gradient artifact reflects the switching of magnetic fields during MRI image acquisition (Allen et al., 2000; Garreffa et al., 2004). Due to its technical origin the gradient artifact can be reliably corrected by averaged artifact template subtraction without limiting further EEG–fMRI analyses (Allen et al., 2000; Ritter et al., 2007). The ballistocardiogram (BCG) artifact, on the other hand, is a bigger methodological challenge. One major problem is its variability.

* Corresponding author at: Department of Psychiatry, Nußbaumstraße 7, 80336 München, Germany. Tel.: +49 89 5160 5550; fax: +49 89 5160 5542.
E-mail address: cmulert@med.uni-muenchen.de (C. Mulert).
[1] These authors contributed equally to this work.

0165-0270/$ – see front matter © 2009 Elsevier B.V. All rights reserved.
doi:10.1016/j.jneumeth.2009.11.009

The BCG artifact occurs about 150–500 ms relative to the QRS complex onset (Allen et al., 1998; Debener et al., 2008) and seems to be caused predominantly by a combination of pulse-related movements of scalp electrodes (Nakamura et al., 2006) and electrically conductive blood (Sijbersa et al., 2000; Srivastava et al., 2005). Some observations have shown that morphology, amplitude and peak-latency of the BCG artifact are usually different between channels and subjects (Allen et al., 1998). BCG artifact correction methods, therefore, have to adjust to both inter- and intrapersonal particularities. Secondly, the BCG artifact contributes to the frequency range (0.5–25 Hz) of interest in the analysis of the ERPs (Allen et al., 1998). This property makes the correction of BCG artifacts both difficult and crucial when considering that EEG informed fMRI analysis requires single-trial information of event-related amplitude modulations without the possibility of increasing the signal-to-noise ratio by averaging prior to analysis. Thirdly, the amplitude of BCG artifacts is directly proportional to the strength of the magnetic field and, as a consequence, both the absolute magnitude and the spatial variability of the BCG are increased (Tenforde et al., 1983). Finding a reliable BCG artifact correction method becomes even more important with the increasing use of high field MR-scanners.

Different methods have been proposed to reduce BCG artifacts offline (Allen et al., 1998; Benar et al., 2003; Debener et al., 2007; Eichele et al., 2005; Ellingson et al., 2004; Niazy et al., 2005; Siniatchkin et al., 2007; Srivastava et al., 2005). However, to our knowledge there are only two published methods correcting the BCG artifacts in real-time (Bonmassar et al., 2002; Masterton et al., 2007) and no published method trying to avoid the effects of the BCG artifacts while measuring the EEG. Here, we present a novel and simple method in order to decrease the effects of the BCG artifacts in event-related EEGs when collected simultaneously with fMRI by avoiding the interference of the BCG artifact with the ERP in real-time. This method is based on the observation that the main influence of the BCG artifact is largely limited to the time interval of 150–500 ms post-QRS complex (Allen et al., 1998; Debener et al., 2008). We propose to time-lock the stimulus presentation to the QRS complex and place the ERP-wave of interest at a time-point where the BCG is less pronounced, thus allowing for a cleaner ERP. We call this measurement method pulse-triggered (PT). Based on real measurements we simulated different signal presentation methods relative to the onset of the BCG artifact for 14 subjects. Our results show that the estimation of the simulated evoked potential was improved by using PT presentation. We investigated how the method can be combined with existing algorithms for BCG correction in order to further improve ERP accuracy. Furthermore we present preliminary data on the actual implementation of the PT measurement method in a real-life situation.

2. Materials and methods

2.1. Simulation of the different signal presentation methods

Fig. 1 shows a flowchart of our three processing steps: (1) Simultaneous EEG–fMRI data were collected from 14 subjects and used to model the BCG artifacts. (2) Data from a single subject participating in a simultaneous EEG–fMRI auditory paradigm were used to extract the averaged ERP (N1). (3) Addition of the N1 potential to the individual BCG artifact datasets relative to the pulse resulted in nine variations of PT measurement and one dataset simulating conventional measurement methods.

2.1.1. Retrieving the individual BCG artifacts

2.1.1.1. Subjects. Participants were 14 healthy volunteers (8 males, 6 females; range 19–35 years) with no history of neurological or psychiatric disorders, or psychopharmacological medication. All subjects were recruited from an academic environment. Written informed consent was obtained after procedures had been fully explained prior to the experiment, in accordance with the local ethics committee guidelines of the Ludwig Maximilians-University, Munich, Germany. Subjects were instructed to keep their eyes closed and lie still during the recordings. No specific task was introduced since the aim was to identify the BCG artifact and then to find a time period in which ERPs would be less affected by the BCG artifact.

2.1.1.2. fMRI. Imaging was performed in a 1.5 T whole body scanner (Siemens Magnetom Sonata) with echo planar capability using a standard eight-channel-head-coil. The subject's head was fixed during the whole experiment thus reducing involuntary movements. For each subject, a three-dimensional MPRAGE dataset (T1*-weighted) was recorded parallel to the anterior commissure-posterior commissure line (193 sagittal slices). For functional BOLD imaging, 12 slices covering the whole brain with a T2*-weighted EPI sequence (TR: 3000 ms; TE: 53 ms; flip angle: 90°; FOV: 180 × 180; matrix: 64 × 64; interleaved slice acquisition; slice thickness 8 mm; interslice gap 0.4 mm; resulting pixel slice: 2.8 mm × 2.8 mm) were acquired in the same position as the anatomical images, resulting in 633 scans within each session (approximately 32 min). The slice thickness is related to our 'sparse sampling design' with EEG acquisition interleaved with MR image acquisition. While this design has two advantages (no disturbance of gradient artifacts concerning our ERP signal and no disturbance of our auditory stimuli with the scanner noise), it was necessary to apply relatively thick slices in order to cover the whole brain.

2.1.1.3. EEG. A 64-channel amplifier system, designed especially for the MR environment was used (BrainAmp MR, Brainproducts, Munich, Germany). The recording was taken from 61 equidistant scalp sites mounted in a cap system (Easycap, Falk Minow Services, Herrsching, Germany). The 61 EEG electrodes (sintered Ag/AgCl ring electrodes) were referred to Cz and placed on the scalp according to the international 10–10 system. The ground electrode was placed between Fz and Fpz. Continuous data were also recorded from one electrode placed below the left eye in order to monitor eye blinks, plus another three electrodes placed on the upper back for electrocardiogram recording (ECG 1–3). The impedance of all channels was held below 5 kΩ. The sampling rate was set to 5000 Hz. Wires in the coil were fixed under weights of sand to reduce artifacts caused by movement. The EEG was recorded using the Brain Vision Recorder Software (Brain Vision Software Munich, Germany).

FMRI gradient artifacts were removed from the EEG using a local averaged artifact subtraction method (Allen et al., 2000) as implemented in Brain Vision Analyzer 1.05.0005 (Brainproducts, Munich, Germany). The scanner artifact was detected at F1 for interleaved scans by a calculated gradient trigger (250 μV/ms). Baseline correction for average (start: −50 ms; end: 0) was enabled. Scanned intervals (based on time: start [−50 ms], end [1300 ms]; length [1350 ms]) for average were selected to start at the fifth scan. No upper limit for selected intervals was chosen. All channels were included. Subsequently, the data were down-sampled to 250 Hz, a cut-off frequency of 80 Hz was selected and the corrected EEG data were stored to history node (compression with 500.0 nV resolution). Finally, the data were filtered (low pass filter 50 Hz, 48 dB/oct; high pass filter 0.5 Hz, 48 dB/oct), re-referenced to common average and exported to Matlab 7.4 (Mathworks, Natick, MA).

Data processing under Matlab was based on EEGLAB 6.01b (Delorme and Makeig, 2004), an open source toolbox running in Matlab and developed by the Schwartz Center for Computational

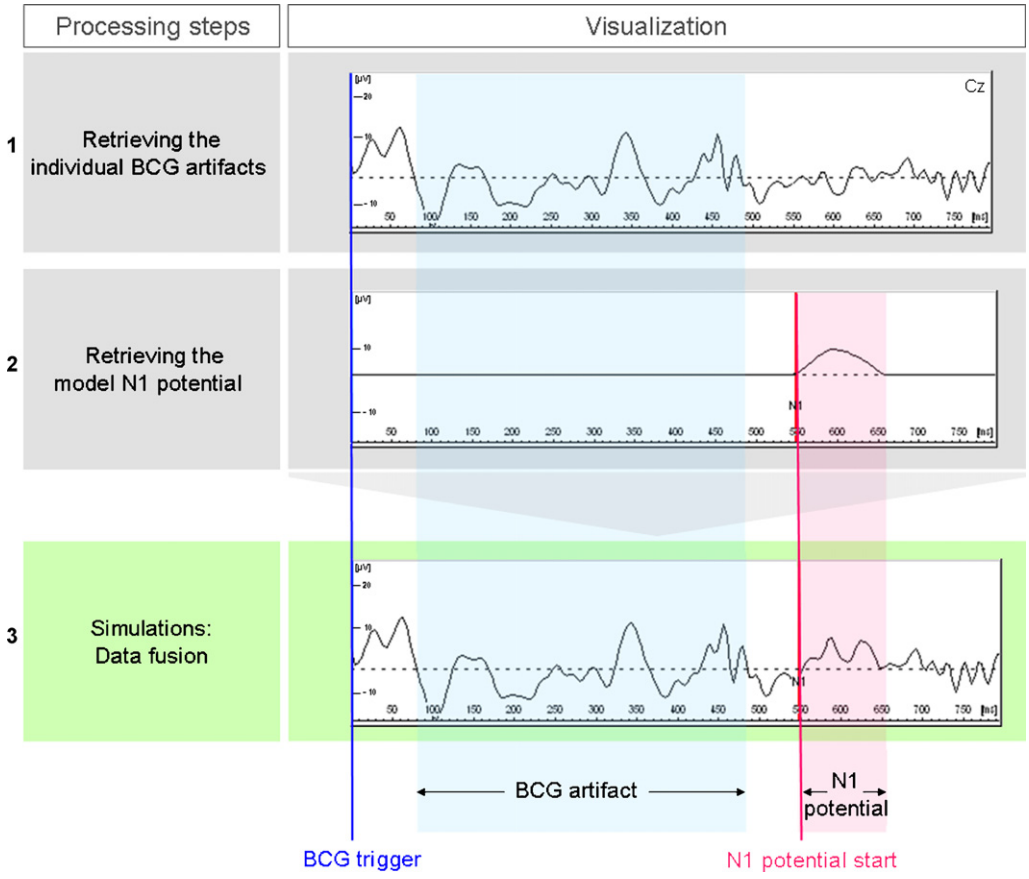

Fig. 1. A flowchart of the three processing steps to simulate the different signal presentation methods. (1) Simultaneous EEG–fMRI data were collected from 14 subjects. The figure shows a single-trial BCG artifact (highlighted in blue) of a single subject. The BCG trigger (blue) marks the onset of the detected R-wave. In the presented single event the BCG artifact starts 80 ms post-BCG trigger and ends after 400 ms. (2) Data from a single subject participating in a simultaneous EEG–fMRI auditory paradigm were used to extract the averaged model N1 potential (highlighted in red). The N1 potential started with the N1 potential start (red). (3) For the simulation of different measurement methods the N1 potential was added to the individual BCG artifacts in different ways relative to the BCG trigger (total 10 variations). In this example, the N1 potential occurs 550 ms after the ECG trigger. These steps were visualized using single-subject data. (For interpretation of the references to color in this figure legend, the reader is referred to the web version of the article.)

Neurosciences, LA Jolla, CA (http://www.sccn.ucsd.edu/eeglab). As a prerequisite to trigger our signal pulse-locked depending on the occurrence of the BCG artifact — a robust QRS complex detection algorithm was needed. The main influence of the BCG artifact in the EEG channels was to be expected in the time interval of 150–500 ms post-QRS complex in the ECG channel (Allen et al., 1998; Debener et al., 2008). The detection of the QRS complexes was performed for all three ECG channels using the FMRIB 1.2 plug-in (Niazy et al., 2005), an advanced algorithm based on Christov and Kim (Christov, 2004; Kim et al., 2004). The results of the QRS detection were inspected by eye and the most appropriate ECG channel was selected accordingly. The most appropriate ECG channel was defined as the channel whose detected R-wave was reliably followed by a BCG artifact. Further on this detected R-wave will be referred to as BCG trigger. The BCG artifact was defined as a systematic polarity reversal on both left and right hemisphere electrodes (F7, F8), about 210 ms after the BCG trigger (Debener et al., 2008). Thereafter, data were epoched from 0 ms to 800 ms relative to the BCG trigger. Since channel Cz is often used to investigate the auditory evoked N1 potential (Hansen and Hillyard, 1980; Naatanen and Picton, 1987; Mulert et al., 2003, 2008b), the resulting BCG artifact segments in channel Cz were used for our simulations. The BCG artifacts of every subject remained in the same order as they were recorded during the experiment. In order to investigate the time course of the BCG artifact in Cz, the resulting segments (1575–2046 segments per subject) were averaged.

2.1.2. Retrieving the model N1 potential

The model signal was retrieved by using the average N1 potential of a single subject recorded simultaneously with fMRI in a former study (Mulert et al., 2008b). We decided in favor of an average ERP to ensure a stable and clean signal. We worked with the auditory evoked N1 potential, since this is a time-bound and well documented ERP even in simultaneous EEG–fMRI measurements (Mulert et al., 2001, 2005, 2008b).

The experimental task was an auditory choice reaction paradigm with 152 tones of different pitches (50%: 800 Hz and 50%: 1300 Hz) and a duration of 250 ms presented by earphones at 85 dB SPL with pseudo-randomized intervals (ISI: 2.5–7.5 s). In the experimental runs, subjects had to press one of two buttons depending on the tone. On hearing the low tone subjects were instructed to press the left button, on hearing the high tone they were instructed to press the right button. In former studies we were able to verify that this paradigm reliably generates a N1 potential (Gallinat et al., 2002; Mulert et al., 2001, 2004). The EEG data were collected in the scanner and thus affected by the BCG artifact. We used these data instead of EEGs collected outside the scanner because firstly, PT measurements will be applied with a signal measured simultaneous to fMRI and secondly, it makes no difference which signal you chose as a model for a simulation. EEG and fMRI settings were the same as described above.

The single-subject EEG dataset was processed in Brain Vision Analyzer, epoched from 0 ms to 400 ms relative to stimulus onset

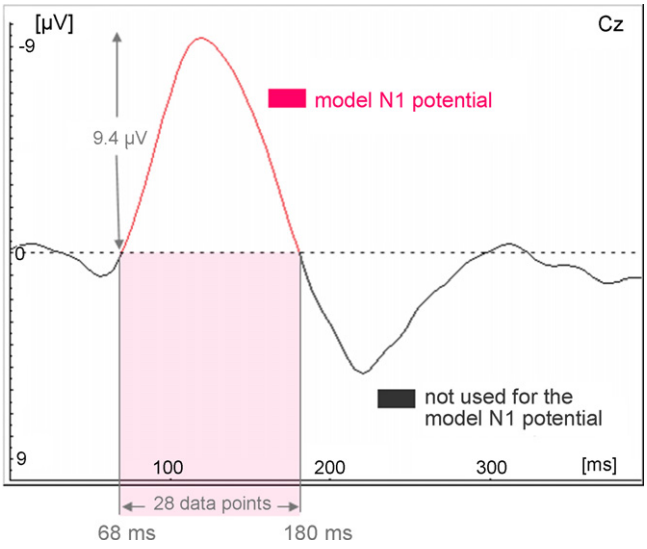

Fig. 2. The model N1 potential (red line). The model signal was retrieved by using the averaged N1 potential of a single subject recorded simultaneously to fMRI. For the design of the model N1 potential only data points (overall 28) in the interval from 68 ms to 180 ms post-stimulus were used (sampling rate 250 Hz). The maximal negative amplitude was −9.4 μV occurring 120 ms post-stimulus. The remaining data points (black line) of the averaged N1 potential were not considered in order to simplify our investigation of the signal distortion after BCG artifact superposition. (For interpretation of the references to color in this figure legend, the reader is referred to the web version of the article.)

(tone) and exported into Matlab. The time domain-averaging of the epochs resulted in an averaged N1 potential (see Fig. 2). For the design of the model N1 potential only data points (28 in total) from 68 ms to 180 ms post-stimulus were used (sampling rate 250 Hz). The remaining data points of the averaged N1 potential were not considered in order to simplify our investigation of the signal distortion after BCG artifact superposition. The maximum negative amplitude of the averaged N1 potential was −9.4 μV, occurring 120 ms post-stimulus. In the following text, the averaged data points from 68 ms to 180 ms post-stimulus will be referred to as N1 potential.

2.1.3. Simulations: data fusion

Simulation of PT measurements was performed by adding the averaged model N1 potential to the BCG artifacts (10 new data structures for every subject). These new data structures differed in the exact time-point the N1 potential was added with respect to the pulse (BCG trigger). Each data structure represented a different signal presentation: It was our intention to investigate the most appropriate time-point in relation to the BCG artifact. Therefore, stimuli were set pulse-triggered at three different time-points (280 ms, 480 ms and 680 ms, see Fig. 3b–d), without a jitter (W: without jitter) and combined with a short (S = 120 ms, see Fig. 3e) or long (L = 240 ms, see Fig. 3f) jitter. We included the jittered versions to allow for a combination of PT with an established BCG artifact correction method, which would otherwise eliminate any un-jittered pulse-triggered signal as belonging to the BCG artifact. The jitter was implemented by using the Matlab function (rand) creating uniformly random numbers and arrays. Therefore, combining PT-680 with the short jitter (PT-680S) meant that the N1 potential was randomly presented 560–680 ms after the BCG trigger (see Fig. 3e). A combination of PT-680 with the long jitter (PT-680L) resulted in a randomly set N1 potential between 440 ms and 680 ms after the BCG trigger (see Fig. 3f). In the measurement strategies used so far, stimuli were presented in random relation to the BCG artifact in between scans. In order to simulate these established measurement methods the N1 potential was set randomized from 0 ms to 680 ms post-BCG trigger (see Fig. 3a). Datasets generated in this way were named CLASSIC.

2.2. Combination with an averaged artifact subtraction method

Averaged artifact subtraction (AAS) was applied to all created datasets with jitter since this method would eliminate any un-jittered pulse-triggered ERP as belonging to the BCG artifact. The algorithm was a channel-wise averaged template subtraction method as implemented in the FMRIB 1.2 EEGLAB plug-in (Niazy et al., 2005), based on the method introduced by Allen et al. (1998). The Gaussian-weighted mean artifact correction method averaged artifacts after multiplying Gaussian window weights in order to emphasize the current artifact shape and to reduce the effect of further artifacts.

2.3. Validation of the signal quality

We investigated the signal quality without BCG correction and after combination with AAS. The distortion of the resulting N1 potentials was evaluated by comparing the model N1 potential to the recovered N1 potential, both after BCG artifact superposition without BCG correction and after BCG artifact correction with AAS. The N1 potential was defined as the maximum negativity 0–112 ms after the N1 potential signal start. Altogether, 28,977 amplitudes were analyzed. The mean failure (MF) showed the grade of deviation from the original N1 potential. The mean failure was calculated in this way: $m = \sum_{i=1}^{n} |c - a_i|/n$; with $c = -9.4$ as the maximum negative amplitude of the model N1 potential, n is the number of amplitudes and a_i is the measured amplitudes (at time of maximum negative amplitude). For an evaluation of the quality of the signal distortion, we classified the amplitude as 'good' or 'bad'. Depending on the reduction of the mean failure when compared to the model N1 potential, we defined 'good amplitudes' (GA) as MF being smaller than 20% and 'bad amplitudes' (BA) as MF exceeding 50%.

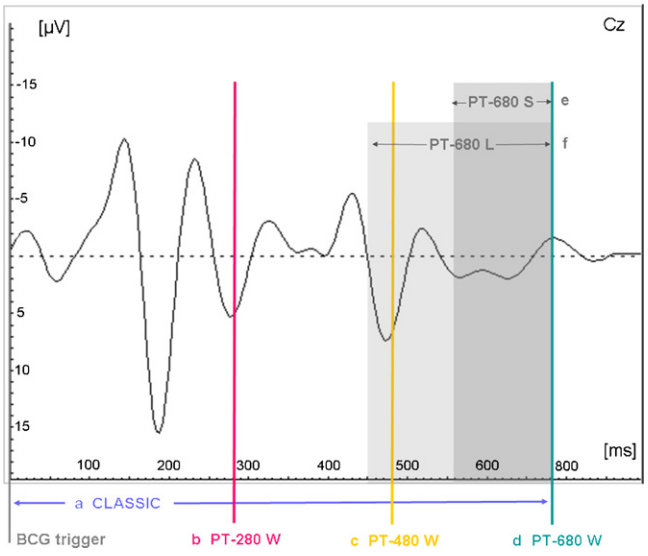

Fig. 3. Simulations were done by adding the N1 potential to the BCG artifacts (10 new data structures for every subject). These new data structures differed in the exact time-point the N1 potential was added in respect of the pulse (BCG trigger). Figure illustrates these time-points. In simultaneous EEG–fMRI measurements stimuli are presented in a random relation to the BCG artifact. Therefore, the N1 potential was set randomized from 0 ms to 680 ms post-BCG trigger. Datasets were named CLASSIC (see part (a)). Three time-points (280 ms, 480 ms and 680 ms; see parts (b–d)) without a jitter (W: without jitter) and combined with a short (S = 120 ms) or long (L = 240 ms) jitter were investigated. For example, for PT-680S the N1 potential was randomly presented 560–680 ms after the BCG trigger (e). PT-680L resulted in a randomly set N1 potential between 440 ms and 680 ms after the BCG trigger (f).

Table 1
The averaged results of CLASSIC and PT without BCG correction.

	CLASSIC	PT-280			PT-480			PT-680		
		W	S	L	W	S	L	W	S	L
Mean failure (μV)	7.4	7.3	7.5	8.4	6.5	6.7	7.1	6.6	6.4	6.4
Standard deviation (μV)	6.3	6.3	6.5	6.9	5.5	5.8	6.1	6.1	6.0	5.8
Good amplitudes (%)	16.2	17.1	13.9	12.0	20.4	19.1	17.1	19.2	19.5	19.7
Bad amplitudes (%)	60.5	59.6	64.1	68.0	53.1	54.6	58.6	49.8	52.8	52.8

2.4. Application of PT in real-life situation

EEG data were recorded in a 3 T scanner by means of the MR compatible amplifier BrainAmp MR (Brainproducts, Munich, Germany). The EEG was recorded using the Brain Vision Recorder Software (Brain Vision Software Munich, Germany). The incoming data were sent to the BrainVision RecView software ("Recording Viewer", Brain Vision Software, Munich, Germany) for high-speed real-time data analyses. BrainVision RecView is an add-on module for the BrainVision Recorder and was used to remove the gradient artifact permitting QRS pulse-detection in real-time during the scan. The correction of the gradient artifact was performed by means of subtraction using the template drift compensation algorithm to remedy template jitter caused by imperfect synchronization between the EEG amplifier and the scanner clocks. During a user defined learning period the pulse artifact correction module filter learned the specific properties of the gradient corrected ECG signal with a template matching approach. Based on this template, the ongoing ECG was inspected for further QRS complexes. The set R-wave-marker represented the first dominant local maximum from the beginning of the template and then sent to the stimulus presentation system. We used Presentation Software (Presentation, Neurobehavioural Systems, http://www.neurobs.com) as stimulus delivery and experimental control software system. Presentation decided on the timing of the PT stimuli presentation after receiving the R-wave- and scanner-information. The experimental task was an auditory choice reaction paradigm with tones of different pitches (50%: 800 Hz and 50%: 1300 Hz) and a duration of 250 ms presented by earphones at 85 dB SPL with pseudo-randomized intervals (ISI: 2.5–7.5 s). The main idea (cp. Fig. 4a) of PT stimulus presentation is to trigger the ERP during a BCG-free period to minimize superposition with the artifact. Therefore presentation was to allow a PT stimulus only when certain conditions were fulfilled: (1) The ERP should appear in between scans. (2) The pseudo-

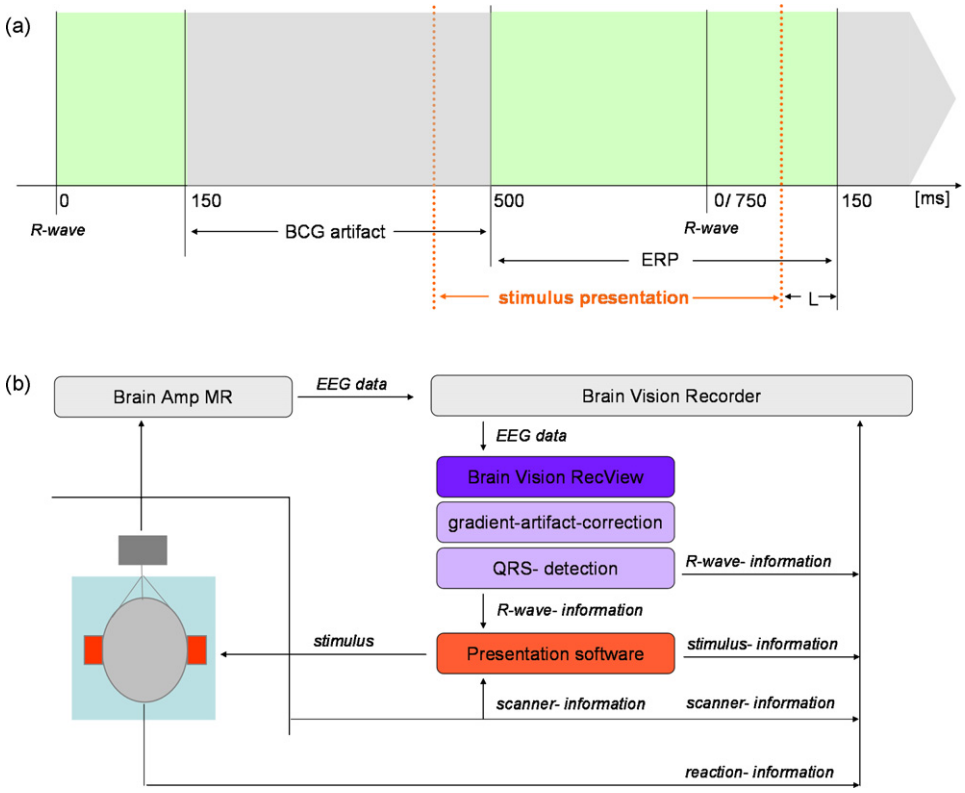

Fig. 4. (a) Schematic illustration of the main idea of the pulse-triggered stimulus presentation: The BCG artifact (highlighted in grey) afflicts the EEG mostly between 150 ms and 500 ms post-QRS complex (R-wave in the schema). Considering an average heartbeat rate (80 bpm) the distance between two QRS complexes should be about 750 ms. Hence an interval of about 400 ms can be considered as BCG free (highlighted in green). We suggest measuring the ERP during this period to minimize superposition of the BCG and the evoked potential. Due to the latency (L) of the ERP (100 ms for the N1 potential) the time period for the stimulus presentation (period between vertical orange lines) starts and ends earlier than the time period considered as BCG free. (b) Schematic illustration of the technical pipeline required for PT measurement. Through the amplifier system (BrainAmp MR), the EEG data are sent to Brain Vision Recorder and Brain Vision RecView ("Recording Viewer") which performs a real-time online gradient-artifact-correction and QRS detection. The detected R-wave information and the MR scanner-information (onset of the scans) are sent to the Presentation software (Neurobehavioural Systems). When all the required conditions are fulfilled (see text for further details) the presentation software sets the stimulus pulse-triggered. The subject reacts to the stimulus. All information (detected R-wave, stimulus onset, scan onset and the subject's reaction) are sent to Brain Vision Recorder, where it appears as marker-information in the recorded EEG data. (For interpretation of the references to color in this figure legend, the reader is referred to the web version of the article.)

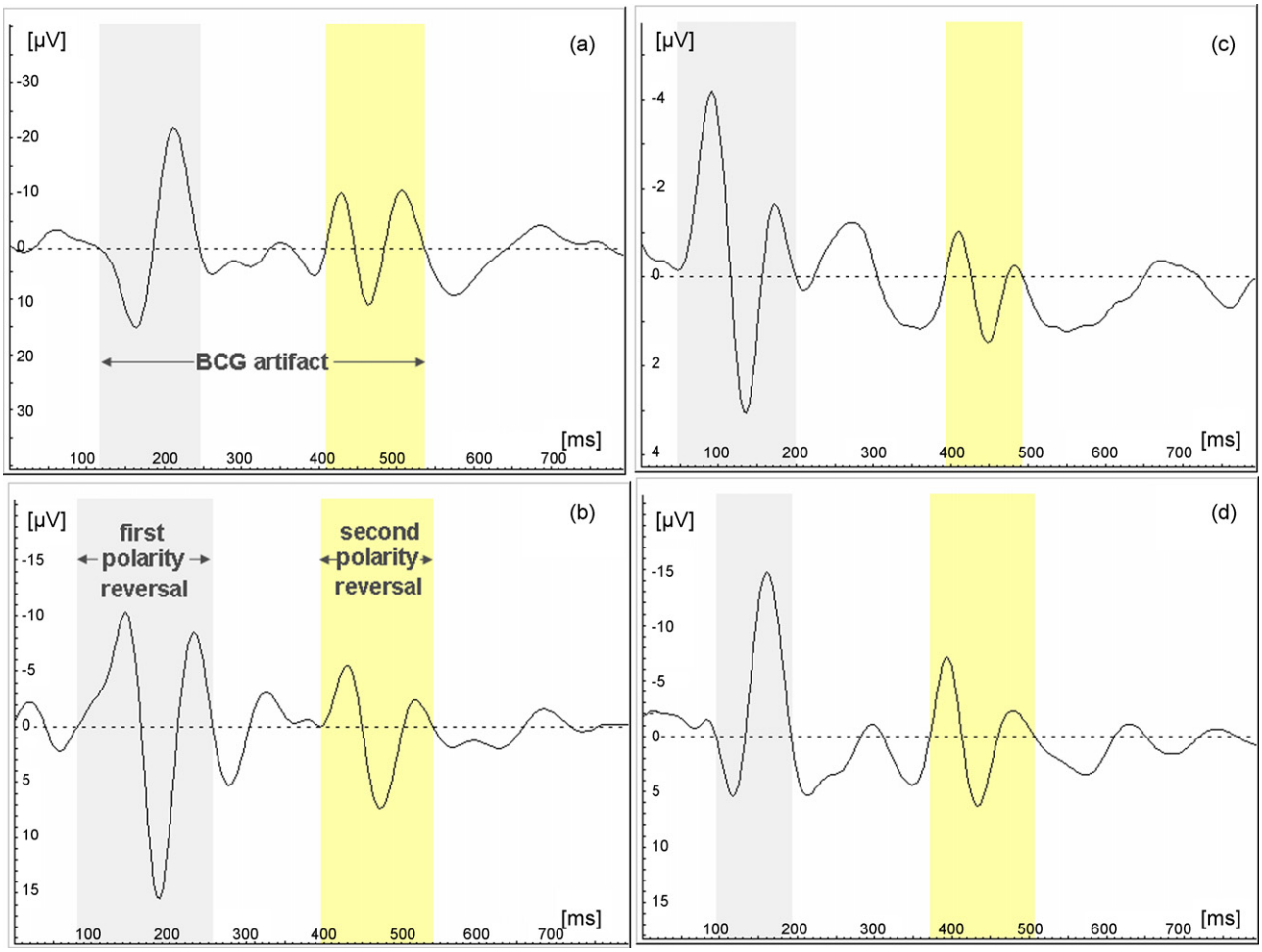

Fig. 5. The averaged time courses of the BCG artifact in Cz for four representative subjects (a–d). After QRS complex detection in the ECG channel the EEG data were epoched from 0 ms to 800 ms relative to the detected R-wave (BCG trigger). The main occurrence of the BCG artifact was identified between 80 ms and 500 ms post-BCG trigger (a). BCG artifacts in Cz can be defined as two successive polarity reversals (b). The first (area highlighted in grey) occurred about 147 ms, the second (area highlighted in yellow) occurred about 451 ms after the QRS complex. (For interpretation of the references to color in this figure legend, the reader is referred to the web version of the article.)

randomized inter-stimulus intervals were to be respected. (3) The ERP was to be set 500 ms post-QRS complex. With an average heartbeat rate (80 bpm) the distance between two QRS complexes was about 750 ms. Hence an interval of about 400 ms could be considered as BCG free. (4) The latency of the ERP (here N1) was to be considered. This meant that the stimulus could be set within the BCG artifact as long as the ERP would appear in the BCG-free period. Fig. 4b gives a schematic overview of the whole technical pipeline required for PT measurement including online MR artifact correction, QRS detection and triggered stimulus presentation.

3. Results

For a thorough overview of all the results after measurement (see Table 1).

3.1. Characterization of the averaged BCG artifact in Cz

Firstly, for a simulation of the pulse-triggered N1 stimuli presentation it was necessary to show that the BCG artifact has a characteristic time course in channel Cz, where the N1 potential is usually analyzed. The following observations refer to the individual BCG artifact averages found in 14 subjects in channel Cz (see Fig. 5). The BCG artifact was identified as a signal with its main influence between 80 ms and 500 ms post-QRS complex. While the BCG artifact had an interpersonal variance, it also exhibited characteristic attributes. BCG artifacts can be defined as two successive polarity reversals. The first high polarity reversal appears about 147 ms after the QRS complex and is then followed by a second smaller polarity reversal, 304 ms later. The mean amplitude of the first polarity reversal was 13.8 μV (standard deviation [SD]: 8.6). The second, smaller polarity reversal occurred 451 ms post-QRS complex, its mean amplitude was 8.0 μV (SD: 5.0 μV).

3.2. Investigation of signal quality without AAS

Secondly, we investigated whether the estimation of the simulated evoked potential was improved by using PT presentation and which point in time would be the most adequate relative to the pulse: (1) The PT presentation of stimuli without a jitter after 480 ms and 680 ms resulted in a 15% (PT-480W) and in a 11% (PT-680W) reduction of the mean failure, compared to measurements with random relation to the BCG artifact (CLASSIC). PT stimuli presentation 280 ms after QRS complex (PT-280W) showed a reduction of the mean failure of 4% compared to CLASSIC. (2) The combination of the PT stimuli presentation with the short (120 ms) and the long (240 ms) jitter showed two different effects, depending on whether the presentation of stimuli fell into the main influence of the BCG artifact or not. PT-280 and PT-480 combined with the short or long jitter resulted in supplementary stimuli presentations within the main influence of the BCG artifact (80–500 ms post-QRS complex) and, therefore, performed worse than PT-280W and PT-480W (see

Table 2
The results after combining the simulated measurement methods (PT and CLASSIC) with an averaged artifact subtraction (AAS) method concerning mean failure (MF), standard deviation (SD), good amplitudes (GA) and bad amplitudes (BA).

	CLASSIC + AAS		PT-480 S + AAS		PT-480 L + AAS		PT 680 S + AAS		PT-680 L + AAS	
Mean failure (μV)	7.4	5.2	6.7	4.0	7.1	4.5	6.4	4.0	6.4	4.4
Standard deviation (μV)	6.3	4.9	5.8	4.1	6.1	4.4	6.0	4.6	5.8	4.6
Good amplitudes (%)	16.2	25.6	19.1	34.4	17.1	31.3	19.5	34.2	19.7	32.2
Bad amplitudes (%)	60.5	42.5	54.6	28.8	58.6	34.6	52.8	28.9	52.8	33.3

Fig. 6). By contrast, PT-680 combined with both short or long jitter presented the stimuli mainly after the main influence of the artifact, hence increasing the signal quality. In general, the short jitter performed better than the long jitter (see below). For a thorough overview of all the results after measurement (see Table 1), whereas for an illustration of the reduction of MF in percentage (see Fig. 6).

3.3. Investigation of signal quality with AAS

Thirdly, we investigated how this method could be combined with existing algorithms for BCG correction (AAS) in order to further improve ERP accuracy. As a signal occurring time-locked to the BCG artifact would be corrected along with the artifact, AAS was combined with the jittered PT stimuli presentation (PT-S and PT-L). The combination with AAS could further improve both the results of CLASSIC and PT: (1) Compared to the signal quality without BCG correction, the combination of CLASSIC and AAS showed an improvement of both mean failure (31%) and good or bad amplitudes. (2) Likewise the combination of AAS and PT-S or PT-L improved the signal quality. Interestingly, PT-S (PT-480S: 47% and PT-680S: 46%) outperformed PT-L (PT-480L: 40%; PT-680L: 41%) when compared to CLASSIC. For a thorough overview of all the results after measurement (see Table 2), and for an illustration of the reduction of MF in percentage (see Fig. 7).

The signal quality of every subject was improved by combining PT-W with AAS (see Table 3). For an overview over the results view Fig. 8.

3.4. Application of PT in real-life situation

Here we present preliminary data on the actual implementation of the PT measurement method in a real-life situation. Fig. 9 shows a 10-s example EEG data from a representative subject wherein the N1 stimulus was set pulse-triggered.

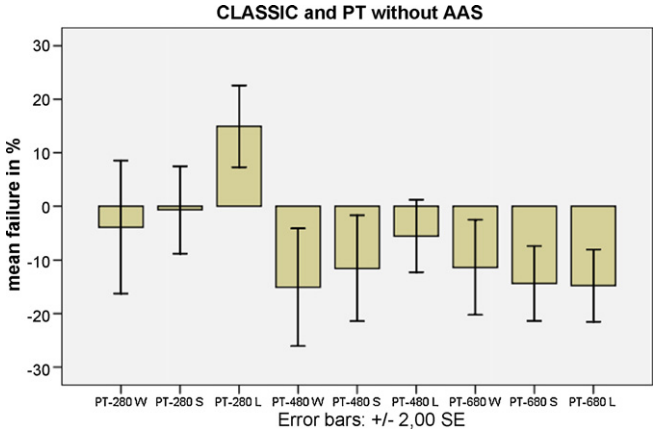

Fig. 6. The average change of the mean failure without BCG artifact correction in percent. Compared to the CLASSIC measurement method the mean failure decreased for PT-280W, PT-480W and PT-680W. Presenting the N1 potential at 480 ms or 680 ms post-BCG artifact was able to reduce the MF also in combination with the short and long jitter, while PT-280S and L enhanced the mean failure.

Table 3
The performance (main failure in [μV]) of *c* of CLASSIC, PT-480S and PT-680S in combination with AAS.

	CLASSIC + AAS		PT-480S + AAS		PT-680S + AAS	
Subject 1	7.3	4.4	9.3	3.1	6.6	3.2
Subject 2	8.4	6.5	8.0	5.3	6.9	5.0
Subject 3	6.9	5.1	6.3	3.6	6.2	3.5
Subject 4	5.6	3.9	4.3	3.1	4.9	3.3
Subject 5	10.6	8.1	12.3	5.9	10.8	6.3
Subject 6	9.6	4.9	6.0	3.8	5.6	4.0
Subject 7	7.0	5.3	5.0	3.5	5.6	3.5
Subject 8	8.0	6.4	7.5	4.2	7.7	4.4
Subject 9	8.6	6.8	7.6	4.7	8.6	4.9
Subject 10	5.9	3.1	5.0	2.8	3.7	2.8
Subject 11	5.1	3.1	3.1	2.7	4.5	2.8
Subject 12	5.7	3.8	5.3	3.3	4.7	3.5
Subject 13	10.6	8.2	10.3	6.7	10.5	6.2
Subject 14	4.9	3.2	3.9	2.8	3.9	3.9

4. Discussion

While simultaneous EEG–fMRI is a promising new approach in functional neuroimaging, the occurrence of BCG artifacts is still a relevant methodological problem today. The current study proposes a PT method of stimulus presentation attempting to avoid interference of BCG artifacts with event-related potentials at the time-point of data acquisition. So far, all other available strategies have been based on real-time or post-hoc artifact subtraction. The current results show that PT outperforms conventional stimuli presentation strategies when measuring the N1 potential 500–800 ms after QRS onset. Furthermore, results can be further improved when

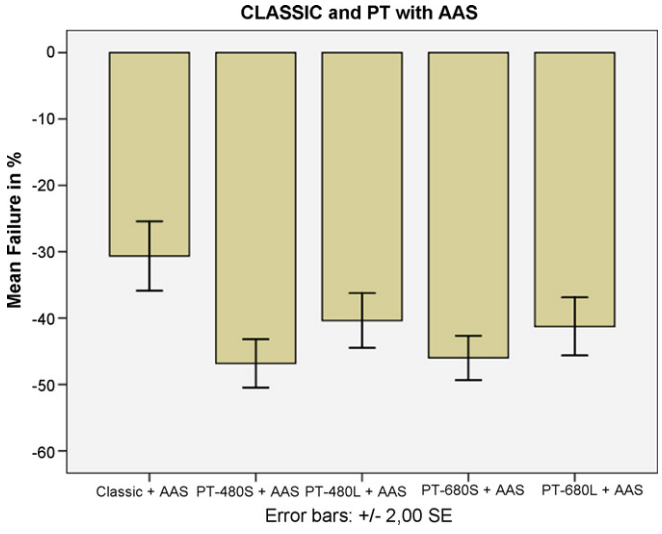

Fig. 7. The averaged reduction of the mean failure after the combination of measurement methods and averaged artifact subtraction (AAS) in percent. AAS improved the accuracy of the measured N1 potential. When joining AAS with pulse-triggered (PT) measurements and the long jitter (240 ms) the mean failure was further reduced. When the PT stimuli presentation time was combined with the short jitter (120 ms), the performance concerning signal quality was improved even more. The combination of AAS and PT-480S showed the best performance.

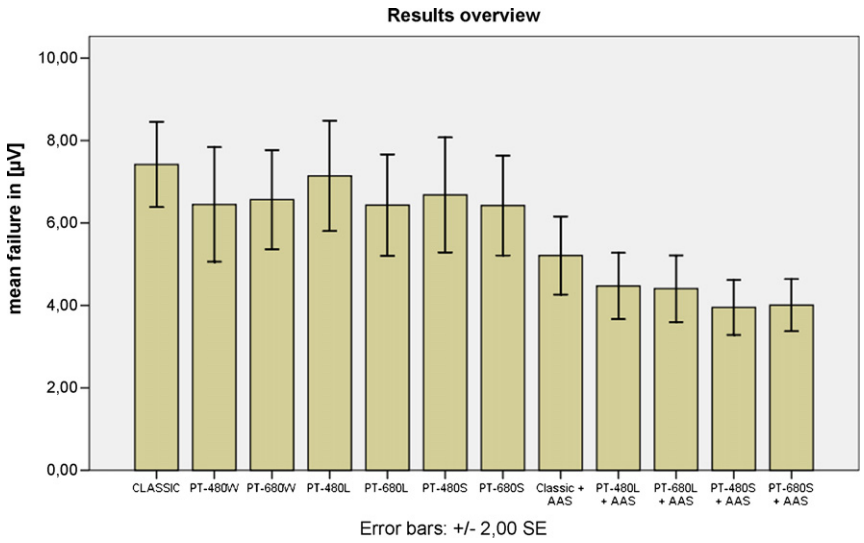

Fig. 8. An overview over the average mean failure without BCG artifact correction and after the combination of measurement methods and averaged artifact subtraction (AAS) in µV.

combined with an offline AAS method. Therefore, we propose to combine PT measurement with a jitter of maximally 120 ms in combination with conventional BCG artifact correction methods. Furthermore we present preliminary data on the actual implementation of the PT measurement method in a real-life situation.

4.1. Simulation of pulse-triggered stimuli presentation

Measuring the N1 potential with PT stimulus presentation depends on a characteristic time course of the BCG artifact in channel Cz. In agreement with earlier findings in F7 and F8 (Allen et al., 1998; Debener et al., 2008), the influence of the BCG artifact in Cz was largely limited to a time interval between 80 and 500 ms post-QRS complex (cp. Fig. 5) and two successive polarity reversals appearing 150 ms and 480 ms post-QRS complex were distinguishable. PT without AAS showed that the time-point of stimulus presentation relative to the onset of the artifact had an influence on the quality of the signal. Regarding the signal quality of the three investigated time-points (PT-280, PT-480 and PT-680), PT measurement performed best when the N1 potentials occurred after 480 ms and 680 ms (cp. Fig. 6). Hence, we suggest stimuli to be presented in such a way that the ERP-component of interest occurs 500–800 ms relative to the onset of the BCG artifact.

It is important to notice that PT stimulus presentation primarily generated ERPs time-locked to the BCG artifacts. Consequently, the combination of PT measurement with AAS resulted in an elimination of the N1 potential, since the N1 potential was falsely recognized as part of the BCG artifact. Therefore, the combination of PT with AAS requires a jitter. We investigated the effects of a short (PT-S: 120 ms) and a long (PT-L: 240 ms) jitter. As a result

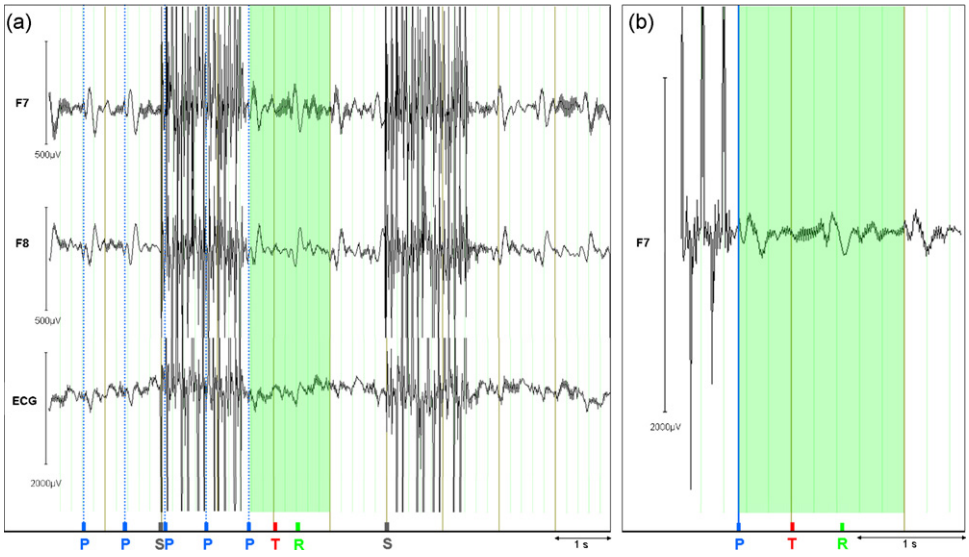

Fig. 9. 10-s (a) example EEG data from a single subject wherein the N1 stimulus was set pulse-triggered (highlighted in green). 3 out of 65 recorded channels are shown. Note the different scaling between panels and the pulsatile nature of the BCG artifact in the EEG channels (F7, F8), which is related to the cardiac cycle (ECG). The corresponding ECG signal is shown together with the identified heartbeat events (vertical blue lines, marker P = pulse). Real-time gradient-artifact-correction and QRS complex detection enables QRS detection during scan. Marker S shows the onset of the MR scans. When all the required conditions were fulfilled (see text for further details) the presentation software set the stimulus (T: tone) pulse-triggered after the pulse (here 440 ms) to which the subject responded (marker R). The corresponding N1 potential should be expected about 100 ms after the stimulus and well after the BCG artifact. A 2½-s (b) example EEG data show the same pulse-triggered period (highlighted in green) on a larger scale. (For interpretation of the references to color in this figure legend, the reader is referred to the web version of the article.)

it was firstly possible to jitter the PT stimuli presentation without loosing the advantages of PT measurements. However, the longer jitter either reached into the first polarity reversal 147 ms after the QRS complex (PT-280L) or into the second smaller polarity reversal 304 ms later (PT-480L, PT-680L). As a consequence, the versions with a short jitter outperformed the versions with the long jitter (cp. Fig. 6). We therefore suggest that PT stimuli presentation jitters should not exceed 120 ms. Secondly, the combination of the jittered PT versions with AAS further enhanced the signal accuracy (at best to +47%) of every subject.

4.2. PT in comparison with other BCG artifact correction methods

Previous BCG artifact correction strategies are based on post-hoc artifact elimination using either real-time or offline approaches to filter the EEG. In contrast to offline BCG artifact correction methods, real-time approaches first measure the BCG artifact itself and then filter it from the EEG. Bonmassar et al. employed a piezoelectric transducer mounted near the subject's temporal artery to acquire an independent measure of ballistocardiographic and gross subject motion (Bonmassar et al., 2002; Hill et al., 1995). A linear adaptive filter was used to remove signals from the EEG that are linearly related to the motion sensor signal. Notably, the relationship between the motion sensor signal and the induced artifact might not be linear, making it unsuitable for a linear filtering approach. As an advancement, Maserton et al. proposed to use loops of carbon fiber wire which are physically attached to, but electrically isolated from the subject's head in order to record subject motion (Laudon et al., 1998; Masterton et al., 2007). The loops are subject to induced voltages from movement in the magnetic field which are recorded using our standard EEG amplifier. Thus, this method ensured that the signal recorded from the loops in the MR scanner was a direct result of the same process leading to the BCG and motion artifacts. In addition, Masterton et al. used a recursive linear filter based upon a multichannel recursive least squares algorithm from multiple motion recordings from different locations on the scalp. Masterton et al. acted on the assumption that three motion channels provide better modeling of the subject's head motion allowing for linear combinations of multiple motion channels. These methods remain dependent on a signal representing the BCG artifact which is, however, locally variable and could restrict the quality of the template. Therefore, the resulting signal may be distorted. Compared to PT, one definite advantage of those measurement methods is that they are not restricted to an ERP of a few milliseconds, but can be applied to any EEG study. Furthermore, PT does not deal with artifacts from spontaneous [non-BCG] motion – unless the non-jittered method is used – it requires inspection by eye and selection of the most appropriate channel for QRS detection. On the other side, PT does not require additional recording coils and does not distort the signal as much. Various methods have been proposed to reduce BCG artifacts offline. At the moment, the most frequently used BCG artifact correction method detects the QRS complex and uses subtraction of a template derived from a sliding window average of previous artifact waveforms (Allen et al., 1998). However, this correction method relies on ECG pulse-detection in order to identify and align BCG artifacts for averaging and subtraction and does not consider the large intrapersonal variance of the BCG artifact. Consequently, several groups have tried to improve the BCG identification via EEG (Kruggel et al., 2000) or EOG (Kim et al., 2004) and developed channel-by-channel algorithms not assuming the exact repetition of the same artifact shape (Ellingson et al., 2004; Niazy et al., 2005) template. Another strategy often applied is a correction of BCG artifacts by means of principal component analysis (PCA) or independent component analysis (ICA). After decomposition of the raw EEG signal, artifact-related components are identified and a filtered signal is obtained by reconstructing the components previously removed. One key improvement provided by these methods is that explicit pulse-detection is not required. Siniatchkin et al. (2007) performed BCG artifact correction using PCA in a multiple source correction approach (MSA). However, in order to prevent the distortion of EEG signals of interest with the aid of the BCG artifact correction, the prior knowledge of meaningful and significant brain activity needs to be taken into account and modeled by multiple equivalent current dipoles (Baumgartner et al., 1989; Scherg and Von Cramon, 1985). The usefulness of this method, however, may be limited to situations in which the BCG artifact is spatially correlated and time-locked with the EEG signal, produced by the focal brain activity of interest, such as late ERP (Ille et al., 2002). Several groups achieved good results with ICA based BCG artifact removal (Benar et al., 2003; Briselli et al., 2006; Moosmann et al., 2007; Nakamura et al., 2006; Srivastava et al., 2005). Still, correction methods involving ICA entail problems concerning the identification of independent components (IC) representing the BCG artifact. Also, ICA-performance seems to be contingent with the strength of the magnetic field. Studies using ICA were successfully based on EEG recordings at 1.5 T (Benar et al., 2003; Briselli et al., 2006; Eichele et al., 2005; Mantini et al., 2007), while studies on 3 and 7 T (Debener et al., 2008) showed that ICA performs worse with increasing magnetic strength. These findings suggest not only the absolute magnitude of the BCG artifact to be smaller at 1.5 T compared to 3 and 7 T recordings, but also the dynamically rotating topography of the BCG artifact to be more pronounced. Therefore, BCG removal techniques assuming fixed spatial topographies may have difficulties accounting for all portions of the artifact (Debener et al., 2007). Some authors suggest the combination of waveform and spatial pattern removal approaches in the assumption that spatial BCG artifact correction approaches might perform better having separated residual BCG artifacts and brain-related EEG signals beforehand. However, the combination of various BCG artifact correction methods seems to hold the risk of overcorrecting the EEG data.

4.3. Online detection of the ECG/real life situation

Compared to the average ECG outside the scanner the ECG signal may be distorted (Allen et al., 1998) inside the MR machine due to blood conductivity (Wendt et al., 1988) occurring specifically during the ejection phase, spanning both the ST and T intervals (Debener et al., 2008). EEG systems often provide limited ECG recording facilities, e.g., one single bipolar channel (Niazy et al., 2005). Reliable online detection of the QRS complex will however be a relevant issue for the application of PT measurements in the real life situation.

4.4. Application of PT: single-trial analysis of ERPs

Correction of the BCG artifact is especially important if EEG data will be used for any kind of single-trial analysis, especially single-trial coupling with fMRI. On the other hand, the influence of BCG artifacts would be smaller, if ERP data could be averaged since BCG artifacts would then be part of the "noise" that would be diminished by averaging of the EEG signal of interest. However, single-trial coupling of EEG–fMRI is a very interesting strategy: The striking feature of single-trial coupling is its ability to separate different aspects of the BOLD signal according to their specific relationship with distinct neural processes. Single-trial coupling of EEG and fMRI predicts the BOLD signal specifically related to amplitude variations of electrophysiological components (Mulert et al., 2008a).

While this study investigating the N1 potential has proved the potential benefit of the new PT method, it is also important to see potential limitations. One aspect is the fact that PT measurement improves the ERP quality only in a small window between two

succeeding BCG artifacts. Accordingly, the improvement is largest, if the ERP of interest has a small width. Apart from the auditory evoked N1 potential used in the present study, good candidates for an application of this method could be for example the visual evoked N1 potential, the P2 potential or the N170. The PT method might be less applicable for potentials with a longer duration such as the late positive potential (LPP) or the contingent negative variation (CNV). While potentials such as the P50 might be short enough to fit in the improved time window but show smaller amplitudes than the auditory evoked N1 potential that was used in the present study, it will be interesting to see whether the improvement in the signal-to-noise ratio will be strong enough to allow for a reliable single-trial coupling of EEG–fMRI.

5. Conclusion

The present study describes a new method to decrease the influence of BCG artifacts in ERP measurements performed in the MR environment. The idea is to present the stimuli in periods devoid of BCG artifact, i.e. triggering the stimulus presentation with respect to the BCG timing. We showed that pulse-triggered stimuli presentation can significantly improve the estimation of the simulated evoked potential and thus could be a suitable method to investigate ERPs. In particular, PT offers an improved quality of EEG data recorded simultaneously with fMRI—an important topic when considering that more sophisticated methods, e.g. EEG informed fMRI analysis, require a good signal-to-noise ratio on a single-trial level and any additional noise, be it instrumental or physiological, should be minimized. The implementation of the PT stimuli presentation requires a high speed (1) real-time scanner artifact correction and QRS pulse-detection, including (2) a stimuli presentation software package that decides on pulse-triggered stimuli presentation after receiving the QRS triggers. In preliminary data we could demonstrate that PT measurement works in a real-life situation. The general topic of evoked potential estimation in the MR scanner is currently raising much attention in the human brain mapping community, and this study could therefore participate usefully in the discussion on how to optimize such recordings.

Acknowledgements

The authors would like to thank Alexander Svojanovsky for insightful comments and discussions. The present study was financially supported by a grant from the Friedrich-Baur-Stiftung of the medical faculty of the Ludwig-Maximilians-University Munich.

References

Allen PJ, Josephs O, Turner R. A method for removing imaging artifact from continuous EEG recorded during functional MRI. Neuroimage 2000;12:230–9.
Allen PJ, Polizzi G, Krakow K, Fish DR, Lemieux L. Identification of EEG events in the MR scanner: the problem of pulse artifact and a method for its subtraction. Neuroimage 1998;8:229–39.
Baumgartner C, Sutherling WW, Di S, Barth DS. Investigation of multiple simultaneously active brain sources in the electroencephalogram. J Neurosci Methods 1989;30:175–84.
Benar C, Aghakhani Y, Wang Y, Izenberg A, Al-Asmi A, Dubeau F, et al. Quality of EEG in simultaneous EEG–fMRI for epilepsy. Clin Neurophysiol 2003;114:569–80.
Benar CG, Schon D, Grimault S, Nazarian B, Burle B, Roth M, et al. Single-trial analysis of oddball event-related potentials in simultaneous EEG–fMRI. Hum Brain Mapp 2007;28:602–13.
Bonmassar G, Anami K, Ives J, Belliveau JW. Visual evoked potential (VEP) measured by simultaneous 64-channel EEG and 3T fMRI. Neuroreport 1999;10:1893–7.
Bonmassar G, Purdon PL, Jaaskelainen IP, Chiappa K, Solo V, Brown EN, et al. Motion and ballistocardiogram artifact removal for interleaved recording of EEG and EPs during MRI. Neuroimage 2002;16:1127–41.
Briselli E, Garreffa G, Bianchi L, Bianciardi M, Macaluso E, Abbafati M, et al. An independent component analysis-based approach on ballistocardiogram artifact removing. Magn Reson Imaging 2006;24:393–400.
Christov II. Real time electrocardiogram QRS detection using combined adaptive threshold. Biomed Eng Online 2004;3:28.
Czisch M, Wehrle R, Kaufmann C, Wetter TC, Holsboer F, Pollmacher T, et al. Functional MRI during sleep: BOLD signal decreases and their electrophysiological correlates. Eur J Neurosci 2004;20:566–74.
Debener S, Mullinger KJ, Niazy RK, Bowtell RW. Properties of the ballistocardiogram artefact as revealed by EEG recordings at 1.5, 3 and 7 T static magnetic field strength. Int J Psychophysiol 2008;67:189–99.
Debener S, Strobel A, Sorger B, Peters J, Kranczioch C, Engel AK, et al. Improved quality of auditory event-related potentials recorded simultaneously with 3-T fMRI: removal of the ballistocardiogram artefact. Neuroimage 2007;34:587–97.
Debener S, Ullsperger M, Siegel M, Fiehler K, von Cramon DY, Engel AK. Trial-by-trial coupling of concurrent electroencephalogram and functional magnetic resonance imaging identifies the dynamics of performance monitoring. J Neurosci 2005;25:11730–7.
Delorme A, Makeig S. EEGLAB: an open source toolbox for analysis of single-trial EEG dynamics including independent component analysis. J Neurosci Methods 2004;134:9–21.
Eichele T, Specht K, Moosmann M, Jongsma ML, Quiroga RQ, Nordby H, et al. Assessing the spatiotemporal evolution of neuronal activation with single-trial event-related potentials and functional MRI. Proc Natl Acad Sci USA 2005;102:17798–803.
Ellingson ML, Liebenthal E, Spanaki MV, Prieto TE, Binder JR, Ropella KM. Ballistocardiogram artifact reduction in the simultaneous acquisition of auditory ERPS and fMRI. Neuroimage 2004;22:1534–42.
Gallinat J, Mulert C, Bajbouj M, Herrmann WM, Schunter J, Senkowski D, et al. Frontal and temporal dysfunction of auditory stimulus processing in schizophrenia. Neuroimage 2002;17:110–27.
Garreffa G, Bianciardi M, Hagberg GE, Macaluso E, Marciani MG, Maraviglia B, et al. Simultaneous EEG–fMRI acquisition: how far is it from being a standardized technique? Magn Reson Imaging 2004;22:1445–55.
Goldman RI, Stern JM, Engel Jr J, Cohen MS. Acquiring simultaneous EEG and functional MRI. Clin Neurophysiol 2000;111:1974–80.
Goldman RI, Stern JM, Engel Jr J, Cohen MS. Simultaneous EEG and fMRI of the alpha rhythm. Neuroreport 2002;13:2487–92.
Hansen JC, Hillyard SA. Endogenous brain potentials associated with selective auditory attention. Electroencephalogr Clin Neurophysiol 1980;49:277–90.
Hill RA, Chiappa KH, Huang-Hellinger F, Jenkins BG. EEG during MR imaging: differentiation of movement artifact from paroxysmal cortical activity. Neurology 1995;45:1942–3.
Iannetti GD, Di Bonaventura C, Pantano P, Giallonardo AT, Romanelli PL, Bozzao L, et al. fMRI/EEG in paroxysmal activity elicited by elimination of central vision and fixation. Neurology 2002;58:976–9.
Ille N, Berg P, Scherg M. Artifact correction of the ongoing EEG using spatial filters based on artifact and brain signal topographies. J Clin Neurophysiol 2002;19:113–24.
Kim KH, Yoon HW, Park HW. Improved ballistocardiac artifact removal from the electroencephalogram recorded in fMRI. J Neurosci Methods 2004;135:193–203.
Kruggel F, Wiggins CJ, Herrmann CS, von Cramon DY. Recording of the event-related potentials during functional MRI at 3.0 Tesla field strength. Magn Reson Med 2000;44:277–82.
Laudon MK, Webster JG, Frayne R, Grist TM. Minimizing interference from magnetic resonance imagers during electrocardiography. IEEE Trans Biomed Eng 1998;45:160–4.
Lemieux L, Krakow K, Fish DR. Comparison of spike-triggered functional MRI BOLD activation and EEG dipole model localization. Neuroimage 2001;14:1097–104.
Mantini D, Perrucci MG, Cugini S, Ferretti A, Romani GL, Del Gratta C. Complete artifact removal for EEG recorded during continuous fMRI using independent component analysis. Neuroimage 2007;34:598–607.
Masterton RA, Abbott DF, Fleming SW, Jackson GD. Measurement and reduction of motion and ballistocardiogram artefacts from simultaneous EEG and fMRI recordings. Neuroimage 2007;37:202–11.
Moosmann M, Eichele T, Nordby H, Hugdahl K, Calhoun VD. Joint independent component analysis for simultaneous EEG–fMRI: principle and simulation. Int J Psychophysiol 2008;67:212–21, Erratum in: Int J Psychophysiol 2008;68:81.
Moosmann M, Ritter P, Krastel I, Brink A, Thees S, Blankenburg F, et al. Correlates of alpha rhythm in functional magnetic resonance imaging and near infrared spectroscopy. Neuroimage 2003;20:145–58.
Mulert C, Gallinat J, Pascual-Marqui R, Dorn H, Frick K, Schlattmann P, et al. Reduced event-related current density in the anterior cingulate cortex in schizophrenia. Neuroimage 2001;13:589–600.
Mulert C, Gallinat J, Dorn H, Herrmann WM, Winterer G. The relationship between reaction time, error rate and anterior cingulate cortex activity. Int J Psychophysiol 2003;47:175–83.
Mulert C, Jager L, Schmitt R, Bussfeld P, Pogarell O, Moller HJ, et al. Integration of fMRI and simultaneous EEG: towards a comprehensive understanding of localization and time-course of brain activity in target detection. Neuroimage 2004;22:83–94.
Mulert C, Menzinger E, Leicht G, Pogarell O, Hegerl U. Evidence for a close relationship between conscious effort and anterior cingulate cortex activity. Int J Psychophysiol 2005;56:65–80.
Mulert C, Pogarell O, Hegerl U. Simultaneous EEG–fMRI: perspectives in psychiatry. Clin EEG Neurosci 2008a;39:61–4.
Mulert C, Seifert C, Leicht G, Kirsch V, Ertl M, Karch S, et al. Single-trial coupling of EEG and fMRI reveals the involvement of early anterior cingulate cortex activation in effortful decision making. Neuroimage 2008b;42:158–68.

Mulert C, Leicht G, Hepp P, Kirsch V, Karch S, Pogarell O, et al. Single-trial coupling of the gamma-band response and the corresponding BOLD signal. Neuroimage, 2009 Oct 27 [Epub ahead of print].
Naatanen R, Picton T. The N1 wave of the human electric and magnetic response to sound: a review and an analysis of the component structure. Psychophysiology 1987;24:375–425.
Nakamura W, Anami K, Mori T, Saitoh O, Cichocki A, Amari S. Removal of ballistocardiogram artifacts from simultaneously recorded EEG and fMRI data using independent component analysis. IEEE Trans Biomed Eng 2006;53:1294–308.
Niazy RK, Beckmann CF, Iannetti GD, Brady JM, Smith SM. Removal of FMRI environment artifacts from EEG data using optimal basis sets. Neuroimage 2005;28:720–37.
Ritter P, Becker R, Graefe C, Villringer A. Evaluating gradient artifact correction of EEG data acquired simultaneously with fMRI. Magn Reson Imaging 2007;25:923–32.
Ritter P, Villringer A. Simultaneous EEG–fMRI. Neurosci Biobehav Rev 2006;30:823–38.
Scherg M, Von Cramon D. Two bilateral sources of the late AEP as identified by a spatio-temporal dipole model. Electroencephalogr Clin Neurophysiol 1985;62:32–44.
Sijbersa J, Van Audekerke J, Verhoye M, Van der Linden A, Van Dyck D. Reduction of ECG and gradient related artifacts in simultaneously recorded human EEG/MRI data. Magn Reson Imaging 2000;18:881–6.
Siniatchkin M, Moeller F, Jacobs J, Stephani U, Boor R, Wolff S, et al. Spatial filters and automated spike detection based on brain topographies improve sensitivity of EEG–fMRI studies in focal epilepsy. Neuroimage 2007;37:834–43.
Srivastava G, Crottaz-Herbette S, Lau KM, Glover GH, Menon V. ICA-based procedures for removing ballistocardiogram artifacts from EEG data acquired in the MRI scanner. Neuroimage 2005;24:50–60.
Tenforde TS, Gaffey CT, Moyer BR, Budinger TF. Cardiovascular alterations in Macaca monkeys exposed to stationary magnetic fields: experimental observations and theoretical analysis. Bioelectromagnetics 1983;4:1–9.
Wendt 3rd RE, Rokey R, Vick 3rd GW, Johnston DL. Electrocardiographic gating and monitoring in NMR imaging. Magn Reson Imaging 1988;6:89–95.

Chapter 3

Concluding remarks

This thesis focuses on two issues: Altered neural synchrony oscillations as a pathophysiological mechanism in schizophrenia and the improvement of simultaneous EEG-fMRI measurements. The first three studies use complementary functional and structural brain mapping approaches to *(i)* localize the early auditory evoked gamma band response (GBR) and then to link *(ii)* long-range synchronization and *(iii)* its changes in white matter volume and organization in the auditory tract to auditory verbal hallucinations (AVH) in schizophrenic patients (SZ). The results of the first study point to a disturbed "gamma-modulated" functional interaction between the anterior cingulated cortex (ACC) and the auditory cortex in schizophrenia. The findings in study two and three complement each other. Taken together, they suggest that a greater propensity for hallucinations in schizophrenia is associated with both increased phase locking of high-frequency oscillations in the auditory cortex and an increased volume of the auditory interhemispheric pathway fibres. Further investigation could establish neural oscillations as a crucial factor in the pathophysiology of schizophrenia and complete the picture of the nature of brain functions and their impairments.

The fourth study describes a new method to decrease the influence of BCG artifacts in event related potentials (ERP) measurements performed in the MR environment. The idea is to present the stimuli in periods devoid of BCG artifact. We show that pulse-triggered (PT) stimuli presentation can significantly improve the estimation of the simulated evoked potential and thus could be a suitable method to investigate ERPs. In particular, PT offers an improved quality of EEG data recorded simultaneously with fMRI—a considerable advantage seeing that more sophisticated methods, e.g. EEG informed fMRI analysis, require a good signal-to-noise ratio on a single-trial level and any additional noise, be it instrumental or physiological, should be minimized. The implementation of the PT stimuli presentation requires a high speed *(i)* real-time scanner artifact correction and QRS pulse-detection, including *(ii)* a stimuli presentation software package that decides on pulse-triggered stimuli presentation after receiving the QRS triggers. In preliminary data we can demonstrate that PT measurement works in a real-life situation. This study could therefore contribute usefully to the discussion on ways of optimizing evoked potential estimation in the MR scanner.

References

Adler LE, Pachtman E, Franks RD, Pecevich M, Waldo MC, Freedman R. Neurophysiological evidence for a defect in neuronal mechanisms involved in sensory gating in schizophrenia. Biol Psychiatry 1982; 17: 639-54.

Ahlfors SP, Simpson GV. Geometrical interpretation of fMRI-guided MEG/EEG inverse estimates. Neuroimage 2004; 22: 323-32.

Ahveninen J, Kahkonen S, Tiitinen H, Pekkonen E, Huttunen J, Kaakkola S, et al. Suppression of transient 40-Hz auditory response by haloperidol suggests modulation of human selective attention by dopamine D2 receptors. Neurosci Lett 2000; 292: 29-32.

Alexander DC. Multiple-fiber reconstruction algorithms for diffusion MRI. Ann N Y Acad Sci 2005; 1064: 113-33.

Allen PJ, Josephs O, Turner R. A method for removing imaging artifact from continuous EEG recorded during functional MRI. Neuroimage 2000; 12: 230-9.

Allen PJ, Polizzi G, Krakow K, Fish DR, Lemieux L. Identification of EEG events in the MR scanner: the problem of pulse artifact and a method for its subtraction. Neuroimage 1998; 8: 229-39.

Anami K, Mori T, Tanaka F, Kawagoe Y, Okamoto J, Yarita M, et al. Stepping stone sampling for retrieving artifact-free electroencephalogram during functional magnetic resonance imaging. Neuroimage 2003; 19: 281-95.

Arthurs OJ, Boniface SJ. What aspect of the fMRI BOLD signal best reflects the underlying electrophysiology in human somatosensory cortex? Clin Neurophysiol 2003; 114: 1203-9.

Assaf Y, Pasternak O. Diffusion tensor imaging (DTI)-based white matter mapping in brain research: a review. J Mol Neurosci 2008; 34: 51-61.

Assecondi S, Vanderperren K, Novitskiy N, Ramautar JR, Fias W, Staelens S, et al. Effect of the static magnetic field of the MR-scanner on ERPs: evaluation of visual, cognitive and motor potentials. Clin Neurophysiol 2010; 121: 672-85.

Babiloni C, Vecchio F, Buffo P, Buttiglione M, Cibelli G, Rossini PM. Cortical responses to consciousness of schematic emotional facial expressions: a high-resolution EEG study. Hum Brain Mapp 2010; 31: 1556-69.

Bandettini PA, Wong EC, Hinks RS, Tikofsky RS, Hyde JS. Time course EPI of human brain function during task activation. Magn Reson Med 1992; 25: 390-7.

Bartos M, Vida I, Jonas P. Synaptic mechanisms of synchronized gamma oscillations in inhibitory interneuron networks. Nat Rev Neurosci 2007; 8: 45-56.

Basser PJ. Inferring microstructural features and the physiological state of tissues from diffusion-weighted images. NMR Biomed 1995; 8: 333-44.

Basser PJ, Mattiello J, LeBihan D. Estimation of the effective self-diffusion tensor from the NMR spin echo. J Magn Reson B 1994; 103: 247-54.

Basser PJ, Pajevic S, Pierpaoli C, Duda J, Aldroubi A. In vivo fiber tractography using DT-MRI data. Magn Reson Med 2000; 44: 625-32.

Baudena P, Halgren E, Heit G, Clarke JM. Intracerebral potentials to rare target and distractor auditory and visual stimuli. III. Frontal cortex. Electroencephalogr Clin Neurophysiol 1995; 94: 251-64.

Bauer M, Oostenveld R, Peeters M, Fries P. Tactile spatial attention enhances gamma-band activity in somatosensory cortex and reduces low-frequency activity in parieto-occipital areas. J Neurosci 2006; 26: 490-501.

Baumgartner C. Controversies in clinical neurophysiology. MEG is superior to EEG in the localization of interictal epileptiform activity: Con. Clin Neurophysiol 2004; 115: 1010-20.
Beaulieu C, Allen PS. Determinants of anisotropic water diffusion in nerves. Magn Reson Med 1994; 31: 394-400.
Behrens TE, Berg HJ, Jbabdi S, Rushworth MF, Woolrich MW. Probabilistic diffusion tractography with multiple fibre orientations: What can we gain? Neuroimage 2007; 34: 144-55.
Behrens TE, Johansen-Berg H, Woolrich MW, Smith SM, Wheeler-Kingshott CA, Boulby PA, et al. Non-invasive mapping of connections between human thalamus and cortex using diffusion imaging. Nat Neurosci 2003a; 6: 750-7.
Behrens TE, Woolrich MW, Jenkinson M, Johansen-Berg H, Nunes RG, Clare S, et al. Characterization and propagation of uncertainty in diffusion-weighted MR imaging. Magn Reson Med 2003b; 50: 1077-88.
Benar C, Aghakhani Y, Wang Y, Izenberg A, Al-Asmi A, Dubeau F, et al. Quality of EEG in simultaneous EEG-fMRI for epilepsy. Clin Neurophysiol 2003; 114: 569-80.
Benar CG, Schon D, Grimault S, Nazarian B, Burle B, Roth M, et al. Single-trial analysis of oddball event-related potentials in simultaneous EEG-fMRI. Hum Brain Mapp 2007; 28: 602-13.
Benes FM. Emerging principles of altered neural circuitry in schizophrenia. Brain Res Brain Res Rev 2000; 31: 251-69.
Benes FM, Berretta S. GABAergic interneurons: implications for understanding schizophrenia and bipolar disorder. Neuropsychopharmacology 2001; 25: 1-27.
Berger H. Über das Elektrenkephalogramm des Menschen. Archiv für Psychiatrie und Nervenkrankheiten 1929; 87: 527-570.
Blamire AM, Ogawa S, Ugurbil K, Rothman D, McCarthy G, Ellermann JM, et al. Dynamic mapping of the human visual cortex by high-speed magnetic resonance imaging. Proc Natl Acad Sci U S A 1992; 89: 11069-73.
Bonmassar G, Hadjikhani N, Ives JR, Hinton D, Belliveau JW. Influence of EEG electrodes on the BOLD fMRI signal. Hum Brain Mapp 2001; 14: 108-15.
Bonmassar G, Purdon PL, Jaaskelainen IP, Chiappa K, Solo V, Brown EN, et al. Motion and ballistocardiogram artifact removal for interleaved recording of EEG and EPs during MRI. Neuroimage 2002; 16: 1127-41.
Boynton GM, Engel SA, Glover GH, Heeger DJ. Linear systems analysis of functional magnetic resonance imaging in human V1. J Neurosci 1996; 16: 4207-21.
Bragin A, Jando G, Nadasdy Z, Hetke J, Wise K, Buzsaki G. Gamma (40-100 Hz) oscillation in the hippocampus of the behaving rat. J Neurosci 1995; 15: 47-60.
Bressler SL. Large-scale cortical networks and cognition. Brain Res Brain Res Rev 1995; 20: 288-304.
Briselli E, Garreffa G, Bianchi L, Bianciardi M, Macaluso E, Abbafati M, et al. An independent component analysis-based approach on ballistocardiogram artifact removing. Magn Reson Imaging 2006; 24: 393-400.
Brosch M, Budinger E, Scheich H. Stimulus-related gamma oscillations in primate auditory cortex. J Neurophysiol 2002; 87: 2715-25.
Brown P, Salenius S, Rothwell JC, Hari R. Cortical correlate of the Piper rhythm in humans. J Neurophysiol 1998; 80: 2911-7.
Bullmore E, Sporns O. Complex brain networks: graph theoretical analysis of structural and functional systems. Nat Rev Neurosci 2009; 10: 186-98.
Buzsaki G, Chrobak JJ. Temporal structure in spatially organized neuronal ensembles: a role for interneuronal networks. Curr Opin Neurobiol 1995; 5: 504-10.
Buzsaki G, Draguhn A. Neuronal oscillations in cortical networks. Science 2004; 304: 1926-9.
Buzsaki G, Geisler C, Henze DA, Wang XJ. Interneuron Diversity series: Circuit complexity and axon wiring economy of cortical interneurons. Trends Neurosci 2004; 27: 186-93.
Calhoun VD, Adali T, Pearlson GD, Kiehl KA. Neuronal chronometry of target detection: fusion of hemodynamic and event-related potential data. Neuroimage 2006; 30: 544-53.
Canolty RT, Edwards E, Dalal SS, Soltani M, Nagarajan SS, Kirsch HE, et al. High gamma power is phase-locked to theta oscillations in human neocortex. Science 2006; 313: 1626-8.
Catani M, ffytche DH. The rises and falls of disconnection syndromes. Brain 2005; 128: 2224-39.
Caton R. The electric currents of the brain. Br Med J 1875; 2: 278.

Ciccarelli O, Catani M, Johansen-Berg H, Clark C, Thompson A. Diffusion-based tractography in neurological disorders: concepts, applications, and future developments. Lancet Neurol 2008; 7: 715-27.

Comon P. Independent component analysis- A new concept? Signal Processing 1994; 36: 287-314.

Conturo TE, Lori NF, Cull TS, Akbudak E, Snyder AZ, Shimony JS, et al. Tracking neuronal fiber pathways in the living human brain. Proc Natl Acad Sci U S A 1999; 96: 10422-7.

Cooper R, Winter AL, Crow HJ, Walter WG. Comparison of Subcortical, Cortical and Scalp Activity Using Chronically Indwelling Electrodes in Man. Electroencephalogr Clin Neurophysiol 1965; 18: 217-28.

Coyle JT. The GABA-glutamate connection in schizophrenia: which is the proximate cause? Biochem Pharmacol 2004; 68: 1507-14.

Csicsvari J, Jamieson B, Wise KD, Buzsaki G. Mechanisms of gamma oscillations in the hippocampus of the behaving rat. Neuron 2003; 37: 311-22.

Dale AM, Halgren E. Spatiotemporal mapping of brain activity by integration of multiple imaging modalities. Curr Opin Neurobiol 2001; 11: 202-8.

Dale AM, Liu AK, Fischl BR, Buckner RL, Belliveau JW, Lewine JD, et al. Dynamic statistical parametric mapping: combining fMRI and MEG for high-resolution imaging of cortical activity. Neuron 2000; 26: 55-67.

Daunizeau J, Grova C, Marrelec G, Mattout J, Jbabdi S, Pelegrini-Issac M, et al. Symmetrical event-related EEG/fMRI information fusion in a variational Bayesian framework. Neuroimage 2007; 36: 69-87.

Davidson RJ, Jackson DC, Larson CL. Human electroencephalography. Cambridge: Cambridge University Press, 2000.

Debener S, Herrmann CS, Kranczioch C, Gembris D, Engel AK. Top-down attentional processing enhances auditory evoked gamma band activity. Neuroreport 2003; 14: 683-6.

Debener S, Makeig S, Delorme A, Engel AK. What is novel in the novelty oddball paradigm? Functional significance of the novelty P3 event-related potential as revealed by independent component analysis. Brain Res Cogn Brain Res 2005; 22: 309-21.

Debener S, Mullinger KJ, Niazy RK, Bowtell RW. Properties of the ballistocardiogram artefact as revealed by EEG recordings at 1.5, 3 and 7 T static magnetic field strength. Int J Psychophysiol 2008; 67: 189-99.

Debener S, Strobel A, Sorger B, Peters J, Kranczioch C, Engel AK, et al. Improved quality of auditory event-related potentials recorded simultaneously with 3-T fMRI: removal of the ballistocardiogram artefact. Neuroimage 2007; 34: 587-97.

Debener S, Ullsperger M, Siegel M, Engel AK. Single-trial EEG-fMRI reveals the dynamics of cognitive function. Trends Cogn Sci 2006; 10: 558-63.

Dierks T, Linden DE, Jandl M, Formisano E, Goebel R, Lanfermann H, et al. Activation of Heschl's gyrus during auditory hallucinations. Neuron 1999; 22: 615-21.

Disbrow EA, Slutsky DA, Roberts TP, Krubitzer LA. Functional MRI at 1.5 tesla: a comparison of the blood oxygenation level-dependent signal and electrophysiology. Proc Natl Acad Sci U S A 2000; 97: 9718-23.

Doesburg SM, Roggeveen AB, Kitajo K, Ward LM. Large-scale gamma-band phase synchronization and selective attention. Cereb Cortex 2008; 18: 386-96.

Dyrholm M, Goldman R, Sajda P, Brown TR. Removal of BCG artifacts using a non-Kirchhoffian overcomplete representation. IEEE Trans Biomed Eng 2009; 56: 200-4.

Edwards E, Soltani M, Deouell LY, Berger MS, Knight RT. High gamma activity in response to deviant auditory stimuli recorded directly from human cortex. J Neurophysiol 2005; 94: 4269-80.

Eichele T, Calhoun VD, Moosmann M, Specht K, Jongsma ML, Quiroga RQ, et al. Unmixing concurrent EEG-fMRI with parallel independent component analysis. Int J Psychophysiol 2007.

Eichele T, Specht K, Moosmann M, Jongsma ML, Quiroga RQ, Nordby H, et al. Assessing the spatiotemporal evolution of neuronal activation with single-trial event-related potentials and functional MRI. Proc Natl Acad Sci U S A 2005; 102: 17798-803.

Ellingson ML, Liebenthal E, Spanaki MV, Prieto TE, Binder JR, Ropella KM. Ballistocardiogram artifact reduction in the simultaneous acquisition of auditory ERPS and fMRI. Neuroimage 2004; 22: 1534-42.

Engel AK, Fries P, Singer W. Dynamic predictions: oscillations and synchrony in top-down processing. Nat Rev Neurosci 2001; 2: 704-16.
Engel AK, Konig P, Kreiter AK, Singer W. Interhemispheric synchronization of oscillatory neuronal responses in cat visual cortex. Science 1991; 252: 1177-9.
Fan J, Byrne J, Worden MS, Guise KG, McCandliss BD, Fossella J, et al. The relation of brain oscillations to attentional networks. J Neurosci 2007; 27: 6197-206.
Fisahn A, Pike FG, Buhl EH, Paulsen O. Cholinergic induction of network oscillations at 40 Hz in the hippocampus in vitro. Nature 1998; 394: 186-9.
Fox PT, Raichle ME, Mintun MA, Dence C. Nonoxidative glucose consumption during focal physiologic neural activity. Science 1988; 241: 462-4.
Frahm J, Merboldt KD, Hanicke W, Kleinschmidt A, Boecker H. Brain or vein--oxygenation or flow? On signal physiology in functional MRI of human brain activation. NMR Biomed 1994; 7: 45-53.
Frank LR. Characterization of anisotropy in high angular resolution diffusion-weighted MRI. Magn Reson Med 2002; 47: 1083-99.
Fries P, Nikolic D, Singer W. The gamma cycle. Trends Neurosci 2007; 30: 309-16.
Fries P, Reynolds JH, Rorie AE, Desimone R. Modulation of oscillatory neuronal synchronization by selective visual attention. Science 2001; 291: 1560-3.
Friston K. Beyond phrenology: what can neuroimaging tell us about distributed circuitry? Annu Rev Neurosci 2002; 25: 221-50.
Friston KJ. Schizophrenia and the disconnection hypothesis. Acta Psychiatr Scand Suppl 1999; 395: 68-79.
Friston KJ, Jezzard P, Turner R. Analysis of functional MRI time-series. Human Brain Mapping 1994; 1: 153-171.
Friston KJ, Josephs O, Rees G, Turner R. Nonlinear event-related responses in fMRI. Magn Reson Med 1998; 39: 41-52.
Fuchs EC, Doheny H, Faulkner H, Caputi A, Traub RD, Bibbig A, et al. Genetically altered AMPA-type glutamate receptor kinetics in interneurons disrupt long-range synchrony of gamma oscillation. Proc Natl Acad Sci U S A 2001; 98: 3571-6.
Fuchs EC, Zivkovic AR, Cunningham MO, Middleton S, Lebeau FE, Bannerman DM, et al. Recruitment of parvalbumin-positive interneurons determines hippocampal function and associated behavior. Neuron 2007; 53: 591-604.
Galambos R, Makeig S, Talmachoff PJ. A 40-Hz auditory potential recorded from the human scalp. Proc Natl Acad Sci U S A 1981; 78: 2643-7.
Gallinat J, Winterer G, Herrmann CS, Senkowski D. Reduced oscillatory gamma-band responses in unmedicated schizophrenic patients indicate impaired frontal network processing. Clin Neurophysiol 2004; 115: 1863-74.
Gao JF, Yang Y, Lin P, Wang P, Zheng CX. Automatic removal of eye-movement and blink artifacts from EEG signals. Brain Topogr 2010; 23: 105-14.
Gaser C, Nenadic I, Volz HP, Buchel C, Sauer H. Neuroanatomy of "hearing voices": a frontotemporal brain structural abnormality associated with auditory hallucinations in schizophrenia. Cereb Cortex 2004; 14: 91-6.
George JS, Schmidt DM, Rector DM, Wood C. Dynamic functional neuroimaging integrating multiple modalities. In: Jezzard P, Matthews PM and Smith SM, editors. Functional MRI. An Introduction to Methods. Oxford: Oxford Univ. Press, 2001: 353–382.
Ghaderi F, Nazarpour K, McWhirter JG, Sanei S. Removal of Ballistocardiogram Artifacts Using the Cyclostationary Source Extraction Method. IEEE Trans Biomed Eng 2010.
Goldman RI, Stern JM, Engel J, Jr., Cohen MS. Acquiring simultaneous EEG and functional MRI. Clin Neurophysiol 2000; 111: 1974-80.
Gray CM, Konig P, Engel AK, Singer W. Oscillatory responses in cat visual cortex exhibit inter-columnar synchronization which reflects global stimulus properties. Nature 1989; 338: 334-7.
Gray CM, McCormick DA. Chattering cells: superficial pyramidal neurons contributing to the generation of synchronous oscillations in the visual cortex. Science 1996; 274: 109-13.
Grouiller F, Vercueil L, Krainik A, Segebarth C, Kahane P, David O. A comparative study of different artefact removal algorithms for EEG signals acquired during functional MRI. Neuroimage 2007; 38: 124-37.

Hajos N, Palhalmi J, Mann EO, Nemeth B, Paulsen O, Freund TF. Spike timing of distinct types of GABAergic interneuron during hippocampal gamma oscillations in vitro. J Neurosci 2004; 24: 9127-37.

Halgren E, Baudena P, Clarke JM, Heit G, Liegeois C, Chauvel P, et al. Intracerebral potentials to rare target and distractor auditory and visual stimuli. I. Superior temporal plane and parietal lobe. Electroencephalogr Clin Neurophysiol 1995a; 94: 191-220.

Halgren E, Baudena P, Clarke JM, Heit G, Marinkovic K, Devaux B, et al. Intracerebral potentials to rare target and distractor auditory and visual stimuli. II. Medial, lateral and posterior temporal lobe. Electroencephalogr Clin Neurophysiol 1995b; 94: 229-50.

Harris KD, Csicsvari J, Hirase H, Dragoi G, Buzsaki G. Organization of cell assemblies in the hippocampus. Nature 2003; 424: 552-6.

Heaton RK, Gladsjo JA, Palmer BW, Kuck J, Marcotte TD, Jeste DV. Stability and course of neuropsychological deficits in schizophrenia. Arch Gen Psychiatry 2001; 58: 24-32.

Heeger DJ, Ress D. What does fMRI tell us about neuronal activity? Nat Rev Neurosci 2002; 3: 142-51.

Helmholtz H. Über einige Gesetze der Vertheilung elektrischer Ströme in körperlichen Leitern mit der Anwendung auf die thierisch-elektrischen Versuche. Annalen der Physik und Chemie 1853: S. 211-233 und 353-377, 89.

Herrmann CS, Debener S. Simultaneous recording of EEG and BOLD responses: A historical perspective. Int J Psychophysiol 2007.

Herrmann CS, Munk MH, Engel AK. Cognitive functions of gamma-band activity: memory match and utilization. Trends Cogn Sci 2004; 8: 347-55.

Hillebrand A, Singh KD, Holliday IE, Furlong PL, Barnes GR. A new approach to neuroimaging with magnetoencephalography. Hum Brain Mapp 2005; 25: 199-211.

Horwitz B, Poeppel D. How can EEG/MEG and fMRI/PET data be combined? Hum Brain Mapp 2002; 17: 1-3.

Huang-Hellinger FR, Breiter HC, McCormack G, Cohen MS, Kwong KK, Sutton JP, et al. Simultaneous functional magnetic resonance imaging and electrophysiological recording. Hum Brain Mapp 1995; 3: 13–23.

Hubl D, Koenig T, Strik W, Federspiel A, Kreis R, Boesch C, et al. Pathways that make voices: white matter changes in auditory hallucinations. Arch Gen Psychiatry 2004; 61: 658-68.

Ives JR, Warach S, Schmitt F, Edelman RR, Schomer DL. Monitoring the patient's EEG during echo planar MRI. Electroencephalogr Clin Neurophysiol 1993; 87: 417-20.

Jefferys JG, Traub RD, Whittington MA. Neuronal networks for induced '40 Hz' rhythms. Trends Neurosci 1996; 19: 202-8.

Jespersen SN, Kroenke CD, Ostergaard L, Ackerman JJ, Yablonskiy DA. Modeling dendrite density from magnetic resonance diffusion measurements. Neuroimage 2007; 34: 1473-86.

Johansen-Berg H, Behrens TE, Sillery E, Ciccarelli O, Thompson AJ, Smith SM, et al. Functional-anatomical validation and individual variation of diffusion tractography-based segmentation of the human thalamus. Cereb Cortex 2005; 15: 31-9.

Johansen-Berg H, Rushworth MF. Using diffusion imaging to study human connectional anatomy. Annu Rev Neurosci 2009; 32: 75-94.

Joliot M, Ribary U, Llinas R. Human oscillatory brain activity near 40 Hz coexists with cognitive temporal binding. Proc Natl Acad Sci U S A 1994; 91: 11748-51.

Kanaan RA, Kim JS, Kaufmann WE, Pearlson GD, Barker GJ, McGuire PK. Diffusion tensor imaging in schizophrenia. Biol Psychiatry 2005; 58: 921-9.

Kandel ER, Schwartz JH, Jessell TM. Principles of neural science. New York, 2000.

Karch S, Feuerecker R, Leicht G, Meindl T, Hantschk I, Kirsch V, et al. Separating distinct aspects of the voluntary selection between response alternatives: N2- and P3-related BOLD responses. Neuroimage 2010; 51: 356-64.

Kilner JM, Mattout J, Henson R, Friston KJ. Hemodynamic correlates of EEG: a heuristic. Neuroimage 2005; 28: 280-6.

Krakow K, Allen PJ, Symms MR, Lemieux L, Josephs O, Fish DR. EEG recording during fMRI experiments: image quality. Hum Brain Mapp 2000; 10: 10-5.

Kreiter AK, Singer W. Stimulus-dependent synchronization of neuronal responses in the visual cortex of the awake macaque monkey. J Neurosci 1996; 16: 2381-96.

Krishnan GP, Hetrick WP, Brenner CA, Shekhar A, Steffen AN, O'Donnell BF. Steady state and induced auditory gamma deficits in schizophrenia. Neuroimage 2009; 47: 1711-9.
Kruggel F, Wiggins CJ, Herrmann CS, von Cramon DY. Recording of the event-related potentials during functional MRI at 3.0 Tesla field strength. Magn Reson Med 2000; 44: 277-82.
Kubicki M, McCarley R, Westin CF, Park HJ, Maier S, Kikinis R, et al. A review of diffusion tensor imaging studies in schizophrenia. J Psychiatr Res 2007; 41: 15-30.
Lakatos P, Chen CM, O'Connell MN, Mills A, Schroeder CE. Neuronal oscillations and multisensory interaction in primary auditory cortex. Neuron 2007; 53: 279-92.
Lakatos P, Karmos G, Mehta AD, Ulbert I, Schroeder CE. Entrainment of neuronal oscillations as a mechanism of attentional selection. Science 2008; 320: 110-3.
Laufs H, Daunizeau J, Carmichael DW, Kleinschmidt A. Recent advances in recording electrophysiological data simultaneously with magnetic resonance imaging. Neuroimage 2008; 40: 515-28.
Laughlin SB, Sejnowski TJ. Communication in neuronal networks. Science 2003; 301: 1870-4.
Lauritzen M. Reading vascular changes in brain imaging: is dendritic calcium the key? Nat Rev Neurosci 2005; 6: 77-85.
Lauritzen M, Gold L. Brain function and neurophysiological correlates of signals used in functional neuroimaging. J Neurosci 2003; 23: 3972-80.
Le Bihan D. Looking into the functional architecture of the brain with diffusion MRI. Nat Rev Neurosci 2003; 4: 469-80.
Le Bihan D, Mangin JF, Poupon C, Clark CA, Pappata S, Molko N, et al. Diffusion tensor imaging: concepts and applications. J Magn Reson Imaging 2001; 13: 534-46.
Leclercq Y, Balteau E, Dang-Vu T, Schabus M, Luxen A, Maquet P, et al. Rejection of pulse related artefact (PRA) from continuous electroencephalographic (EEG) time series recorded during functional magnetic resonance imaging (fMRI) using constraint independent component analysis (cICA). Neuroimage 2009; 44: 679-91.
Lee K, Yoshida T, Kubicki M, Bouix S, Westin CF, Kindlmann G, et al. Increased diffusivity in superior temporal gyrus in patients with schizophrenia: a Diffusion Tensor Imaging study. Schizophr Res 2009; 108: 33-40.
Lee KH, Williams LM, Breakspear M, Gordon E. Synchronous gamma activity: a review and contribution to an integrative neuroscience model of schizophrenia. Brain Res Brain Res Rev 2003; 41: 57-78.
Lemieux L, Allen PJ, Franconi F, Symms MR, Fish DR. Recording of EEG during fMRI experiments: patient safety. Magn Reson Med 1997; 38: 943-52.
Lemieux L, Salek-Haddadi A, Josephs O, Allen P, Toms N, Scott C, et al. Event-related fMRI with simultaneous and continuous EEG: description of the method and initial case report. Neuroimage 2001; 14: 780-7.
Lewis DA, Hashimoto T, Volk DW. Cortical inhibitory neurons and schizophrenia. Nat Rev Neurosci 2005; 6: 312-24.
Light GA, Hsu JL, Hsieh MH, Meyer-Gomes K, Sprock J, Swerdlow NR, et al. Gamma band oscillations reveal neural network cortical coherence dysfunction in schizophrenia patients. Biol Psychiatry 2006; 60: 1231-40.
Lim KO, Hedehus M, Moseley M, de Crespigny A, Sullivan EV, Pfefferbaum A. Compromised white matter tract integrity in schizophrenia inferred from diffusion tensor imaging. Arch Gen Psychiatry 1999; 56: 367-74.
Lim KO, Helpern JA. Neuropsychiatric applications of DTI - a review. NMR Biomed 2002; 15: 587-93.
Lisman JE, Coyle JT, Green RW, Javitt DC, Benes FM, Heckers S, et al. Circuit-based framework for understanding neurotransmitter and risk gene interactions in schizophrenia. Trends Neurosci 2008; 31: 234-42.
Logothetis NK. The underpinnings of the BOLD functional magnetic resonance imaging signal. J Neurosci 2003; 23: 3963-71.
Logothetis NK, Pauls J, Augath M, Trinath T, Oeltermann A. Neurophysiological investigation of the basis of the fMRI signal. Nature 2001; 412: 150-7.
Logothetis NK, Wandell BA. Interpreting the BOLD signal. Annu Rev Physiol 2004; 66: 735-69.
Magaro PA, Page J. Brain disconnection, schizophrenia, and paranoia. J Nerv Ment Dis 1983; 171: 133-40.

Malonek D, Dirnagl U, Lindauer U, Yamada K, Kanno I, Grinvald A. Vascular imprints of neuronal activity: relationships between the dynamics of cortical blood flow, oxygenation, and volume changes following sensory stimulation. Proc Natl Acad Sci U S A 1997; 94: 14826-31.

Malonek D, Grinvald A. Interactions between electrical activity and cortical microcirculation revealed by imaging spectroscopy: implications for functional brain mapping. Science 1996; 272: 551-4.

Mann EO, Radcliffe CA, Paulsen O. Hippocampal gamma-frequency oscillations: from interneurones to pyramidal cells, and back. J Physiol 2005; 562: 55-63.

Mansfield P, Grannell PK. NMR 'diffraction' in solids? J Phys C 1973; 6: 442-426.

Mantini D, Perrucci MG, Cugini S, Ferretti A, Romani GL, Del Gratta C. Complete artifact removal for EEG recorded during continuous fMRI using independent component analysis. Neuroimage 2007; 34: 598-607.

Marin G, Guerin C, Baillet S, Garnero L, Meunier G. Influence of skull anisotropy for the forward and inverse problem in EEG: simulation studies using FEM on realistic head models. Hum Brain Mapp 1998; 6: 250-69.

Masterton RA, Abbott DF, Fleming SW, Jackson GD. Measurement and reduction of motion and ballistocardiogram artefacts from simultaneous EEG and fMRI recordings. Neuroimage 2007; 37: 202-11.

McBain CJ, Fisahn A. Interneurons unbound. Nat Rev Neurosci 2001; 2: 11-23.

McCarley RW, Shenton ME, O'Donnell BF, Faux SF, Kikinis R, Nestor PG, et al. Auditory P300 abnormalities and left posterior superior temporal gyrus volume reduction in schizophrenia. Arch Gen Psychiatry 1993; 50: 190-7.

Mesulam M. Imaging connectivity in the human cerebral cortex: the next frontier? Ann Neurol 2005; 57: 5-7.

Moosmann M, Eichele T, Nordby H, Hugdahl K, Calhoun VD. Joint independent component analysis for simultaneous EEG-fMRI: Principle and simulation. Int J Psychophysiol 2007.

Mori S, van Zijl PC. Fiber tracking: principles and strategies - a technical review. NMR Biomed 2002; 15: 468-80.

Mori S, Zhang J. Principles of diffusion tensor imaging and its applications to basic neuroscience research. Neuron 2006; 51: 527-39.

Mulert C, Gallinat J, Pascual-Marqui R, Dorn H, Frick K, Schlattmann P, et al. Reduced event-related current density in the anterior cingulate cortex in schizophrenia. Neuroimage 2001; 13: 589-600.

Mulert C, Jager L, Schmitt R, Bussfeld P, Pogarell O, Moller HJ, et al. Integration of fMRI and simultaneous EEG: towards a comprehensive understanding of localization and time-course of brain activity in target detection. Neuroimage 2004; 22: 83-94.

Mulert C, Leicht G, Hepp P, Kirsch V, Karch S, Pogarell O, et al. Single-trial coupling of the gamma-band response and the corresponding BOLD signal. Neuroimage 2009.

Mulert C, Leicht G, Pogarell O, Mergl R, Karch S, Juckel G, et al. Auditory cortex and anterior cingulate cortex sources of the early evoked gamma-band response: relationship to task difficulty and mental effort. Neuropsychologia 2007; 45: 2294-306.

Mulert C, Seifert C, Leicht G, Kirsch V, Ertl M, Karch S, et al. Single-trial coupling of EEG and fMRI reveals the involvement of early anterior cingulate cortex activation in effortful decision making. Neuroimage 2008.

Murthy VN, Fetz EE. Coherent 25- to 35-Hz oscillations in the sensorimotor cortex of awake behaving monkeys. Proc Natl Acad Sci U S A 1992; 89: 5670-4.

Nakamura W, Anami K, Mori T, Saitoh O, Cichocki A, Amari S. Removal of ballistocardiogram artifacts from simultaneously recorded EEG and fMRI data using independent component analysis. IEEE Trans Biomed Eng 2006; 53: 1294-308.

Ngai AC, Jolley MA, D'Ambrosio R, Meno JR, Winn HR. Frequency-dependent changes in cerebral blood flow and evoked potentials during somatosensory stimulation in the rat. Brain Res 1999; 837: 221-8.

Niazy RK, Beckmann CF, Iannetti GD, Brady JM, Smith SM. Removal of FMRI environment artifacts from EEG data using optimal basis sets. Neuroimage 2005; 28: 720-37.

Nunez PL, Silberstein RB. On the relationship of synaptic activity to macroscopic measurements: does co-registration of EEG with fMRI make sense? Brain Topogr 2000; 13: 79-96.

Nunez PL, Silberstein RB, Cadusch PJ, Wijesinghe RS, Westdorp AF, Srinivasan R. A theoretical and experimental study of high resolution EEG based on surface Laplacians and cortical imaging. Electroencephalogr Clin Neurophysiol 1994; 90: 40-57.

Nunez PL, Sirinivasan R, editors. Electric Fields of the Brain: The Neurophysics of EEG: Oxford Univ. Press, 2005.

Ogawa S, Lee TM, Kay AR, Tank DW. Brain magnetic resonance imaging with contrast dependent on blood oxygenation. Proc Natl Acad Sci U S A 1990; 87: 9868-72.

Ogawa S, Lee TM, Stepnoski R, Chen W, Zhu XH, Ugurbil K. An approach to probe some neural systems interaction by functional MRI at neural time scale down to milliseconds. Proc Natl Acad Sci U S A 2000; 97: 11026-31.

Oh JS, Kubicki M, Rosenberger G, Bouix S, Levitt JJ, McCarley RW, et al. Thalamo-frontal white matter alterations in chronic schizophrenia: a quantitative diffusion tractography study. Hum Brain Mapp 2009; 30: 3812-25.

Pantev C, Makeig S, Hoke M, Galambos R, Hampson S, Gallen C. Human auditory evoked gamma-band magnetic fields. Proc Natl Acad Sci U S A 1991; 88: 8996-9000.

Parker GJ, Alexander DC. Probabilistic anatomical connectivity derived from the microscopic persistent angular structure of cerebral tissue. Philos Trans R Soc Lond B Biol Sci 2005; 360: 893-902.

Pascual-Marqui RD. Standardized low-resolution brain electromagnetic tomography (sLORETA): technical details. Methods Find Exp Clin Pharmacol 2002; 24 Suppl D: 5-12.

Pascual-Marqui RD, Lehmann D, Koenig T, Kochi K, Merlo MC, Hell D, et al. Low resolution brain electromagnetic tomography (LORETA) functional imaging in acute, neuroleptic-naive, first-episode, productive schizophrenia. Psychiatry Res 1999; 90: 169-79.

Pascual-Marqui RD, Michel CM, Lehmann D. Low resolution electromagnetic tomography: a new method for localizing electrical activity in the brain. Int J Psychophysiol 1994; 18: 49-65.

Passingham RE, Stephan KE, Kotter R. The anatomical basis of functional localization in the cortex. Nat Rev Neurosci 2002; 3: 606-16.

Penfield W. Mechanisms of voluntary movement. Brain 1954; 77: 1-17.

Perry W, Light GA, Davis H, Braff DL. Schizophrenia patients demonstrate a dissociation on declarative and non-declarative memory tests. Schizophr Res 2000; 46: 167-74.

Pesaran B, Pezaris JS, Sahani M, Mitra PP, Andersen RA. Temporal structure in neuronal activity during working memory in macaque parietal cortex. Nat Neurosci 2002; 5: 805-11.

Phillips WA, Silverstein SM. Convergence of biological and psychological perspectives on cognitive coordination in schizophrenia. Behav Brain Sci 2003; 26: 65-82; discussion 82-137.

Pierpaoli C, Jezzard P, Basser PJ, Barnett A, Di Chiro G. Diffusion tensor MR imaging of the human brain. Radiology 1996; 201: 637-48.

Poupon C, Clark CA, Frouin V, Regis J, Bloch I, Le Bihan D, et al. Regularization of diffusion-based direction maps for the tracking of brain white matter fascicles. Neuroimage 2000; 12: 184-95.

Rees G, Friston K, Koch C. A direct quantitative relationship between the functional properties of human and macaque V5. Nat Neurosci 2000 a; 3: 716-23.

Ritter P, Becker R, Graefe C, Villringer A. Evaluating gradient artifact correction of EEG data acquired simultaneously with fMRI. Magn Reson Imaging 2007; 25: 923-32.

Ritter P, Villringer A. Simultaneous EEG-fMRI. Neurosci Biobehav Rev 2006; 30: 823-38.

Rodriguez E, George N, Lachaux JP, Martinerie J, Renault B, Varela FJ. Perception's shadow: long-distance synchronization of human brain activity. Nature 1999; 397: 430-3.

Rotarska-Jagiela A, Schonmeyer R, Oertel V, Haenschel C, Vogeley K, Linden DE. The corpus callosum in schizophrenia-volume and connectivity changes affect specific regions. Neuroimage 2008; 39: 1522-32.

Salek-Haddadi A, Merschhemke M, Lemieux L, Fish DR. Simultaneous EEG-Correlated Ictal fMRI. Neuroimage 2002; 16: 32-40.

Schoffelen JM, Oostenveld R, Fries P. Neuronal coherence as a mechanism of effective corticospinal interaction. Science 2005; 308: 111-3.

Schwartz WJ, Smith CB, Davidsen L, Savaki H, Sokoloff L, Mata M, et al. Metabolic mapping of functional activity in the hypothalamo-neurohypophysial system of the rat. Science 1979; 205: 723-5.

Seok JH, Park HJ, Chun JW, Lee SK, Cho HS, Kwon JS, et al. White matter abnormalities associated with auditory hallucinations in schizophrenia: a combined study of voxel-based analyses of

diffusion tensor imaging and structural magnetic resonance imaging. Psychiatry Res 2007; 156: 93-104.
Shelley AM, Ward PB, Catts SV, Michie PT, Andrews S, McConaghy N. Mismatch negativity: an index of a preattentive processing deficit in schizophrenia. Biol Psychiatry 1991; 30: 1059-62.
Shenton ME, Whitford TJ, Kubicki M. Structural neuroimaging in schizophrenia: from methods to insights to treatments. Dialogues Clin Neurosci 2010; 12: 317-32.
Shibasaki H. Human brain mapping: hemodynamic response and electrophysiology. Clin Neurophysiol 2008; 119: 731-43.
Shulman RG, Rothman DL. Interpreting functional imaging studies in terms of neurotransmitter cycling. Proc Natl Acad Sci U S A 1998; 95: 11993-8.
Sibson NR, Dhankhar A, Mason GF, Rothman DL, Behar KL, Shulman RG. Stoichiometric coupling of brain glucose metabolism and glutamatergic neuronal activity. Proc Natl Acad Sci U S A 1998; 95: 316-21.
Sijbers J, Van Audekerke J, Verhoye M, Van der Linden A, Van Dyck D. Reduction of ECG and gradient related artifacts in simultaneously recorded human EEG/MRI data. Magn Reson Imaging 2000; 18: 881-6.
Silva LR, Amitai Y, Connors BW. Intrinsic oscillations of neocortex generated by layer 5 pyramidal neurons. Science 1991; 251: 432-5.
Singer W. Synchronization of cortical activity and its putative role in information processing and learning. Annu Rev Physiol 1993; 55: 349-74.
Singer W. Neuronal synchrony: a versatile code for the definition of relations? Neuron 1999; 24: 49-65, 111-25.
Siniatchkin M, Moeller F, Jacobs J, Stephani U, Boor R, Wolff S, et al. Spatial filters and automated spike detection based on brain topographies improve sensitivity of EEG-fMRI studies in focal epilepsy. Neuroimage 2007; 37: 834-43.
Sotero RC, Trujillo-Barreto NJ. Biophysical model for integrating neuronal activity, EEG, fMRI and metabolism. Neuroimage 2008; 39: 290-309.
Speckmann E, Elger C. Introduction to the neurophysiological basis of the EEG and DC potentials. Baltimore: Lippincott Williams and Wilkins, 1999.
Spencer KM, Nestor PG, Niznikiewicz MA, Salisbury DF, Shenton ME, McCarley RW. Abnormal neural synchrony in schizophrenia. J Neurosci 2003; 23: 7407-11.
Spencer KM, Nestor PG, Perlmutter R, Niznikiewicz MA, Klump MC, Frumin M, et al. Neural synchrony indexes disordered perception and cognition in schizophrenia. Proc Natl Acad Sci U S A 2004; 101: 17288-93.
Spencer KM, Niznikiewicz MA, Nestor PG, Shenton ME, McCarley RW. Left auditory cortex gamma synchronization and auditory hallucination symptoms in schizophrenia. BMC Neurosci 2009; 10: 85.
Spencer KM, Niznikiewicz MA, Shenton ME, McCarley RW. Sensory-evoked gamma oscillations in chronic schizophrenia. Biol Psychiatry 2008a; 63: 744-7.
Spencer KM, Salisbury DF, Shenton ME, McCarley RW. gamma-Band Auditory Steady-State Responses Are Impaired in First Episode Psychosis. Biol Psychiatry 2008b.
Srinivasan R, Nunez PL, Tucker DM, Silberstein RB, Cadusch PJ. Spatial sampling and filtering of EEG with spline laplacians to estimate cortical potentials. Brain Topogr 1996; 8: 355-66.
Srivastava G, Crottaz-Herbette S, Lau KM, Glover GH, Menon V. ICA-based procedures for removing ballistocardiogram artifacts from EEG data acquired in the MRI scanner. Neuroimage 2005; 24: 50-60.
Stopfer M, Bhagavan S, Smith BH, Laurent G. Impaired odour discrimination on desynchronization of odour-encoding neural assemblies. Nature 1997; 390: 70-4.
Strogatz SH. Exploring complex networks. Nature 2001; 410: 268-76.
Sundgren PC, Dong Q, Gomez-Hassan D, Mukherji SK, Maly P, Welsh R. Diffusion tensor imaging of the brain: review of clinical applications. Neuroradiology 2004; 46: 339-50.
Sweet RA, Bergen SE, Sun Z, Marcsisin MJ, Sampson AR, Lewis DA. Anatomical evidence of impaired feedforward auditory processing in schizophrenia. Biol Psychiatry 2007; 61: 854-64.
Tallon-Baudry C, Bertrand O, Delpuech C, Pernier J. Stimulus specificity of phase-locked and non-phase-locked 40 Hz visual responses in human. J Neurosci 1996; 16: 4240-9.

Tenforde TS, Gaffey CT, Moyer BR, Budinger TF. Cardiovascular alterations in Macaca monkeys exposed to stationary magnetic fields: experimental observations and theoretical analysis. Bioelectromagnetics 1983; 4: 1-9.

Thomason ME, Thompson PM. Diffusion imaging, white matter, and psychopathology. Annu Rev Clin Psychol 2011; 7: 63-85.

Tiitinen H, Sinkkonen J, Reinikainen K, Alho K, Lavikainen J, Naatanen R. Selective attention enhances the auditory 40-Hz transient response in humans. Nature 1993; 364: 59-60.

Tournier JD, Calamante F, Gadian DG, Connelly A. Direct estimation of the fiber orientation density function from diffusion-weighted MRI data using spherical deconvolution. Neuroimage 2004; 23: 1176-85.

Traub RD, Whittington MA, Stanford IM, Jefferys JG. A mechanism for generation of long-range synchronous fast oscillations in the cortex. Nature 1996; 383: 621-4.

Tsai G, Passani LA, Slusher BS, Carter R, Baer L, Kleinman JE, et al. Abnormal excitatory neurotransmitter metabolism in schizophrenic brains. Arch Gen Psychiatry 1995; 52: 829-36.

Tuch DS. Q-ball imaging. Magn Reson Med 2004; 52: 1358-72.

Tuch DS, Reese TG, Wiegell MR, Wedeen VJ. Diffusion MRI of complex neural architecture. Neuron 2003; 40: 885-95.

Uhlhaas PJ, Haenschel C, Nikolic D, Singer W. The role of oscillations and synchrony in cortical networks and their putative relevance for the pathophysiology of schizophrenia. Schizophr Bull 2008; 34: 927-43.

Uhlhaas PJ, Pipa G, Lima B, Melloni L, Neuenschwander S, Nikolic D, et al. Neural synchrony in cortical networks: history, concept and current status. Front Integr Neurosci 2009; 3: 17.

Uhlhaas PJ, Singer W. Abnormal neural oscillations and synchrony in schizophrenia. Nat Rev Neurosci 2010; 11: 100-13.

Ullsperger M, von Cramon DY. Subprocesses of performance monitoring: a dissociation of error processing and response competition revealed by event-related fMRI and ERPs. Neuroimage 2001; 14: 1387-401.

Ureshi M, Kershaw J, Kanno I. Nonlinear correlation between field potential and local cerebral blood flow in rat somatosensory cortex evoked by changing the stimulus current. Neurosci Res 2005; 51: 139-45.

Usrey WM, Reid RC. Synchronous activity in the visual system. Annu Rev Physiol 1999; 61: 435-56.

van de Ven VG, Formisano E, Roder CH, Prvulovic D, Bittner RA, Dietz MG, et al. The spatiotemporal pattern of auditory cortical responses during verbal hallucinations. Neuroimage 2005; 27: 644-55.

van der Loo E, Gais S, Congedo M, Vanneste S, Plazier M, Menovsky T, et al. Tinnitus intensity dependent gamma oscillations of the contralateral auditory cortex. PLoS One 2009; 4: e7396.

Vanderperren K, De Vos M, Ramautar JR, Novitskiy N, Mennes M, Assecondi S, et al. Removal of BCG artifacts from EEG recordings inside the MR scanner: a comparison of methodological and validation-related aspects. Neuroimage 2010; 50: 920-34.

Vanzetta I, Grinvald A. Increased cortical oxidative metabolism due to sensory stimulation: implications for functional brain imaging. Science 1999; 286: 1555-8.

Viola FC, Thorne J, Edmonds B, Schneider T, Eichele T, Debener S. Semi-automatic identification of independent components representing EEG artifact. Clin Neurophysiol 2009; 120: 868-77.

Vreugdenhil M, Jefferys JG, Celio MR, Schwaller B. Parvalbumin-deficiency facilitates repetitive IPSCs and gamma oscillations in the hippocampus. J Neurophysiol 2003; 89: 1414-22.

Wedeen VJ, Wang RP, Schmahmann JD, Benner T, Tseng WY, Dai G, et al. Diffusion spectrum magnetic resonance imaging (DSI) tractography of crossing fibers. Neuroimage 2008; 41: 1267-77.

Wespatat V, Tennigkeit F, Singer W. Phase sensitivity of synaptic modifications in oscillating cells of rat visual cortex. J Neurosci 2004; 24: 9067-75.

Whitford TJ, Kubicki M, Schneiderman JS, O'Donnell LJ, King R, Alvarado JL, et al. Corpus callosum abnormalities and their association with psychotic symptoms in patients with schizophrenia. Biol Psychiatry 2010; 68: 70-7.

Whittington MA, Traub RD. Interneuron diversity series: inhibitory interneurons and network oscillations in vitro. Trends Neurosci 2003; 26: 676-82.

Whittington MA, Traub RD, Jefferys JG. Synchronized oscillations in interneuron networks driven by metabotropic glutamate receptor activation. Nature 1995; 373: 612-5.

Womelsdorf T, Fries P, Mitra PP, Desimone R. Gamma-band synchronization in visual cortex predicts speed of change detection. Nature 2006; 439: 733-6.

Wu W, Wheeler DW, Staedtler ES, Munk MH, Pipa G. Behavioral performance modulates spike field coherence in monkey prefrontal cortex. Neuroreport 2008; 19: 235-8.

Yan WX, Mullinger KJ, Geirsdottir GB, Bowtell R. Physical modeling of pulse artefact sources in simultaneous EEG/fMRI. Hum Brain Mapp 2009; 31: 604-20.

Yan Y, Nunez PL, Hart RT. Finite-element model of the human head: scalp potentials due to dipole sources. Med Biol Eng Comput 1991; 29: 475-81.